EXPERIMENTAL INVESTIGATION OF THE AEROELASTIC INSTABILITY OF BLUFF TWO-DIMENSIONAL CYLINDERS

by

PETER NOEL HAMILTON BROOKS
B.A.Sc., University of British Columbia, 1958

A THESIS SUBMITTED IN PARTIAL FULFILLMENT OF THE

REQUIREMENTS FOR THE DEGREE OF

M.A.Sc.

in the Department of

Mechanical Engineering

We accept this thesis as conforming to the

required standard

The University of British Columbia

August 1960

In presenting this thesis in partial fulfilment of the requirements for an advanced degree at the University of British Columbia, I agree that the Library shall make it freely available for reference and study. I further agree that permission for extensive copying of this thesis for scholarly purposes may be granted by the Head of my Department or by his representatives. It is understood that copying or publication of this thesis for financial gain shall not be allowed without my written permission.

P.N.H.Brooks.

Department of Mechanical Engineering,

The University of British Columbia,
Vancouver 8, Canada.

Date August 12, 1960

ABSTRACT

Aerodynamically bluff elastic structures such as suspension bridges and industrial smokestacks have been observed to vibrate violently in the presence of a low speed wind. Although a number of theories such as Den Hartog's quasi-steady instability criterion and the vortex resonance theory have been proposed to explain the phenomenon, the problem is still not completely solved nor yet fully understood. The purpose of this research was to dynamically test a number of two-dimensional cylinders of simple cross-section and to observe whether or not the results correlated with either of the two theories mentioned above. Necessary aerodynamic coefficients were obtained by the graphical integration of measured surface pressure distributions. Tests were performed on models mounted elastically with six degrees of freedom. Generally only one of two modes of vibration was excited at a given airspeed. Dynamic response curves are presented for several lightly damped cylinders. For cylinders with rectangular cross-section of length/width (b/h/ greater than 0.75, vibration occurred at any airspeed above a certain minimum which depended on the structural damping (galloping). Cylinders with b/h less than 0.683 were found to vibrate over a limited range of airspeeds which always included the critical velocity for resonance with the periodic formation of vortices in the wakes. Using quasi-steady theory, it was found that the D-section and rectangles with

with b/h less than 0.683 have zero aerodynamic damping to large relative angles of attack, due to the symmetry of the wake pressures at angles of attack greater than zero. Because of this the D-section is subject to galloping only when given a substantial initial amplitude. Vortex resonance was observed for all the cylinders tested with two exceptions; the reversed D-section and the D-section with the flat face initially at an angle of attack greater than 40°, both of which appear to be completely stable. Measurements of the frequency of vortex formation for stationary cylinders gave Strouhal numbers which showed only slight variation over the speed range used in the tests. However, a strong variation with b/h was noted for the rectangles $1.0 < b/h < 3.0$. During vibration of any kind, the frequency of vortex formation was controlled at the frequency of vibration which in all cases was a natural frequency of the system being tested. An energy balance based on quasi-steady theory and neglecting structural damping yields velocity-amplitude curves which give good agreement with the experimental data for the galloping D-section and the square section at various initial angles of attack. The test results indicate that the steady state aerodynamic coefficients provide a useful approximation to the dynamic values; they also indicate that any theory which will completely predict the behaviour of such systems must include the effects of both negative aerodynamic damping and vortex resonance.

CONTENTS

	Page No.
INTRODUCTION	1
TEST FACILITIES AND APPARATUS	6
MEASUREMENT TECHNIQUES	10
CALIBRATION AND ACCURACY	13
REVIEW OF CURRENT THEORIES	20
TEST RESULTS	24
DISCUSSION OF RESULTS	41
CONCLUSIONS	61
APPENDICES	
A. Use of the Lissajous ellipse for the determination of the frequency of an unknown signal	66
B. Wind Tunnel Corrections	68
C. The Den Hartog Instability criterion	70
D. Definition of force coeffients	72
E. Aerodynamic coefficients for the D-section cylinder	73
F. Aerodynamic coefficients for the rectangular cylinder	77
REFERENCES	78
SUPPLEMENTARY BIBLIOGRAPHY	80
ILLUSTRATIONS	84

ILLUSTRATIONS

Figure Number

1 WIND TUNNEL AERODYNAMIC OUTLINE

2 ESTIMATION OF TEST SECTION TURBULENCE LEVEL

3 TYPICAL DYNAMIC MODEL

4 MOUNTING OF DYNAMIC MODEL

5 CROSS-SECTIONS OF DYNAMIC MODELS

6 MODELS FOR WAKE WIDTH MEASUREMENTS

7 D-SECTION PRESSURE MODEL

8 LOCATION OF PRESSURE TAPS ON D-SECTION PRESSURE MODEL

9 DETAILS OF PRESSURE MODEL

10 SQUARE SECTION PRESSURE MODEL

11 LOCATION OF PRESSURE TAPS ON SQUARE SECTION MODEL

12 LOCATION OF PRESSURE TAPS ON RECTANGULAR SECTION MODEL

13 MOUNTING OF PRESSURE MODEL

14 CROSS-SECTIONS OF PRESSURE MODELS

15 MEASUREMENT OF SHEDDING FREQUENCY

16 MEASUREMENT OF AMPLITUDE BUILD-UP WITH TIME

17 CALIBRATION OF AUDIO OSCILLATOR

18 CALIBRATION OF PHOTOCELL

19 SHAPE OF PHOTOVOLTAIC CELL USED FOR AMPLITUDE MEASUREMENT

20 NON-AERODYNAMIC DAMPING FOR DYNAMIC TESTS

21 EFFECT OF STREAMWISE POSITION IN HOLE ON AMPLITUDE

22 ZONES OF INSTABILITY

23 PROJECTION OF C_p ON UPSTREAM SURFACE ($\alpha = 0^\circ$)

24 PROJECTION OF C_p ON UPSTREAM SURFACE ($\alpha = 15^\circ$)

25 MID-SPAN SECTIONAL COEFFICIENTS FOR D-SECTION. NR = 66,000

26 PROJECTION OF C_p ON UPSTREAM SURFACE. TWO-DIMENSIONAL D-SECTION ($\alpha = 0$ & 15°)

27 PROJECTION OF C_p ON UPSTREAM SURFACE. TWO-DIMENSIONAL D-SECTION ($\alpha = 35$ & 40°)

28 SECTIONAL LIFT COEFFICIENT FOR TWO-DIMENSIONAL D-SECTION

29 SECTIONAL DRAG COEFFICIENT FOR TWO-DIMENSIONAL D-SECTION

30 PRESSURE ON CENTERLINE OF WAKE DOWNSTREAM OF VARIOUS CYLINDERS

31 AMPLITUDE AND VORTEX FREQUENCY OF D-SECTION -- PLUNGING MODE

32 AMPLITUDE AND VORTEX FREQUENCY OF D-SECTION -- TORSIONAL MODE

33 PLUNGING AND TORSIONAL AMPLITUDES FOR D-SECTION AT VARIOUS ANGLES OF ATTACK β

34 $dC_{Fv}/d\alpha$ FOR D-SECTION CYLINDER

35 STROUHAL NUMBER FOR D-SECTION CYLINDER AT VARIOUS β

36 PLUNGING AND TORSIONAL MODES FOR CIRCULAR CYLINDER

37 AMPLITUDE VARIATION FOR RECTANGULAR CYLINDERS (PLUNGING MODE)

38 AMPLITUDE VARIATION FOR RECTANGULAR CYLINDERS (TORSIONAL MODE)

39 AMPLITUDE AND VORTEX FREQUENCY FOR SQUARE SECTION (PLUNGING MODE)

40 C_p ON 2:1 RECTANGLE FOR VARIOUS α

41 C_p ON SQUARE CYLINDER FOR VARIOUS α

42 C_p ON 1:2 RECTANGLE FOR VARIOUS α

43 SECTIONAL LIFT COEFFICIENTS FOR RECTANGULAR CYLINDERS

44 SECTIONAL DRAG COEFFICIENTS FOR RECTANGULAR CYLINDERS

45 COMPARISON OF C_{Fv} FOR VARIOUS CYLINDER CROSS-SECTIONS

46 COMPARISON OF VELOCITY-AMPLITUDE CHARACTERISTICS

47 VARIATION OF STROUHAL NUMBER WITH DEPTH OF RECTANGLE

48 VARIATION OF WAKE WIDTH WITH DEPTH OF RECTANGLE

49 TYPICAL TIME-AMPLITUDE CURVE FOR 1" SQUARE SECTION (f_p = 8.9 cps)

50 NUMBER OF CYCLES TO MAXIMUM AMPLITUDE (SQUARE SECTION)

51 DYNAMIC RESPONSE -- GALLOPING

52 SPRING-MASS SYSTEM FOR ENERGY THEORY

53 AMPLITUDE RESPONSE FOR 1.0" SQUARE SECTION CYLINDERS

54 AMPLITUDE RESPONSE FOR 0.75" SQUARE SECTION CYLINDERS

55 AMPLITUDE RESPONSE FOR SEVERAL SQUARE SECTION CYLINDERS

56 AMPLITUDE RESPONSE FOR SQUARE SECTION CYLINDER FOR $\beta = 5^\circ$ & 9°

57 AMPLITUDE RESPONSE FOR D-SECTION SHOWING GALLOPING VIBRATION

ACKNOWLEDGMENT

The author wishes to acknowledge the advice and encouragement given by Dr. G.V. Parkinson who supervised the research. He also wishes to thank the Mechanical Engineering Department for the extensive use of the U.B.C. wind tunnel. Financial assistance was received from the National Research Council of Canada, Grant A-586.

SYMBOLS AND ABBREVIATIONS

A	Amplitude measured at the tips of the model
A_p	Reduced plunging amplitude $(A_p = A/h)$
A_t	Reduced torsional amplitude $(A_t = A/h)$
b	Streamwise dimension of rectangle
C_d	Sectional drag coefficient $(D/0.5\,\rho V_R^2 h)$ or $D/q_R h$
C_ℓ	Sectional lift coefficient $(L/0.5\,\rho V_R^2 h)$
C_D	Total drag coefficient $(D/0.5\,\rho V_R^2 h\ell)$
C_L	Total lift coefficient $(L/0.5\,\rho V_R^2 h\ell)$
C_{Fv}	Aerodynamic damping force coefficient $(F_v/0.5\,\rho V^2 h)$
C_p	Pressure coefficient $(p - p_\infty)/q_\infty$
C_{pw}	Wake pressure coefficient
D	Drag force
h	Characteristic width of model
f_a	Frequency of formation of vortices downstream of model -- cps
f_p	Natural frequency in plunging -- cps
f_t	Natural frequency in torsion -- cps
F_v	Aerodynamic damping force
ℓ	Length of model
ℓ_s	Distance between spring mounts $(\ell/\ell_s = 1.905$ for all models
L	Lift force
NR	Reynolds number (Vh/ν)
p	Pressure
p_∞	Static pressure far upstream
p_n	Static pressure drop across tunnel nozzle

$p_{t\infty}$	Total pressure far upstream of models
p_{tw}	Total pressure in wake
p_w	Static pressure in wake
q	Velocity pressure
q_∞	Velocity pressure far upstream
S	Strouhal's Number ($f_a h/V$)
t	Time
v	Velocity of vibrating model
V_∞	Fluid velocity far upstream of model
V_{nc}	Fluid velocity calculated from p_n, corrected for room temperature and barometric pressure
V_{cp}	Fluid critical velocity for plunging ($f_p h/S$)
V_{tp}	Fluid critical velocity for torsion ($f_t h/S$)
V_R	Fluid relative velocity
x	Streamwise position of model in wall opening
α	Angle of attack
β	Initial angle of attack
Δ	Area of wall opening upstream of model
Δ_o	Area of wall opening upstream of model when $A_p = 0.025$
δ	Wake width ($\delta = W/h$, where W = the distance between two points at which $p_{tw} = 0.95\ p_{t\infty}$)
Γ	Vortex strength
ν	Kinematic viscosity
ρ	Density
ω_p	Natural circular frequency in plunging (Rad/sec)
ω_t	Natural circular frequency in torsion (Rad/sec)
ξ	Distance between upstream surface and static holes of probe in wake

EXPERIMENTAL INVESTIGATION OF THE AEROELASTIC INSTABILITY OF BLUFF TWO-DIMENSIONAL CYLINDERS

INTRODUCTION

This work was done as part of a general program to study the aeroelastic instability of aerodynamically bluff cylinders. In all cases the cylinders tested were geometrically two-dimensional. Dynamic tests involving measurements of vortex formation and vibration amplitude were performed with elastically supported models having six degrees of freedom. Static tests provided data for the determination of the aerodynamic coefficients of various cross-sections.

Historical Background

The earliest mention we have of periodic vortex formation behind a bluff object was given by Leonardo da Vinci[1] in 1510. In an illustration of the flow downstream of a wall, he shows the vortices to be alternating in direction (which is incorrect) but more important, he shows their periodicity.

In 1907, Lanchester[2] gave an explanation for the "aerial tourbillion". This apparatus consists of a short length of D-section cylinder pivoted about its center point

and held in a uniform airstream incident on the flat face. If it is given an inital spin, the rotor will gain speed and auto-rotate. He reasons that there will be a force in the direction of rotation, if the flow re-attaches on the upstream edges of the rotor. The initial angular velocity required to cause autorotation will thus depend on the velocity of the free stream.

In 1911, Theodor von Karman[3] gave a mathematical analysis for the stability of straight, parallel vortex filaments arranged in two staggered rows. Only for one case in which the ratio of the distance between the two rows of vortices to the distance between successive vortices in the same row is 0.283, does stability exist. This arrangement is now known as the Karman vortex street. Experimental observation of such flows has verified von Karman's analysis, if the vortices have fairly definite cores. This pattern may be observed behind a circular cylinder below a Reynolds Number of 150. At higher Reynolds Numbers the vortices are still formed periodically but they tend to diffuserapidly.

The earliest systematic investigation of the vortical structure of wakes was done by A.Fage and F. Johannsen[4] in 1927. They studied the flow behind an inclined flat plate at several angles of attack, making measurements of the frequency and speed with which the individual vortices passed downstream, the dimensions of the vortex system, the average strength of the vortices, and the rate at which vorticity left the edges of the plate. This paper was extended by the

authors in 1928[5] to include work on cylinders of widely differing forms -- an aerofoil, a circular cylinder, and several wedges.

More recently, the vibration of bluff cylinders in a uniform airstream has attracted the attention of a large number of researchers, (see supplementary bibliography) due to the increasing importance of this phenomenon in industry, and also to the need to relate the potential theory which is applicable upstream of the body, to the statistical theories which are used to describe the completely turbulent flow far downstream.

Self-excited Vibrations in Industry

In industry, the self-excited vibration of bluff cylinders has caused many practical problems. The best known example is that of the Tacoma Narrows bridge[6]. This bridge was designed to withstand the static side thrust of a 200 mph wind, yet in 1940, six months after completion, it failed under the action of a steady 42 mph wind.

Another well-known example is the galloping of transmission lines. The usual description of the conditions necessary for the occurrence of this phenomenon is as follows:

a. There is a steady wind.

b. The temperature is close to freezing and the humidity is high.

c. There are ice formations on the wires which alter the aerodynamic characteristics of the wires.

A typical case is reported by the Shawinigan Power and Water Company:

700 ft. spans between 190 ft. towers in a 40 mph wind. The span vibrated at its natural frequency with a center span amplitude of 17 ft.

In all cases, the span has been observed to vibrate at one of its natural frequencies. These vibrations have been known to last for periods up to 24 hours, which eliminates the possibility of a forced vibration caused by the wind gusting at exactly the natural frequency of the system.

There have been many reports of the periodic oscillations of smokestacks as cantilevers, and "ovalling" of the cross-section at both subcritical and supercritical Reynolds' numbers.

Two other examples which have received attention are the vibration of aerial pipelines and submarine periscopes.

It is generally agreed that there are at least two types of vibration involved in these industrial manifestations. In the case of vibrating transmission lines, J.P.Den Hartog[7] differentiates between two forms; galloping and vortex resonance. He suggests that a system subject to galloping is unstable at any airspeed and that the vibration is characterised by large amplitudes and low frequencies. The other form, vortex resonance, produces small amplitudes and high frequencies.

This report will deal with tests of these effects performed on two-dimensional cylinders of several cross-sections, including semi-circular, circular, and a wide range of rectangles.

TEST FACILITIES AND APPARATUS

Wind Tunnel

All the tests described in this report were performed in the University of British Columbia low-speed, closed-circuit, single return wind tunnel (see Fig. 1). The test section is octagonal, formed by a 27 in. x 36 in. rectangle with 45° fillets, and is 9.0 ft. in length. The fillets decrease from 6.0 in. at the upstream end to 4.5 in. at the downstream end to offset the effect of boundary layer growth[8]. The flow is smoothed by three screens placed as shown, and enters the test section through a 7:1 contraction cone which accelerates the flow and improves its uniformity. In the test area, the spatial variation in velocity is approximately 0.25%, and the turbulence level[9] is less than 0.5% (see Fig. 2). The tunnel is capable of providing a steady flow indefinitely at an airspeed which may be varied continuously from 4.0 fps to 140 fps. Tests were performed within a Reynolds Number range of 4000 to 70,000.

Models Tested

All dynamic models tested were fabricated from balsa wood with a sanded finish smooth to the touch. The spring attachments were located as far apart as possible in order to obtain a flow about the center-span that was closely two-dimensional. Because of this consideration, together with the geometry of the test section, it was found

that there was coincidence between the natural frequencies of the two most important modes of vibration. To avoid this it was necessary to add a concentrated mass to the center-span of all the models tested. A typical example of a dynamic model is shown in Figure 3. Such a model weighed approximately 200 grams, 100 grams being located at mid-span.

In all cases, the dynamic models were freely mounted on four coil springs (Fig. 4) allowing six degrees of freedom. In general, only two modes of vibration were excited; a translational vibration perpendicular to the longitudinal axis of the model in a plane normal to the mean flow, and a torsional oscillation about the mid-span, also in a plane normal to the mean flow. Other modes that were excited on particular occasions were: torsion of the cross-section; torsion about a mid-span axis in a plane parallel to the flow (pitching); and translation parallel to the longitudinal axis (diving). The same set of springs was used for all the dynamic tests. These springs were closely matched, weighing 44.0, 44.0, 43.7, and 43.7 grams respectively, and having spring constants of 1.32 lbs/in. The springs were designed to have linear load-deflection characteristics for deflections up to nine inches. The initial extension varied between 4.0 and 4.5 inches. All dynamic models were 26.63 inches in length, allowing a clearance of 3/16 of an inch at either end. The cross-section and dimensions of all dynamic models are shown in Figure 5.

A series of static models of rectangular cross-section was used to study the variation of wake properties with the ratio b/h (see Fig. 6). These were of hardwood construction and were fitted in the test section with no end gaps.

Models used for the measurement of surface pressures were of two types. The first, a two inch diameter D-section cylinder (see Fig. 7), was made of hardwood with a brass central section. The brass section was hollow and fitted with pressure taps machined flush with the surface. There were twenty-five pressure taps 0.020 in. I.D. distributed around the section (see Fig. 8). On the inside of the brass section, the pressure taps were connected by 0.070 in. O.D. copper tubing to 0.100 in. O.D. polyethylene tubing which passed through the wooden sections to the outside of the test section. The second type was made of aluminum box section tubing. Mid-span sections of the aluminum were removed and replaced with brass sections similarly instrumented with pressure taps (see Figs. 9,10,11, & 12).

Both types of pressure model were mounted in the same manner (see Fig. 13) and kept as two-dimensional as possible. As shown the models pierced the roof and floor of the test section, and the hole was sealed with cardboard shields mounted flush with the inside surface. The mounting permitted the models to be adjusted to any angle of attack. Four cross-sections were tested in this manner; one D-section, and three rectangles (see Fig. 14).

Experimental Apparatus

For pressure measurement, two instruments were used. The first, a Betz micromanometer which could be read to ± 0.005 mm.w.g., was used as the tunnel speed gauge. The second, a Lambrecht inclined micromanometer, could be read to ± 0.01 millimeters of alcohol on the 1:5 scale, and ± 0.025 on the 1:2 scale. This instrument was used for all pressure measurements associated with the models.

A Flow Corporation CR3-B constant resistance-ratio hotwire anemometer was used for monitoring the large scale velocity fluctuations associated with the wakes of both stationary and vibrating models.

Used in conjunction with the anemometer were a Heathkit A.O.1 audio frequency oscillator modified to give frequencies down to 5 cps, and a Dumont type 350, 110 watt cathode ray oscillograph with continuously variable sweep frequency. The oscillator dial could be read to ± 0.2 cps at 25 cps and ± 1.0 cps at 60 cps.

An international Rectifier type B-17 selenium photovoltaic cell was used with a Heathkit model V-7A vacuum tube voltmeter and a Brush amplifier-chart recorder combination for time-amplitude studies. The voltmeter could be read to ± 0.005 volts.

The frequencies of vibration in dynamic tests were determined by visual observation using a strobolight. The scale of this instrument could be read to ± 5 cpm.

MEASUREMENT TECHNIQUES

Frequency of Vortex Formation

The frequency of vortex formation in the wake of both stationary and dynamic models was obtained by the method of Lissajous ellipses[10] (see Appendix A). A hot-wire probe was located approximately five inches downstream of the model and eight inches from the centerline of the wake (see Fig. 15). At this position a strong signal could be picked up from the passing vortices without the effect of the full spectrum of strong turbulence in the wake. This signal was amplified by the CR3-B anemometer and put across the vertical deflection plates of an oscilloscope. The horizontal sweep voltage of the oscilloscope was supplied by an audio frequency oscillator with continuously variable frequency. To obtain the predominant frequency of the signal from the hot-wire probe, the audio oscillator was tuned until a stable Lissajous ellipse appeared on the oscilloscope. The frequency of the oscillator signal was then the same as the frequency of vortex formation on one side of the model.

Vibration Amplitude

In the dynamic tests performed, two types of amplitude measurement were required. First, it was necessary to measure the maximum amplitude reached at a given airspeed. This was accomplished simply by visual observa-

tion of the model moving across a scale on the tunnel floor using a strobolight. Second, the transient amplitude build-up starting from rest at a given airspeed was required. To measure this, a slot was cut in the wall at one end of the model; a rigid strip of aluminum was attached to this end of the model and extended through the slot. A light cardboard shield was attached to this metal strip in such a manner that it just prevented the light from a 200w. D.C. source from falling on a selenium photovoltaic cell. When the model started vibrating, the card moved allowing light to fall on the cell. The cell was calibrated so that the vibration amplitude was proportional to the voltage output of the cell. This voltage was passed to a Brush amplifier-recorder system which provided a chart record of the amplitude build-up (see Fig. 16).

Aerodynamic Coefficients

Owing to the lack of a tunnel balance it was necessary to obtain lift and drag coefficients indirectly by the graphical integration of surface pressures. Although this method is tedious, less accurate, and not to be recommended when a balance is available, it did provide very useful information on the pressure distribution on the wake side of the models which would not otherwise have been obtained. The variation of this pressure distribution with angle of attack is shown later to have great importance with regard to the stability of the cylinder under observation. The type of model used for these tests is shown in Figure 10. Two steel rods were rigidly attached to the

model outside the test section. When the model was adjusted to a particular angle of attack, the rods were screwed directly to the panels of the test section, thus eliminating any possibility of model movement during a test. The method was simple to use and did not require any special fittings to accommodate the different cross-sections tested. In all cases, there were no end gaps and the system was kept as geometrically two-dimensional as possible.

Wake Width

The width of the wake at any point downstream of a model was defined as the cross-stream distance between two points at which the total head was ninety-five percent of the total head upstream of the model. The total head profile was taken by traversing a 0.125 in. diameter Pitot probe across the wake. The traversing mechanism could move the probe in accurate increments down to 0.01 in. The total head was measured on the 1:2 scale of a Lambrecht inclined manometer. Due to the large scale vortical flow in the wake, the reading from the probe was very unsteady. It was found that by inserting a choke with approximately 0.005 in. I.D. in the lead to the manometer, a fairly steady reading could be obtained.

CALIBRATION AND ACCURACY

Tunnel Speed

The Betz micromanometer used to measure the tunnel airspeed could be read to $\pm$ 0.005 mm.w.g. At the lowest velocity pressure (p_n = 0.11 mm.w.g.) there is a possible error of 5%. This error decreases as the airspeed increases. The corresponding error in velocity is then 2.5% for the worst case. The zero position was checked after each run. This instrument is provided with a ground glass screen on which the reading is projected so that parallax is prevented. All measurements of velocity pressure were referred to standard temperature (520°R) and pressure (29.92 in. hg.). Corrections due to the presence of the model in the tunnel are listed in Appendix B. These corrections were applied only when it was necessary to compare some test data with published data. In the case of a vibrating model, the corrections are not applied, since the vibration itself may be characteristic of the restrained flow.

The spatial variation of velocity in the test section has been found to be of the order of 0.25% -- a negligible amount. It was noted that the pressure field of the models extended upstream to the piezometer ring at the downstream end of the contraction cone. When a 2 in. D-section was mounted 24 inches downstream of the piezometer ring, the tunnel speed gauge gave a velocity which was 1.5% low. At

a distance of 29 in. the error was 1.1% and at 34 in. it was 0.25%. This correction was applied for all 2 in. models tested. For a 1.0 in. diameter model it is estimated that the upstream effect is approximately one fourth of that for the 2 inch model. This was neglected. Thus the possible error in velocity was less than 3.2% for a 1.0" model.

Strouhal Number

The variation in cross-section dimensions along the span was less than 3% for $h = 1$ inch, and less than 2% for 2 inch models. Curvature of the span between tangents at the extremities was less than one degree. The modified Heathkit audio oscillator was calibrated by passing the output to a Brush amplifier-recorder. The frequency of the oscillator signal was obtained directly from a chart record. This was done for a suitable range of frequencies and the results are presented in Figure 17. The scale could be read to $\pm$ 0.2 cps at 25 cps, and $\pm$ 2.0 cps at 60 cps -- the maximum possible error is 3.3% at 60 cps. As stated previously, the possible error in velocity is less than 3.2%. Assuming the worst condition for all variables at a velocity pressure of 4.0 mm.w.g., a model with $h = 1$ inch and $S = .13$ yields a maximum possible error in S of 10%. This is of course based on a single determination. Values of S obtained by taking a point from the average curve of shedding frequency against velocity should have a maximum error comparable to that encountered in measuring h. The error involved in deciding when the Lissajous ellipse becomes stationary is negligibly small. Cyclic movement at 0.02 cps

is clearly discernible, and would cause an error of approximately 0.2% for a typical measurement. The above estimate represents an upper limit for this error.

Vibration Amplitude

The measurement of the maximum amplitude at a given airspeed was accurate to $\pm$ .05 inch. Thus for a 2 inch amplitude the possible error was less than 2.5%.

For time-amplitude measurement, a photocell was used. The active surface of the cell was masked so as to give a voltage output proportional to the length of cell exposed.(see Fig. 18). This calibration was done with a Heathkit vacuum tube voltmeter which could be read to $\pm$ 5 m.v. The output from the photocell was passed to a Brush amplifier-recorder system. This recorder was calibrated and found to give a pen deflection which was directly proportional to the input voltage. Thus the amplitude of the trace on the recorder was proportional to the amplitude of vibration. The largest deviation from linearity in the photocell calibration is approximately 4.5%. The error involved in converting the chart amplitude to vibration amplitude could be as much as 20% for very small amplitudes and less than 10% for $A > 1/4$ inch. Figure 19 shows the approximate shape of the active surface of the photocell.

Lift and Drag Coefficients

The error involved in measuring the lift and drag coefficients was a combination of several possible errors.

(a) The error in positioning the model in the tunnel

(b) Neglect of the viscous shear forces

(c) Error in pressure measurement

(d) Error in graphical integration

(e) Error in measuring the upstream velocity.

(a) This error is difficult to isolate, and should be combined with any asymmetry of the basic tunnel flow. However, the experimental lift curves all pass through zero at $\alpha = 0$ suggesting that there is no asymmetry in the flow, and that the error in locating the model is small. The slopes of the drag curves at $\alpha = 0$ are close to zero, so that errors in positioning the model have little effect. These models were located to within $\pm$ 10 minutes of arc.

(b) When fluid flows over a surface a velocity gradient exists in the fluid next to the surface. A shear stress between the fluid and the surface also exists which is proportional to this velocity gradient. For all the dynamic tests the separation point occurs at the upstream edge with the exception of the circular cylinder. Because of this, the contribution of the shear to the drag is very small (Ref. 1, p. 3-12, Fig. 22), and the neglect of this contribution causes an error of less than 0.5%. This is within the accuracy of the measurement techniques.

(c) Here again, the percentage error varies with the pressure. However, there were a large number of pressure taps, at each of which several readings were taken. This would tend to average out any random errors.

(d) The error in graphically integrating the curves of

pressure coefficient versus model width was less than $\pm$ 1%.

(e) All pressure tests were done at 63.0 fps. The error involved for that speed, with $h = 2$ inches, is less than $\pm$ 1.0%. Since it is the slope near $\alpha = 0$ rather than the ordinate of the lift curve that is important we can consider the error in taking the slope between $\alpha = 0$ & $\alpha = 3$ degrees. For the lift, (b) causes a negligible error at small α and (c) is assumed to be zero. Including the effects of (a), (d), and (e), we get errors of $\pm$ 0.5%, $\pm$ 1.0%, and $\pm$ 1.0% respectively, a total of $\pm$ 2.5%. For the drag, (a) is small, and (c) is again taken to be zero. For (b), (d), and (e) we get -0.5%, $\pm$ 1.0%, and $\pm$ 1.0% respectively, or a maximum error of -2.5%. The standard wind tunnel corrections (Appendix B) are applied only for purposes of comparison with published data.

Measurement of Wake Width

To obtain the wake width, a total head tube was traversed across the wake and a continuous profile was obtained. The definition of the wake width was arbitrary and the actual values of total head were unimportant. Thus any errors would be found in the traversing mechanism and in the model diameters. The main element of the traversing mechanism was a 1/2" x 20 screw thread. No error was found in this. For this particular measurement, the model width h was accurate to within $\pm$ 1%.

Two-Dimensionality of Tests

In the "Two-Dimensional" pressure tests, the models were supported outside the tunnel so that geometrically they were two-dimensional. The pressure taps were located within one inch on either side of mid-span. In the case of the D-section and square cylinders, tests with the measuring sections located 3.0 inches from the walls gave the same results as the mid-span tests. This, together with the fact that the force coefficients obtained from integrating the surface pressures agreed closely with published results, indicated that the flow also was two-dimensional.

In the dynamic tests it was very difficult to obtain two-dimensional conditions. It was decided that mounting the model with springs inside the tunnel and a 3/16 inch gap at either end had less effect on the two-dimensionality of the flow than mounting the springs on the outside and allowing the model to pass through holes large enough to permit the vibration amplitudes encountered. Dynamic tests with end gaps of 1/4 in., 1/2 in., and 3/4 in. showed no appreciable change in the amplitude at a given velocity, whereas allowing the model to extend through a 6.0 in. diameter hole produced a completely different set of vibration characteristics.

Structural Damping

In all the dynamic tests the structural damping

was kept constant in that the same springs and mounts were used throughout. The damping was measured by obtaining the time-amplitude decay of a flat plate of comparable mass in still air (Fig.20). It should be noted that at large amplitudes the spring forces became large enough to cause the tunnel walls to vibrate appreciably. This effect would make the actual damping greater than the measured value for the higher airspeeds and would tend to reduce the amplitude reached at a given airspeed. It is also noted that as the airspeed increases the vibration caused by the tunnel fan increases. Since the dynamic tests were performed at relatively low airspeeds, this effect should be small.

REVIEW OF CURRENT THEORIES

Den Hartog's "Negative Slope" Theory[7]

This theory considers an elastically mounted cylindrical body with negative aerodynamic damping; i.e. the cross-sectional shape of the cylinder is such that, if the body is moving downward in the presence of a steady wind, it will experience a downward force due to the wind. Den Hartog expresses this condition for instability in a simple relationship between the steady state lift and drag coefficients for the cross-section (see Appendix C). He shows that if $(dC_\ell/d\alpha)_{\alpha=0} + C_{do} < 0$, then the cross-section will be unstable. Thus a cross-section which satisfies this criterion should be unstable at all airspeeds. The lowest airspeed at which vibration will occur should depend only on the structural damping, and the amplitude of vibration should depend on the air velocity; i.e., a maximum amplitude for a given air velocity should be reached when the net input of energy per cycle from the wind is just equal to the energy dissipated by structural damping. Cross-sections which do not satisfy this criterion should be aerodynamically stable. It should be noted that it has yet to be proved that the steady state aerodynamic coefficients can be used to replace the instantaneous dynamic coefficients.

Parkinson[11] has obtained a solution for the non-linear differential equation of motion that results from

Den Hartog's criterion when the steady state aerodynamic coefficients are expressed as polynomial functions. His results for a square section cylinder are presented later on.

D.B. Steinman[12] has put forward a theory which also makes use of the steady state aerodynamic coefficients. He also disregards any effect of vortex formation other than the fact that the aerodynamic coefficients are influenced by the time-average of the vortex induced pressures. This theory was developed to predict the vibration characteristics of a wide section, such as a bridge deck, but can be applied to any aeroelastic system.

The Vortex Theory

When fluid flows past a bluff cylindrical object separation occurs and two shear layers are formed. These surfaces of discontinuity are extremely unstable and break up to form large vortices centered approximately on the shear layers. It was observed by Strouhal[13] that the frequency f at which the vortices are formed on each side is directly proportional to the fluid velocity V_∞ and inversely proportional to the cylinder diameter h. This relation was expressed by Strouhal in the form of a dimensionless parameter, the Strouhal Number

$$S = fh/V_\infty \tag{1}$$

Upstream of the cylinder the flow is assumed to be ir-

rotational, so that when a vortex is formed in the wake, then, in accordance with Helmholtz' Laws[14], circulation of opposite direction is set up about the cylinder. The interaction of this circulation with the mean flow causes a force to act on the body in a direction normal to the flow (Kutta-Joukowski[14]). This vortex induced force will alternate at the frequency of vortex formation. The vortex theory attributes the aerodynamic excitation of an elastically mounted cylinder to the action of this periodic force having a certain degree of resonance with one of the natural modes of vibration of the system. If the lowest natural frequency of the system is f_p, then the system should start vibrating near a critical velocity V_{cp} where

$$V_{cp} = f_p h/S \tag{2}$$

Once the vibration has started it controls the frequency of formation of the vortices so that two vortices are formed every cycle. In this way the vibration remains in a condition of resonance over a range of airspeeds. As the airspeed is increased, the vortices grow stronger and the amplitude increases, until finally the vibration loses control of the vortex action and dies down. At this point the frequency is again determined by the velocity, the Strouhal number, and the diameter. Vibration will reappear at the next critical velocity.

This theory indicates that elastically mounted

cylinders of any cross-section should be excited within certain ranges of airspeed if the damping is not too high. Here the amplitude of vibration will depend on both the structural and aerodynamic damping, the shape of the cross-section, and the air velocity. There should also be ranges of airspeed in which such systems are not excited.

Flutter

The flutter type of aerodynamic excitation differs from those mentioned previously in that two degrees of freedom are excited simultaneously instead of just one. Usually this takes the form of a transverse vibration coupled with twisting of the cross-section. Generally, because the exciting forces are not small compared to the elastic and inertia forces, the two natural frequencies will differ from those measured in still air. Since the aerodynamic forces vary with the wind speed, so will the natural frequencies and a critical speed can be reached at which they coincide. When this occurs the result will be a very rapid buildup to large amplitudes.

TEST RESULTS

D-Section -- Open Holes at Ends

Preliminary dynamic testing was performed on a 2" D-section cylinder piercing the floor and roof through 6.5 inch circular holes and suspended on four coil springs placed outside the tunnel. It was noted for a given airspeed that the resulting amplitude of vibration in the plunging mode was a function of the streamwise position of the model in the hole. Because of the awkward geometry of the circular hole, it was decided to investigate this variation further by using rectangular openings. The model was tested with 8" x 10" openings and the same effect was observed. Some degree of correlation was obtained between the two cases by plotting the amplitude of vibration versus the ratio Δ/Δ_o, where Δ is the area of the opening upstream of the model and Δ_o is the area upstream of the model when the reduced amplitude A_p is 0.025. The results are shown in Figure 21. Both sets of data plot on a single curve. The aeroelastic behaviour over a wide range of airspeeds is shown in Figure 22. Three modes of vibration were observed: plunging, a translational vibration perpendicular to the longitudinal axis of the model and in a plane normal to the mean flow; diving, a translational vibration parallel to the longitudinal axis; and pitching, a torsional vibration about a mid-span axis in a plane

parallel to the flow. Below 62.0 fps, and for any position in the hole, the plunging mode occurs. At higher airspeeds, both pitching and diving modes occur. This wide range of airspeeds over which plunging occurred suggests that the D-section shows instability of the "galloping" type. However, at an airspeed of 66.0 fps, plunging occurred at X = 9.875 inches but not at X = 8.50 inches. This suggests that Den Hartog's instability criterion (Appendix C) for this section should be a function of the hole position at this particular airspeed, i.e.:

at X = 9.875 inches

$$(dC_{F_V}/d\alpha)_{\alpha=0} < 0 \tag{3}$$

and at X = 8.5 inches

$$(dC_{F_V}/d\alpha)_{\alpha=0} > 0 \tag{4}$$

In order to check this, a static model was constructed and instrumented to measure surface pressures. The pressure coefficient C_p was measured at the mid-span for both positions in the hole (see Figs. 23, 24). Both showed the same C_p variation on the upstream face and constant wake pressures with respect to the chord, the value being slightly lower for X = 9.875 inches. The sectional lift and drag coefficients (see Fig. 25) were obtained by graphical integration and the aerodynamic damping force coefficient C_{F_V} was calculated. It was found for both cases that $(dC_{F_V}/d\alpha)_{\alpha=0} = 0$ within the accuracy of the measurement techniques. Thus Den Hartog's criterion

cannot be applied here. It is shown (Appendix E) that the damping force coefficient C_{F_V} is exactly zero if the wake pressure is constant or symmetrical with respect to the chord for $\alpha \geqslant 0^\circ$. The lift and drag coefficients obtained were approximately 30% lower than values quoted by Cheers[15]. This was due to the outflow through the end holes from points upstream of the model, and the inflow to the wake downstream of the model. Because of the obvious effect of the holes on the elastic behaviour of the system, it was decided to eliminate the holes, to place the springs in the airstream (as close to the ends as possible) and to allow only a small gap at the ends of the model. It was felt that the effect of the springs on the flow would be small compared to that of the holes.

Two-Dimensional D-Section

Pressure tests were performed on a 2" D-section at various angles of attack with the end holes completely sealed. A check, with the measuring section three inches from the floor, showed that the flow was two-dimensional. Typical C_p distributions are shown in Figures 26, 27. The upstream variation at $\alpha = 0^\circ$ shows good agreement with that of a flat plate given by Fage[4]. The wake pressure at $\alpha = 0^\circ$ is no longer constant but is still symmetrical with respect to the chord. This symmetry in the wake persists up to $\alpha = 25^\circ$ while the stagnation point upstream moves toward the leading edge. At $\alpha = 35^\circ$ the wake pressure has become noticeably asymmetric, and at 40° there

is a sudden rise in the level of the wake pressure and a suction peak forms downstream of the leading edge, indicating that the flow has re-attached.

The sectional lift and drag coefficients were obtained again by graphical integration and are shown in Figures 28 and 29. The lift curve, uncorrected for wind tunnel effects, shows values of lift approximately 13% higher than those presented by Cheers[15] for $0 < \alpha < 35^{\circ}$. However, Cheers data reaches a peak at $\alpha = 40^{\circ}$ which was not found in the present test. The data corrected for wind tunnel effects show better agreement with Cheers' data over most of the range. It should be noted that small end holes were permitted in the tests done by Cheers which would have the effect of reducing the slope of the lift curve. The other curve presented is that of $-C_d \tan\alpha$. It is shown in Appendix E that if the wake pressure is symmetrical with respect to the chord for $\alpha = 0^{\circ}$, then

$$C_{\ell} = -C_d \tan\alpha \tag{5}$$

This curve follows the experimental lift data very closely up to 25°, the angle of attack at which the wake pressure becomes asymmetric. Thus for the two-dimensional D-section $(dC_{Fv}/d\alpha)_{0<\alpha<25^{\circ}} = 0$, i.e., Den Hartog's criterion is not satisfied, and the D-section should not gallop when released from rest. Cheers[15] finds that the D-section is initially stable, and Harris[16] finds that it is unstable. The drag (Fig. 29) is also found to be higher than that

given by Cheers.

A static pressure traverse along the center line of the wake shows a gradual increase in suction to a maximum at approximately 1.25 diameters downstream of the flat face (see Fig. 30). These data were obtained by placing a static probe in the wake parallel to the flow. Because of the vortical cross flow, the pressure level read is lower than the actual value. The readings are adjusted by a constant factor to the pressure at the cylinder surface obtained from previous tests and show a distribution which is similar to that obtained by Roshko[17] for the circular cylinder. However, Roshko's results for a flat plate show the point of vortex formation to be approximately 2.0 diameters downstream. It is noted that the pressure at the surface of the plate is higher than that obtained for the D-section. This suggests that Roshko's tests may have been performed with small end gaps which would have increased the pressure and which may also have affected the point of vortex formation. To check this, the wake traverse was repeated for the D-section cylinder with the 8" x 10" holes open. It was found that there was only a slight decrease in pressure to a minimum at approximately 2.75 diameters downstream of the flat face, and that the general pressure level was much higher than for the two-dimensional case. If the holes at the ends of the model are open, the inflow to the wake tends to suppress the pressure gradient along the wake in that the maximum

inflow is directed toward the point of minimum pressure. It is suggested that the suction peak in the wake close to the afterbody of the D-section causes the surface pressure profile to achieve a minimum for the two-dimensional case, whereas the surface pressure for the 'open-end' case is not affected in this way and the profile is flat (see Figs. 23, 26).

In the dynamic tests on the two-dimensional D-section only two modes of vibration were excited; (a) a translational oscillation perpendicular to the longitudinal axis of the model and in a plane normal to the flow, hereafter referred to as 'plunging', and (b) a torsional oscillation about the mid-span also in a plane normal to the flow and hereafter referred to as 'torsion'. The model tested had the following characteristics:

Diameter - 2.0 ins.

Natural frequency in plunging - 8.5 cps

Natural frequency in torsion - 10.35 cps

Weight - 283 gms.

The dynamic response for this D-section at $\beta = 0^{o}$, where β is the initial angle of attack of the section, is shown in Figures 31 and 32. Two sets of data are presented - the ratio of amplitude to diameter and the ratio of the frequency of formation of vortices downstream of one edge of the model to the natural frequencies in plunging and torsion. The abscissa is the ratio of the upstream velocity to the "critical" velocity, where V_{cp} and V_{ct}

are defined as follows:

$$V_{cp} = f_p h/S \tag{6}$$

$$V_{ct} = f_t h/S \tag{7}$$

where h is the diameter, S the Strouhal number, and f_p and f_t the two natural frequencies.

The dynamic response may be described as follows:

a) If the model is restrained at an airspeed at which it is known to plunge, the frequency of vortex formation will be determined by the Strouhal number.

b) When it is released, plunging oscillation begins and gradually builds up. It requires no initial amplitude.

c) At an amplitude estimated at $A_p = 0.15$, the vortex frequency changes abruptly to the plunging natural frequency.

d) The rate of build-up increases and a maximum amplitude is reached.

e) If the vibration is stopped, the frequency reverts to the Strouhal frequency.

The control of the vortex frequency will be referred to as "capture". For the model tests, vibration began at $V_{nc}/V_{cp} = 0.54$ with capture occurring at one half the natural frequency. This continued to $V_{nc}/V_{cp} = 0.71$ at which speed the captured vortex frequency jumped between $0.5\ f_p$ and f_p. From $V_{nc}/V_{cp} = 0.71$ to 1.07, A_p increased to a maximum, and capture was maintained at f_p. Be-

yond 1.07 a mixture of plunging and torsion occurred. Both the torsional and plunging reduced amplitudes are defined as the ratio of the tip amplitude A to the model width h. In order to provide a basis for comparing the two amplitudes, one can consider the potential energy stored at maximum amplitude for both cases. If this is done we find that the torsional amplitude involving the same potential energy as the plunging amplitude A_p is given by

$$A_t = \frac{\ell}{\ell_s} A_p \tag{8}$$

where ℓ is the length of the model and ℓ_s is the distance between spring mounts. For all dynamic tests performed $\frac{\ell_s}{\ell} = 0.525$. At $V_{nc}/V_{ct} = 0.95$ pure torsion occurred accompanied by capture at f_t. A maximum amplitude was reached at $V_{nc}/V_{ct} = 1.05$ above which the amplitude decayed rapidly until at $V_{nc}/V_{ct} = 1.2$ there was no vibration. Below $V_{nc}/V_{cp} = 0.54$, and above $V_{nc}/V_{ct} = 1.2$, the only motion observed was a random buffeting and if the model was released from an initial displacement the vibration would steadily die out.

Dynamic tests were next performed on a two inch D-section for a wide range of β (see Fig. 33). The vibration characteristics obtained were similar to those for the model initially at $\beta = 0$, except that the maximum amplitudes decreased steadily with increasing β until at $\beta = 40^\circ$ no vibration occurred. The instability criterion,

$dC_{Fv}/d\alpha$ is presented for different values of β (Fig. 34). It is noted that for $\beta = 0^{o}$ a high positive value of $dC_{Fv}/d\alpha$ occurs at $\alpha = 42^{o}$. This peak moves as β varies until $dC_{Fv}/d\alpha > 0$ at $\alpha = 0$. This explains why the amplitudes decrease with increasing β. Since the relative angle of attack α depends on the maximum amplitude, and the maximum relative angle of attack is limited by the onset of high positive damping, then as β increases the maximum possible α decreases and hence the maximum amplitude decreases.

The Strouhal numbers for the D-section held stationary at different β show good correlation by the Fage and Johannsen method (Fig. 35). The average value given by

$$S_{ave} = f_a(h\mathrm{Cos}\beta)/V_{nc} \tag{9}$$

is 0.135. This value is comparable to values for a flat plate[5,17].

Circular Cylinder

It is shown in Appendix D by quasi-steady theory that the aerodynamic damping coefficient for a body moving transverse to a uniform stream may be written as follows:

$$C_{Fv} = (C_L + C_D\mathrm{Tan}\,\alpha)\mathrm{Sec}\,\alpha \tag{10}$$

For the circular cylinder, C_L is always zero and C_D is always positive, i.e.:

$$C_{Fv} = C_D \tan\alpha \sec\alpha \tag{11}$$

$$\therefore \quad dC_{Fv}/d\alpha = (2\tan^2\alpha + 1)\sec\alpha\, C_D + \tan\alpha \sec\alpha\, dC_D/d\alpha$$

For small values of α ,

$$dC_{Fv}/d\alpha = C_D \tag{12}$$

Thus, the circular cylinder has positive aerodynamic damping and should therefore be subject only to vortex excitation close to resonance. A circular cylinder with the following characteristics was tested dynamically:

Diameter - 1.9 inches

Natural frequency in plunging - 8.40 cps

Natural frequency in torsion - 10.15 cps

Weight - 280 gms

The dynamic response curves in plunging and torsion are presented in Figure 36. The amplitude curves are similar to those obtained for the D-section cylinder in that vibration occurs only within a limited range of airspeed that includes the critical velocities V_{cp} and V_{ct}. However, the range of airspeeds for plunging is smaller and for torsion is larger. The plunging mode starts at $V_{nc} = 0.86V_{cp}$ and reaches a maximum at $V_{nc} = 1.12\ V_{cp}$. The torsional mode starts at $V_{nc} = 1.12\ V_{ct}$ and extends to $V_{nc} = 1.65\ V_{ct}$ with the maximum amplitude occurring at $V_{nc} = 1.20\ V_{ct}$. Unlike the D-section, the circular cylinder shows only fundamental resonance with the formation of vortices. As before, capture of the vortex frequency occurs

at both f_p and f_t. Between $V_{nc} = 1.15\ V_{cp}$ and $V_{nc} = 1.10\ V_{ct}$ a combination of plunging and torsion occurs. This is not a "flutter" type vibration but occurs because the two natural frequencies are quite close to one another. For a given airspeed vortices are formed at a wide range of frequencies with one fundamental frequency dominating the spectrum. When the airspeed is such that this fundamental frequency falls approximately midway between the two natural frequencies of the model, both modes are excited and a mixed vibration occurs in which one of the natural frequencies predominates. A small speed change either way usually serves to eliminate one or other of the modes from the mixture. The amplitude curve for torsion shows a much wider range than the D-section. This test was repeated on four occasions using models of different mass and wider separation of natural frequency. In each case, the amplitude curve for torsion showed the same characteristics. The reason for the extended range is not understood. The amplitudes for the circular cylinder are not as large as those for the D-section. It is suggested that because of its clearly defined separation point, the D-section will have better span-wise correlation of vortex formation than the circular cylinder. This, together with the fact that the circular cylinder has positive aerodynamic damping from $\alpha = 0$, indicates that the D-section should have a larger amplitude.

Reversed D-Section

A dynamic test was performed on the D-section model with the curved surface upstream. No motion other than random buffeting was observed over a range of airspeeds from $V_\infty = 0$ to 50 fps. This section appears to be completely stable.

Two-Dimensional Rectangular Section

Dynamic tests were performed on a wide range of rectangular cylinders varying from b/h = 0.38 to 2.48 where "b" is the streamwise dimension and "h" is the width. Pressure tests were performed on models with the dimensions b/h = 2.0, 1.0, and 0.5, and the lift, drag, and aerodynamic damping force coefficients were obtained as before by graphical integration of the pressure coefficient. Wake width and vortex frequency measurements were also made for a series of static models in the range of b/h = 0.38 to 4.45.

In the series of dynamic tests, two"types" of vibration were observed -- true galloping and vortex induced. Curves of amplitude in the plunging mode for all sections tested dynamically are shown in Figure 37. Ratios of b/h from 0.375 to 0.683 showed characteristics that are similar to those obtained for the D-section cylinder. From b/h = 0.75 to 2.01 a new behaviour was observed in that the amplitude of vibration in plunging was found to increase almost linearly with the airspeed. At b/h = 2.48,

this behaviour was observed at higher airspeeds but was preceded by the occurrence of the usual torsional mode and two other torsional modes, one, twisting of the cross-section about an axis passing approximately through the quarter-chord point, and the other, with the axis passing through the mid-point of the section. The second, occurring at a higher airspeed than the first, was the more violent of the two modes. No measurements were made but the angular double amplitudes reached in the second mode were of the order of 40°. Another noticeable difference is that this curve is widely separated from the others. This is due to a large difference in the Strouhal number between b/h = 2.01 and 2.48. This phenomenon will be discussed elsewhere.

Some of the models which showed the galloping type of plunging instability also had a range of airspeed in which the usual torsional mode occurred. This range included V_{ct} in all cases. It should also be noted that the speed at which plunging first occurred was close to the critical velocity V_{cp}. The humps in the curves may originate from a certain degree of vortex resonance at double and four times the natural frequency.

The torsional mode for b/h = 0.375 to 0.683 is presented in Figure 38. As b/h decreases, the range of velocities over which torsion occurs also decreases, and the value of V_{nc}/V_{ct} at which the maximum amplitude occurs approaches 1.0. At small values of b/h the shape of

the amplitude curve is similar to that of the D-section.

A typical example of the galloping type of vibration is shown in Figure 39. In all cases the frequency of vortex formation was measured and it was found that during vibration capture occurred at f_p.

Pressure tests were next performed in order to correlate the aerodynamic characteristics of the cross-sections with the observed dynamic behaviour. Models chosen were b/h = 2.0, 1.0, and 0.5.

For b/h = 2.0 measurements of C_p were taken every 2° from $\alpha = 0^o$ to $\alpha = 10^o$. A comparison of the profiles at various α's is given in Figure 40. At $\alpha = 0^o$ the wake pressure is symmetrical with two suction peaks at the corners c and d. At $\alpha = 2^o$, the suction along the side bc remains constant but along da it decreases -- a noticeable asymmetry. This asymmetry increases steadily with increasing angle of attack. For b/h = 1.0 the pressure in the wake behaves in the same way. At $\alpha = 0^o$ it is symmetrical and at $\alpha = 2^o$ an asymmetry has developed which increases with α (Fig. 41). For b/h = 0.5 there is a noticeable difference in the variation of the wake pressure with α (Fig. 42). At $\alpha = 0^o$ it is symmetrical and remains so to 4° where a slight asymmetry develops. The main variation with increasing α is a general increase in the level of the suction. Any asymmetry is very small compared to that encountered with b/h = 2.0 or 1.0.

From the above measurements, lift and drag coefficients were obtained (Figs. 43, 44). The curves for the three sections differ considerably. The lift curve for b/h = 2.0 reaches a maximum negative value and the drag curve a minimum value at $\alpha = 7^{\circ}$. The drag coefficient at $\alpha = 0^{\circ}$ is the smallest of the three. This is reasonable since it is also the most slender rectangle of the three. For b/h = 1.0 the lift and drag curves reach a maximum and minimum at $\alpha = 14^{\circ}$ and $\alpha = 13^{\circ}$ respectively. The test data give curves which are somewhat higher than those presented by Cowdrey and Lawes[18]. However the test data have not been corrected for wind tunnel effects which would lower the ordinates by approximately 5%. For b/h = 0.5 the drag is the highest of the three cases and remains nearly constant at 2.4 to $\alpha = 10^{\circ}$. This value of drag is comparable to that of the D-section at $\alpha = 0^{\circ}$. The lift curve has the smallest slope and increases linearly with α.

The aerodynamic damping force coefficients for the three sections were calculated from the lift and drag data and are presented in Figure 45 for comparison with the coefficients for the D-section and the circular cylinder. The rectangles b/h = 2.0 and 1.0 show strong negative damping; the rectangle b/h = 0.5 and the D-section show zero damping; and the circular section is positively damped. The test curves show good agreement with those calculated from data presented in Refs. 15 and 18. In

Figure 46, the amplitude characteristics for these sections are compared and their behaviour agrees with what would be predicted from the damping curves. (The curve for b/h = 2.0 is shown more completely in Fig. 37).

Dynamic tests were performed on a rectangle, b/h = 1.0 at initial angles of attack $\beta = 5^{\circ}$ and $\beta = 9^{\circ}$. The shape of the amplitude curves was closely similar to that of $\beta = 0^{\circ}$ but the average slope decreased as β increased.

A series of static tests was made on rectangles varying from b/h = 0.38 to b/h = 4.45 to measure the variation of Strouhal number with b/h (Fig. 47). At the same time corresponding measurements of wake width were made at a distance of 7h downstream of the upstream surface of the model (Fig. 48). It was observed that as b/h increased from 0.385 to approximately 2.4 the frequency of vortex formation (f_a) decreased for a given velocity and the Strouhal number (S) decreased from 0.139 to 0.055. Between b/h = 2.4 and 3.0 a sharp increase occurred in f_a and S increased to 0.16. Thereafter, to b/h = 4.45, there was a slow and steady decrease in S to 0.122. The wake width δ also decreases with increasing b/h. At b/h = 0.38, $\delta = 5.5$ and at b/h = 2.9, $\delta = 3.5$. From b/h = 2.9 to 4.45, δ remains approximately constant. There is no abrupt change in δ corresponding to the rise in S between b/h = 2.4 and 3.

Measurements of the time-amplitude response were made on the square section cylinder. Figure 49 shows the response curve at $V_{nc} = 4.74\ V_{cp}$ and indicates that the model will achieve its maximum amplitude approximately 250 cycles after being released from rest. The shape of this curve is similar for all airspeeds but the time to maximum amplitude varies with V_{nc}/V_{cp}. Similar measurements were made on a square section cylinder for which the structural damping was increased approximately by a factor of four. The effect of this was to shift the velocity at which the vibration initiates to a higher value (Fig. 39). The time required to reach maximum amplitude at various airspeeds was measured for the two levels of structural damping (Fig. 50). The curve for the more highly damped case is displaced to the right of the other and tends to infinity for $V_{nc} = 3.8\ V_{cp}$. The other curve shows the same trend but at $V_{nc} = 2\ V_{cp}$ the number of cycles required to build up to maximum amplitude begins to decrease and the lowest value reached is approximately 80 cycles at $V_{nc} = 1.2\ V_{cp}$.

DISCUSSION OF RESULTS

D-Section Cylinder

It is noted in the case of the D-section passing through holes in the roof and floor that a form of galloping occurs. $(dC_{F_V}/d\alpha)_{\alpha=0}$ was measured for the midspan and found to be exactly zero. However, there were strong end flows and $(dC_{F_V}/d\alpha)_{\alpha=0}$ for the whole model may have been negative. It was not possible to measure this because the pressure taps were not all in the same horizontal plane and the spanwise pressure gradient was large. In a similar way the desk model D-section proposed by Den Hartog may satisfy the galloping criterion. The fact that $dF/d\alpha$ becomes negative at $\alpha = 25^{\circ}$ agrees with the observed fact that Lanchester's tourbillion[2] does auto-rotate if given a substantial initial spin.

During vibration the D-section appears to move in a plane normal to the flow. If the cross-section twists about the longitudinal axis it does so with an amplitude that is not discernible; i.e., less than one half of one degree. It is felt that the observed vibrations are "pure" plunging or torsion, and not a flutter type combination. This is borne out by the fact that the systems always vibrate at their natural frequencies over the entire range of airspeed. As the pressure tests suggest, the response is

not of the "galloping" type but rather a form of extended resonance with the vortex formation. Capture at 0.5 f_p corresponds to resonance with the first harmonic, and at f_p and f_t to fundamental resonance. Resonance with the first harmonic is difficult to reconcile with the physical picture since it implies that a vortex is formed every second cycle. It is thought that during capture at f_p, one vortex is formed just after the model reaches the maximum amplitude, thus inducing an equal and opposite circulation about the model and causing a force to act on it in the direction of the motion.

For the D-section, the aerodynamic damping is zero up to $\alpha = 25^\circ$. For $25^\circ < \alpha < 40^\circ$ it is negative and for $\alpha > 40^\circ$ it becomes positive. It appears then that the dynamic response is initially a result of vortex excitation over the range of zero aerodynamic damping; a combination of vortex and negative damping excitation from $25^\circ < \alpha < 40^\circ$; and finally a balance between vortex excitation, structural damping and positive aerodynamic damping for some value of α greater than 40°. When the system reaches a steady state, the maximum relative angle of attack (ϵ) that is reached during a cycle is given by

$$\tan \epsilon = A_{max} \omega_p / V \tag{13}$$

where A_{max} is the maximum amplitude reached at the airspeed V. Since the aerodynamic forces increase with increasing velocity, the relative effect of structural damp-

ing will decrease. Because of this the angle ϵ will depend on the velocity but will gradually lose this dependence as the airspeed increases. It can be seen from Figure 34 that ϵ will decrease as β increases. The variation of maximum amplitudes in plunging for different values of β agrees qualitatively with the curves of $dC_{Fv}/d\alpha$ versus α, the stability of the section at $\beta = 40^{\circ}$ resulting from the high positive damping which occurs for small α (Figs. 33, 34).

It should be pointed out at this time that the possibility of galloping vibration does exist for the D-section. In all the dynamic tests mentioned the model was released from rest at the given airspeed. It was found that the range of velocities for the plunging mode could be extended by approximately 15% if the airspeed was increased continuously and the vibration was not started from rest for each airspeed. However, in all cases, as the airspeed increased, mixed vibration occurred when the torsional mode was excited. It is suggested that if f_t had been less than f_p then the vibration range could have been extended indefinitely because the D-section does have negative aerodynamic damping for $25^{\circ} < \alpha < 40^{\circ}$. Previously, tests at higher velocities failed to show any excitation of the section even when given substantial initial amplitudes. It is suggested that the initial amplitudes were insufficient to produce the required relative angle of attack of 25° for negative damping to occur, and

that the initial energy input was simply dissipated by the structural damping. In order to check for galloping a test was performed on a D-section with the suspension modified to make $f_p > f_t$. The characteristics of the section tested were as follows:

$$h = 2 \text{ inches}$$
$$f_p = 8.75 \text{ cps}$$
$$f_t = 3.33 \text{ cps}$$

In this test, two sets of amplitude data were taken:

a) the vibration was allowed to build up continuously with increasing velocity,

b) the model was initially at rest for each airspeed as in all other dynamic tests.

Both sets of data give the same amplitude curve (Fig. 57) except that for case b, the vibration would not build up for $V_{nc}/V_{cp} > 1.02$. This agrees with the result obtained in the previous test, as does the speed at which plunging first starts, i.e. close to $0.5\ V_{cp}$. It is noted that the amplitudes are considerably larger for a given value of V_{nc}/V_{cp} (Fig. 31). In the present test the spring constant of the elastic system and the mass of the model were less than in the previous test, however f_p was approximately the same. With the lighter system, less energy was transferred to the tunnel than in the previous test in which the vibration of the tunnel walls, caused by the greater spring forces, became appreciable at the larger amplitudes. It is felt that the difference in amplitudes observed in the two tests is attributable to this.

Circular Cylinder

The circular cylinder has positive aerodynamic damping and is subject only to fundamental resonance with the formation of vortices in its wake. The dynamic response is typical of a resonance phenomenon, and differs from the D-section in that it is excited over a smaller range of airspeeds and the amplitude curve shows a more localized peak.

Reversed D-Section

This section showed no instability at any airspeed including $V_{nc} = V_{cp}$ and V_{ct}. It is expected that all elastic structures which shed vortices in a steady airstream should show some excitation when the frequency of vortex formation approaches a natural frequency of the structure. However, there are two reasons why the reversed D-section would tend to be stable. First, the aerodynamic damping is high and positive. Like the circular cylinder, C_L is zero for $\alpha = \pm 20^{\circ}$, thus

$$C_{Fv} = C_D \tan\alpha \sec\alpha \tag{14}$$

and for small α

$$dC_{Fv}/d\alpha = C_D = 1.15 \quad \text{(Cheers}^{15}\text{)}$$

Second, the reversed D-section, unlike any other section tested, has no afterbody extending into the wake. Since the point of vortex formation is determined by the point

of flow separation, the reversed D-section will be relatively further from the point of vortex formation and from the entire vortex street than any section with an afterbody. This effect may be sufficient to reduce the exciting force to a level that is insufficient to overcome the structural and aerodynamic damping.

The Rectangular Cylinder

The rectangular cylinder shows both galloping and vortex-induced vibration. For small values of b/h the wake pressure remains symmetrical with respect to the chord for $\alpha \geqslant 0$, and consequently the aerodynamic damping is exactly zero for a wide range of α. For larger values of b/h the wake pressure becomes asymmetric at small α and the damping becomes negative. However, as b/h increases, the angle at which the aerodynamic damping becomes positive decreases and hence the plunging amplitude at a given airspeed decreases. A similar effect was noticed in tests on a square section cylinder at various initial angles of attack β. As β is increased, the range of α over which negative damping occurs decreases, and the possible amplitude at a given airspeed also decreases. All the amplitude curves (Fig.37) appear to start close to the critical velocity. This is a characteristic of the galloping type of vibration[19]. The airspeed at which vibration will start usually depends on the structural damping, but below a certain level the starting speed becomes independent of the damping and

remains fixed at the critical velocity V_{cp}. For the particular level of damping the vibration is started by vortex resonance and at a slightly higher airspeed it combines with galloping. As the airspeed increases the initial vortex effect decreases, and the vibration tends toward pure galloping. For an elastic system with greater structural damping (Figs. 38, 39) the curves for $b/h < 0.68$ would be grouped about $V_{nc} = V_{cp}$ as before. For $b/h > 0.75$ vortex induced plunging would also occur at $V_{nc} = V_{cp}$, but this would not change to galloping. It would die out as V_{nc} increases until finally at a sufficiently high V_{nc} the galloping type of vibration would start.

For $b/h > 2.5$ the rectangle starts to behave like a flat plate. The natural frequency of torsion of the cross-section decreases and exposes that mode of vibration to vortex excitation within the range of airspeeds used. It should be noted that these torsional modes were pure and there was no suggestion of a flutter type combination with plunging, and no variation of frequency with airspeed.

When the rectangular cylinder was galloping, capture occurred at speeds up to $V_{nc} = 7\ V_{cp}$, the highest used in these tests. It will therefore be necessary to include the effects of vortex formation in any theory that will describe the motion completely.

Roshko[17] has proposed a wake Strouhal number S^* defined by

$$S^* = nd'/U_s$$

where n is the vortex frequency, d' is the distance between the two shear layers, and U_s is velocity at the edge of the wake. He proposes that S^* should have a constant value for all bluff bodies. In his paper he refers to tests done on a circular cylinder with a splitter plate in the wake. As the splitter plate is moved downstream, it forces the vortices to form further from the cylinder base. The result of this is to decrease the vortex frequency n, and the velocity U_s, and increase the wake width d', and to maintain a roughly constant S^*. As the distance between the splitter plate and the cylinder is increased, a point is reached at which the vortices suddenly start forming upstream of the splitter plate. When this occurs the effect of the plate on the flow is substantially reduced. The frequency, velocity, and wake width abruptly return to values which are close to the original ones and S^* is maintained. A similar phenomenon may occur with the rectangular cylinder. In terms of the test variables, S^* is defined as

$$S^* = f_a \delta h/kV_{nc} \tag{16}$$

where $k = \sqrt{1 - C_{pw}}$ and C_{pw} is the pressure coefficient on the downstream surface of the cylinder. Now as b/h increases, f_a decreases, and C_{pw} becomes less negative, causing k to decrease. However, unlike Roshko's case, δ also decreases, and so does S^*. Values of S^* for

b/h = 0.5, 1.0, and 2.0 are 0.47, 0.46, and 0.28 respectively.

Between b/h = 2.4 and 3.0, f_a suddenly increases. It is suggested that this change is caused by the shift in the point of vortex formation from downstream of the trailing edge to a point between the leading and trailing edges, similar to the shift encountered with the circular cylinder and splitter plate. It should be mentioned while referring to Roshko's work that the mathematical models proposed by himself and Kirchhoff[20] would show no dynamic instability other than vortex excitation in that the wake pressure is considered to be constant, i.e.: $dC_{F_V}/d\alpha = 0$.

Observations of the time required for the vibration to build up at a given airspeed show clearly the effect of vortex excitation and structural damping on galloping (Fig. 50). The test with increased structural damping is not influenced by vortex excitation other than the capture which occurs after galloping has started. As V_{nc} decreases toward the speed at which galloping starts, the time to maximum amplitude approaches infinity. However, for the lightly damped case, the speed at which galloping starts coincides with the region of maximum vortex excitation, Thus as V_{nc} decreases, the time to build-up increases until it comes under the influence of the vortex excitation, after which it decreases rapidly as V_{nc} approaches V_{cp}.

The slope of the time amplitude curve (Fig. 49) is of interest because of the abrupt manner in which it decreases near the maximum amplitude. It is suggested that this corresponds to the sudden onset of high positive damping when a certain value of α is reached. This value of α can be determined by obtaining an energy balance for a limit cycle of the vibration; i.e., the net energy transferred from the airstream to the elastic structure should be exactly equal to the energy dissipated by the structural damping. An approximate energy balance is presented.

Approximate Theory for Galloping

For a given α, the aerodynamic damping force, F_V, is directly proportional to the square of the airspeed V and the structural damping is taken to be constant over the range of airspeeds considered. If the system is lightly damped, then at high airspeeds the aerodynamic damping forces will be much greater than the structural damping forces and the latter can be neglected. In the analysis given here, the structural damping is assumed to be negligibly small. This assumption obviously will not be valid at low airspeeds, and agreement is not expected.

During galloping, it is found that the phenomenon of capture occurs. This periodic vortex formation will have some effect on the maximum amplitude reached at a given airspeed. The strength (Γ) of the individual vortices formed will vary directly with the airspeed,

and inversely with the frequency of formation. During capture, the frequency of formation is fixed at the natural frequency of the system, and therefore Γ will depend only on the velocity V_∞. The Kutta Jowkowski Law[14] gives the force on a body with circulation Γ in a uniform airstream of velocity V_∞,

$$P = \rho V \Gamma \tag{17}$$

Assuming that Helmholtz' Laws apply in this case, the force on a model due to vortex excitation will be

$$P \propto \rho V^2 \tag{18}$$

Thus both the vortex excitation and the negative damping excitation vary with V^2 and should therefore remain in a constant ratio to one another.

Since we are neglecting both structural damping and vortex excitation, the vibration will build up from rest until the relative angle of attack reaches the angle ϵ defined by equation 13. Since the structural damping is taken to be zero, ϵ is independent of V and therefore the amplitude will be directly proportional to V.

Thus the analysis presented here should give a velocity-amplitude curve as shown in Figure 51. It is to be expected in the experimental case that the structural damping will prevent vibration until a certain minimum velocity is reached at which velocity the aerodynamic damping forces become comparable to the structural damping

forces. The broken line represents the amplitude response if the vortex excitation due to capture is included, and is also the asymptote to which the experimental curve will tend. The position of this line relative to the line representing aerodynamic damping only will depend on the natural frequency in two ways. First, a system with large f_p should show less effect of vortex excitation than one for which f_p is small, and second, the quasi-steady theory is less applicable if f_p is large.

Consider a spring-mass system placed in a uniform horizontal airstream as shown (Fig. 52). The mass M is assumed to be perfectly elastic.

By definition $$C_{F_V}(\alpha) = F_V(\alpha,V)/0.5\,\rho V^2 h$$

where $F_V(\alpha,V)$ is obtained from wind tunnel tests.
If A = the maximum amplitude reached at velocity V
and $\omega = \sqrt{k/M}$
then $$y = A\sin\omega t \tag{19}$$

Considering a limit cycle, the net energy transfer over each cycle will be zero.

i.e., $$\oint C_{F_V}(\alpha)dy = 0 \tag{20}$$

Let $\omega t = \theta$

Then $$\int_0^{\pi} C_{F_V}(\alpha)A\cos\theta d\theta = 0 \tag{21}$$

Now $$\alpha = \arctan \dot{y}/V = \arctan(A\omega\cos\theta)/V$$

Differentiating we get,

$$- \operatorname{Sin}\theta d\theta = (V/A\omega)(\operatorname{Sec}^2\alpha\, d\alpha)$$

Substituting

$$\tan\theta = \sqrt{(1/\operatorname{Cos}^2\theta) - 1}$$

we get, $$\operatorname{Cos}\theta d\theta = \frac{- V\operatorname{Sec}^2\alpha\, d\alpha}{A\omega\sqrt{(A\omega/V)^2\operatorname{Cot}^2\alpha - 1}}$$

i.e., $$\int_{-\epsilon}^{\epsilon} \frac{C_{F_V}(\alpha)\operatorname{Sec}^2\alpha\, d\alpha}{\sqrt{(A\omega/V)^2\operatorname{Cot}^2 \quad - 1}} = 0 \qquad (22)$$

Where $\alpha = \epsilon$ when $\theta = 0$

and $\alpha = -\epsilon$ when $\theta = \pi$

For a body that is symmetrical with respect to the air-stream, the integration can be performed over a quarter cycle i.e., from 0 to ϵ. Integrating by parts and writing the trigonometric function as $P(\alpha)$ we get

$$\int_0^{\epsilon} C_{F_V}(\alpha)P(\alpha)d\alpha = C_{F_V}(\alpha)\Big]_0^{\epsilon}\int_0^{\epsilon}P(\alpha)d\alpha - \int_0^{\epsilon}\left(\int P(\alpha)d\alpha\right)\left(\frac{dC_{F_V}(\alpha)}{d\alpha}\right)d\alpha$$

or, $$\int_0^{\epsilon} C_{F_V}P d\alpha = C_{F_V}(\alpha)\Big]_0^{\epsilon}\int_0^{\epsilon}\frac{\operatorname{Sec}^2\alpha\, d\alpha}{\sqrt{(\operatorname{Tan}\epsilon\operatorname{Cot}\alpha)^2 - 1}}$$

$$- \int_0^{\epsilon}\left(\int\frac{\operatorname{Sec}^2\alpha\, d\alpha}{\sqrt{(\operatorname{Tan}\epsilon\operatorname{Cot}\alpha)^2 - 1}}\right)\left(\frac{dC_{f_V}}{d\alpha}\right)d\alpha \qquad (23)$$

Consider $\displaystyle\int \frac{\mathrm{Sec}^2\alpha\, d\alpha}{\sqrt{(\mathrm{Tan}\epsilon\mathrm{Cot}\alpha)^2 - 1}}$

Let $\mathrm{Cot}\epsilon = k$ and $\mathrm{Cot}\alpha = x$

The integral becomes

$$-\int \frac{k\,dx}{x^2\sqrt{x^2 - k^2}} = -\sqrt{1/k^2 - 1/x^2}$$

Changing back to α and ϵ,

$$\int_0^{\epsilon} P(\alpha)d\alpha = -\mathrm{Tan}\epsilon\left(\sqrt{1 - (\mathrm{Cot}\epsilon\mathrm{Tan}\alpha)^2}\right)\Big]_0^{\epsilon} \qquad (24)$$

Substituting (24) in (23), we obtain

$$\int_0^{\epsilon} (dC_{Fv}/d\alpha)\left(\sqrt{1-(\mathrm{Cot}\alpha\mathrm{Tan}\alpha)^2}\right)d\alpha + C_{Fv}(0) = 0 \qquad (25)$$

Equation (25) is general and may be applied to a body of any cross-section that is symmetrically disposed with respect to the airstream. For the square cylinder at $\beta = 0$, $C_{Fv}(0) = 0$ and equation (25) is satisfied by $\epsilon = 19^\circ$ and $\epsilon = 0^\circ$. $\epsilon = 0^\circ$ is the unstable initial condition and $\epsilon = 19^\circ$ the stable maximum. Thus when the vibration reaches a limit cycle,

$$A = V\mathrm{Tan}\epsilon/\omega = 0.344V/\omega \qquad (26)$$

with A in feet

V in feet/second

ω in radians/second

It can be seen from equation (26) that the amplitude is

completely independent of the size of the vibrating mass.

Velocity-amplitude curves were obtained experimentally for the following square sections at $\beta = 0^{o}$.

1.00" x 1.00"	ω = 42.4 rad/sec.
1.00" x 1.00"	ω = 56.0 rad/sec.
0.75" x 0.75"	ω = 52.4 rad/sec.
0.75" x 0.75"	ω = 70.1 rad/sec.

The data are compared with the theory and are found to give very good agreement at the higher velocities (Figs.53,54). This may be interpreted in two ways. First the vortex excitation may be very small compared to that of the negative damping. Second, the structural damping may still be having an effect on the amplitude, i.e., at higher velocities the experimental curve may cross the theoretical curve. It is interesting to note that the system with the highest natural frequency shows the largest deviation from the theory. The lack of dependence of the amplitude on the size of the model is emphasized by plotting A versus V/ω for all the models tested (Fig.55).

If equation (22) is integrated between $\pm\epsilon$, the second term in equation (25) drops out, and we get;

$$\int_{-\epsilon}^{\epsilon} (dC_{F_V}/d\alpha)(\sqrt{1 - (\mathrm{Cot}\epsilon\,\mathrm{Tan}\alpha)^2})d\alpha = 0 \qquad (27)$$

Applying equation (27) to the square initially at 5° and 9°, it is found to be satisfied by $\epsilon = 15.2^{o}$ and $\epsilon = 9.0^{o}$

respectively. These values were substituted in equation (26) and the curves are compared with experimental data (Fig. 56). For the airspeeds covered, the theoretical curve gives larger amplitudes for both values of β. This is possibly due to the fact that as β increases the energy involved in negative aerodynamic damping at a given airspeed decreases and the effects of the structural damping will be noticeable to higher velocities. If (25) is applied to the D-section, it is satisfied by $\epsilon = 56^{\circ}$. Thus for $V_{cp} = 10.8$ fps, $\omega_p = 55$ rad/sec, and $h = 2$ inches, equation (13) gives $A_p = 1.75\ V_{nc}/V_{cp}$. This curve is compared with the experimental response for the galloping D-section (Fig. 57) and shows very good agreement.

General Discussion

For all the models tested, regardless of cross-section, the observed vibrations were restricted to a single plane normal to the flow, except at high velocities when the streamwise deflection of the model due to the drag force became appreciable. In all cases, the wind induced vibrations occurred at frequencies which corresponded to the natural frequencies obtained in still air. Mixed torsion and plunging did occur but only when the frequency of the vortex formation was halfway between the two natural frequencies. It is felt that flutter is not the mechanism governing the observed vibrations.

The test results supported to a certain extent

the vortex theory for the excitation of bluff cylinders. The D-section, the circular cylinder, and the short rectangles ($b/h < 0.683$), showed amplitude responses when released from rest which are similar, and characteristic of a resonance phenomenon. The circular cylinder, which has positive aerodynamic damping for $\alpha > 0^{\circ}$, showed a more localized peak than the other two sections, but all three are found to vibrate within a limited speed range which includes the critical velocity. However, the reversed D-section, the D-section initially at 40°, and the long rectangle ($b/h > 0.75$) showed characteristics which are not in agreement with the vortex theory. The reversed D-section is apparently quite stable for two reasons. First, it has positive aerodynamic damping, and second, it has no afterbody extending into the wake. The D-section at $\beta > 40^{\circ}$ is also unaffected by vortex resonance, apparently because of very high positive aerodynamic damping. On the other hand, the long rectangles were found to vibrate at any airspeed above a certain minimum value. This behaviour is characteristic of the galloping type of vibration and lends support to Den Hartog's theory of instability.

If Den Hartog's criterion is applied to all the sections tested, the following result is obtained:

a.	D-Section $\beta = 0^{\circ}$	Neutral i.e. $dC_{Fv}/d\alpha = 0$
b.	Reverse D-section	Stable
c.	D-section with $\beta = 40^{\circ}$	Stable
d.	Circular cylinder	Stable

e. Short rectangles ($b/h < 0.683$) Neutral, $dC_{F_V}/d\alpha = 0$

f. Long rectangles ($b/h > 0.75$) Unstable

Thus the theory is valid in that none of the sections from "a" to "e" shows galloping behaviour when released from rest whereas "f" does. However, the theory does not explain the large amplitude oscillations obtained for "a", "d", and "e".

The galloping theory has been applied by Parkinson[11] to a square section cylinder with the same physical characteristics as one of those tested. The results of his analysis are compared with the experimental amplitude response curves (Figs. 39, 53) with the time-amplitude curve (Fig. 49) and with the time to maximum amplitude curves (Fig. 50). The theoretical results show good agreement with all the main features of the dynamic response of this section. His analysis includes the effect of structural damping and gives good quantitative agreement with the shift in starting speed for increased damping. The slope of the asymptote to his curve was calculated and found to agree with the curve given by the energy balance, indicating that the polynomial approximations that he used for the aerodynamic coefficients were appropriate. The ordinates of his curve are also slightly lower than the experimental values at the higher velocities. This could be attributable to the effect of vortex capture which was not accounted for in his analysis.

The sections which showed limited instability did so over a range of airspeeds which in all cases included the critical velocity V_{cp}. It therefore seems unlikely that the dynamic response of these sections could be predicted by Steinman's theory since he does not consider the effect of vortex formation. It appears necessary that any theory that will account for aerodynamic excitation in general will have to use a combination of both negative aerodynamic damping and vortex excitation.

In the physical phenomenon, both effects are observed in every case, During galloping, capture occurs, and the energy involved in vortex formation becomes available to the vibration. Similarly, the maximum amplitude that is reached during a vortex type vibration is largely governed by the angle of attack at which the aerodynamic damping becomes strongly positive. Again, the lift and drag coefficients from which the damping force is calculated are dependent on the wake pressure distribution, which in turn depends on the time average of vortex induced pressures.

The ideal theory must be able to account for the two effects separately, (as in the case of the more heavily damped square section), in combination near the critical velocity, or a combination of capture and galloping. It must be able to predict the dynamic response of the following types of cross-sections:

a. Stable

   i. No afterbody and positive aerodynamic damping, i.e., the reversed D-section.

   ii. Very high positive aerodynamic damping, i.e., the D-section initially at $\beta = 45^{\circ}$.

b. Unstable over limited speed range

   i. Small but positive aerodynamic damping, i.e., the circular cylinder.

   ii. Zero aerodynamic damping for wide range of α, i.e., the D-section cylinder when released from rest.

c. Unstable

   i. Negative aerodynamic damping for small α i.e., the rectangles with $b/h > 0.75$.

   ii. Zero aerodynamic damping for small α, followed by a range of α with negative aerodynamic damping, i.e., the D-section when given a sufficiently large initial amplitude.

CONCLUSIONS

Tests performed on a D-section cylinder which pierced the tunnel walls through large openings showed that the aeroelastic response of such a system has a strong dependence on the end effects. This particular model showed plunging vibration over a wide range of airspeeds. No amplitude measurements were made, but the lack of dependence of the instability on airspeed indicated some form of excitation other than vortex resonance.

The two-dimensional D-section was tested and found to have zero aerodynamic damping for $0 < \alpha < 25^{\circ}$, negative damping for $25^{\circ} < \alpha < 40^{\circ}$, and positive damping for $\alpha > 40^{\circ}$. Near the critical velocity it is subject to a combination of vortex and negative damping excitation. If the model is initially at rest, the D-section shows instability over a limited range of airspeed. If the model is not brought to rest between changes in airspeed, or if it is given a sufficiently large initial amplitude, a D-section system with low structural damping is found to vibrate at any airspeed with an amplitude which is approximately proportional to the airspeed.

During vibration of any form, capture occurs when an amplitude of approximately 0.15h is reached. This phenomenon persists to any airspeed if the vibration is maintained, and should be accounted for in any theory which

will fully describe the galloping type of vibration.

Den Hartog's criterion, which defines the nature of the aerodynamic damping, predicts correctly whether or not a cross-section will show galloping instability. From the experimental results obtained, it would appear that the instantaneous dynamic force coefficients effective during vibration are adequately approximated by the steady state coefficients obtained in static pressure tests. Any deviation from the static values would necessarily include the effect of capture. An energy balance which neglected structural damping and vortex excitation, yielded amplitude curves for the square section and the galloping D-section which were in close agreement with the experimental values at the higher velocities.

It was shown that cross-sections with a flat face upstream and a wake pressure distribution that remains symmetrical with respect to the chord for $\alpha \geqslant 0$ have zero aerodynamic damping, and lift and drag coefficients which are directly related so long as the wake symmetry persists, i.e.:

$$C_\ell = -C_d \tan \alpha$$

The D-section and the short rectangles ($b/h < 0.683$) were found to be of this type. The long rectangles ($b/h > 0.75$) developed an asymmetry at small α which resulted in negative aerodynamic damping and galloping response. It is

felt that this is caused by the effect of the afterbody on the point of vortex formation which was found to be approximately 1.25 diameters downstream of the separation edges for a D-section.

There is a steady decrease in amplitude with increasing β for the square section at a given airspeed. There is a corresponding decrease in the angle at which the aerodynamic damping force becomes positive. It was shown that the two variations are related. A similar variation was observed for the rectangular sections with increasing b/h.

Wake measurements behind a series of static rectangular models show a steady decrease in S as b/h increases. At b/h = 2.5, there is a sudden increase in S. Observations in the smoke tunnel have supported the suggestion that the sudden jump is caused by the point of vortex formation shifting from downstream of the trailing edge, to a point between the trailing and leading edges.

Increasing the non-aerodynamic damping for a square section was found to increase the velocity at which galloping started and also to separate the vortex resonance effect from the galloping. The effect of the critical velocity on galloping was demonstrated by observation of the time required for the system to reach maximum amplitude at various airspeeds. For the high damping case the time required near the speed at which the vibration starts is very

large. For the low damping case, the starting speed coincides with the critical velocity and the additional excitation due to vortex resonance results in a much shorter time to build-up. It is felt that for high velocities, the effects of the non-aerodynamic damping will die out.

In conclusion, it is recommended that some of the following tests be performed:

1) Measurement of C_L and C_D for a square section cylinder with a splitter plate in the wake. The plate inhibits the formation of vortices close to the cylinder and the test would show whether or not the vortex induced pressures cause asymmetry of the wake pressure with .
2) Measurement of amplitude for a square section cylinder over a full range of β. Comparison with amplitude calculated from an energy balance would serve as a check on the accuracy involved in using the steady state coefficients in the dynamic problem.
3) Measurement of amplitude for a square section cylinder with increased damping at high velocities to observe whether or not the effect of the damping dies out.
4) Measurement of C_{Fv} at larger values of α for the short rectangles to check for negative damping. Also dynamic tests at higher velocities and large initial amplitudes to check for galloping instability.

5) Measurement of spanwise correlation of vortex formation for both stationary and vibrating models of all cross-sections.

6) Measurement of wake geometry and stability while stationary and during vibration. Smoke tunnel tests indicate rapid diffusion of the vortices downstream of the model for NR = 1500 to 8000.

Finally, it is suggested that in future dynamic tests, smaller, lighter models should be used together with lighter springs in order to reduce the vibration of the tunnel walls as much as possible.

APPENDIX A

Use of the Lissajous Ellipse for the Determination of the Frequency of an Unknown Signal

Let $u = a\mathrm{Cos}(2\pi nt - q)$ be a signal of unknown frequency n, and let $v = b\mathrm{Cos}2\pi n't$ be a signal of known frequency;

Assume $n = n'$, and let $2\pi nt = p$

Then $$u = a\mathrm{Cos}(p - q) \tag{1}$$

and $$v = b\mathrm{Cos}p \tag{2}$$

Expanding (1) $$u = a(\mathrm{Cos}p\mathrm{Cos}q + \mathrm{Sin}p\mathrm{Sin}q) \tag{3}$$

Squaring (2) and (3) and adding,

$$(u/a)^2 + (v/b)^2 = \mathrm{Cos}^2p\mathrm{Cos}^2q + 2\mathrm{Sin}p\mathrm{Sin}q(\mathrm{Cos}p\mathrm{Cos}q) + \mathrm{Sin}^2p\mathrm{Sin}^2q + \mathrm{Cos}^2p$$

Now, $$(2uv\mathrm{Cos}q)/ab = 2\mathrm{Cos}^2p\mathrm{Cos}^2q + 2\mathrm{Sin}p\mathrm{Sin}q(\mathrm{Cos}p\mathrm{Cos}q)$$

$$\therefore\ (u/a)^2 + (v/b)^2 = \mathrm{Cos}^2p - \mathrm{Cos}^2p\mathrm{Cos}^2q + \mathrm{Sin}^2p\mathrm{Sin}^2q + (2uv\mathrm{Cos}q)/ab$$

$$= \mathrm{Cos}^2p(1 - \mathrm{Cos}^2q) + \mathrm{Sin}^2p\mathrm{Sin}^2q + (2uv\mathrm{Cos}q)/ab$$

$$= \mathrm{Sin}^2q(\mathrm{Cos}^2p + \mathrm{Sin}^2p) + (2uv\mathrm{Cos}q)/ab$$

$$= \mathrm{Sin}^2q + (2uv\mathrm{Cos}q)/ab$$

$$\therefore\ (u/a)^2 + (v/b)^2 - (2uv\mathrm{Cos}q)/ab - \mathrm{Sin}^2q = 0 \tag{4}$$

Eqn.(4) is the equations of an ellipse whose major and minor axes depend on the amplitude of the signals u and v, and on the phase difference q.

If the signals u and v are put across the horizontal and vertical input plates of an oscilloscope, the frequency of the signal u can be determined by varying the frequency of the known signal v, until a stable Lissajous ellipse appears on the screen. The frequency of the known input will then be exactly equal to that of the unknown signal.

APPENDIX B

Wind Tunnel Corrections

There are only two wind tunnel corrections which are applicable to the bluff cylinders tested; solid blocking and wake blocking.

Solid Blocking.

$$\sigma_{sb} = 0.333\,\lambda(\pi h/2a)^2$$

where h = model width

a = tunnel width

λ = a parameter which depends on a/chord.

Wake Blocking.

$$\sigma_{wb} = 0.25cC_D/a$$

where c = chord of model

If $\sigma = \sigma_{sb} + \sigma_{wb}$,

then

$$V_\infty = V_T(1 + \sigma)$$

$$C_{L\infty} = C_{LT}(1 - 2\sigma)$$

$$C_{D\infty} = C_{DT}(1 - 2\sigma)$$

The subscript 'T' denotes a wind tunnel measurement.

MODEL	CORRECTIONS			
	σ	V_∞/V_T	$C_{L\infty}/C_{LT}$	$C_{D\infty}/C_{DT}$
2" D-Section	0.0185	1.018	0.963	0.963
2" Circular Cylinder	0.0191	1.019	0.962	0.962
2"x1" Rectangle (b/h = 2)	0.0229	1.023	0.955	0.955
2"x2" Rectangle (b/h = 1)	0.0342	1.034	0.932	0.932
1"x2" Rectangle (b/h = 0.5)	0.0185	1.018	0.963	0.963

APPENDIX C

The Den Hartog Instability Criterion

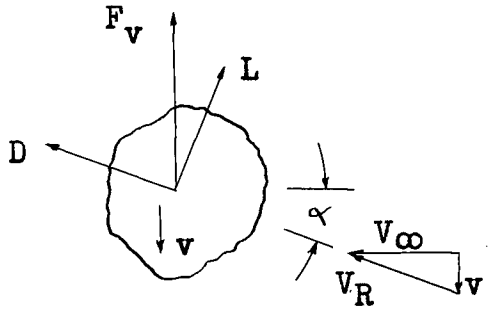

Forces and angles are positive as shown

Consider a body moving downward as shown with a velocity v, in the presence of a steady, uniform airstream of velocity V_∞. Let V_R be the relative velocity at an angle α to the horizontal.

Then, $$V_R = V_\infty - v \tag{1}$$

and, $$\alpha = \mathrm{Arctan}(v/V_\infty) \tag{2}$$

The total upward damping force due to air pressure is given by,

$$F_v = D\mathrm{Sin}\alpha + L\mathrm{Cos}\alpha \tag{3}$$

If $dF_v/d\alpha$ is negative, then the upward wind force, F_v, increases for negative $d\alpha$ and decreases for positive $d\alpha$, i.e., the aerodynamic damping is negative.

Setting $dF_v/d\alpha < 0$, we get,

$$(dL/d\alpha + D)\mathrm{Cos}\alpha + (dD/d\alpha - L)\mathrm{Sin}\alpha < 0 \tag{4}$$

Considering the initial instability of a stationary body, or one moving such that v is small compared to V_∞, we

can set $\alpha = 0$,

then, $$(dL/d\alpha + D) < 0$$

or, $$(dC_L/d\alpha + C_D) < 0 \qquad (5)$$

Thus the body is unstable if " the negative slope of the lift curve is greater than the ordinate of the drag." However as the vibration builds up, α increases, and the sign of the aerodynamic damping will be decided by equation (4).

APPENDIX D

Definition of Force Coefficients

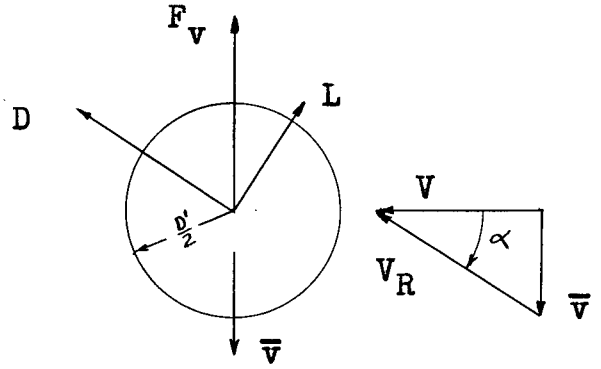

Forces and velocities are positive as shown.

$$V = V_R \cos\alpha$$

$$F_v = L\cos\alpha + D\sin\alpha$$

$$C_L = L/(0.5\rho V_R^2 D')$$

$$C_D = D/(0.5\rho V_R^2 D')$$

$$C_{Fv} = F_v/(0.5\rho V^2 D') = F_v/(0.5\rho V_R^2 D')\cos^2\alpha$$

or,

$$C_{Fv} = (C_L + C_D \tan\alpha)\sec\alpha$$

APPENDIX E

Aerodynamic Coefficients for the D-Section Cylinder

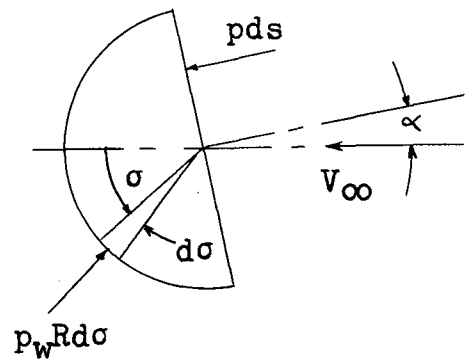

Diameter = 2R

By definition,

$$C_\ell = L/2Rq_\infty$$

$$C_d = D/2Rq_\infty$$

From the diagram,

$$L = -\int_0^{2R} pds\,\mathrm{Sin}\alpha + \int_{-(\pi/2-\alpha)}^{(\pi/2+\alpha)} p_w R\,\mathrm{Sin}\sigma d\sigma \tag{1}$$

$$D = \int_0^{2R} pds\,\mathrm{Cos}\alpha - \int_{-(\pi/2-\alpha)}^{(\pi/2+\alpha)} p_w R\,\mathrm{Cos}\sigma d\sigma \tag{2}$$

$$\therefore \quad C_\ell = -\frac{\mathrm{Sin}\alpha}{2Rq_\infty}\int_0^{2R} pds + \frac{1}{2q_\infty}\int_{-(\pi/2-\alpha)}^{(\pi/2+\alpha)} p_w \mathrm{Sin}\sigma d\sigma \tag{3}$$

and,

$$C_d = \frac{\mathrm{Cos}\alpha}{2Rq_\infty}\int_0^{2R} pds - \frac{1}{2q_\infty}\int_{-(\pi/2-\alpha)}^{(\pi/2+\alpha)} p_w \mathrm{Cos}\sigma d\sigma \tag{4}$$

Now let $p_w = (P + n(\alpha,\sigma))$, where P is a constant.

Then,

$$C_\ell = -\frac{\sin\alpha}{2Rq_\infty}\int_0^{2R} p\,ds + \frac{P}{2q_\infty}\int_{-(\pi/2-\alpha)}^{(\pi/2+\alpha)} \sin\sigma\,d\sigma$$

$$+ \frac{1}{2q_\infty}\int_{-(\pi/2-\alpha)}^{(\pi/2+\alpha)} n(\alpha,\sigma)\sin\sigma\,d\sigma \qquad (5)$$

Now,

$$\int_{-(\pi/2-\alpha)}^{(\pi/2+\alpha)} \sin\sigma\,d\sigma = 2\sin\alpha$$

$$\therefore\ C_\ell = -\frac{\sin\alpha}{2Rq_\infty}\int_0^{2R} p\,ds + \frac{P\sin\alpha}{q_\infty} + \frac{1}{2q_\infty}\int_{-(\pi/2-\alpha)}^{(\pi/2+\alpha)} n(\alpha,\sigma)\sin\sigma\,d\sigma \qquad (6)$$

Let $\frac{1}{2q_\infty R}\int_0^{2R} p\,ds - P/q_\infty = \tilde{C}_p(\alpha)$, and let $\frac{n(\alpha,\sigma)}{2q_\infty} = Z(\alpha,\sigma)$

Then

$$C_\ell = -\tilde{C}_p(\alpha)\sin\alpha + \int_{-(\pi/2-\alpha)}^{(\pi/2+\alpha)} Z(\alpha,\sigma)\sin\sigma\,d\sigma \qquad (7)$$

and

$$C_d = C_p(\tilde{\alpha})\cos\alpha + \int_{-(\pi/2-\alpha)}^{(\pi/2+\alpha)} Z(\alpha,\sigma)\cos\sigma\,d\sigma \qquad (8)$$

If we assume that the pressure $Z(\alpha\sigma)$ remains symmetrical with respect to the chord, then $Z(\alpha\sigma)$ is an even function and it can be expanded as a Fourrier cosine series in $(\alpha + \sigma)$

i.e.

$$Z(\alpha\sigma) = \sum_{n=o}^{\infty} A_n \mathrm{Cos}n(\alpha + \sigma) \tag{9}$$

Let $$(\alpha + \sigma) = \beta$$

Then

$$C_\ell = -\widetilde{C}_p(\alpha)\mathrm{Sin}\alpha + \int_{-\pi/2}^{\pi/2} \sum_{n=o}^{\infty} A_n \mathrm{Cos}n\beta \mathrm{Sin}(\beta - \alpha)d\beta \tag{10}$$

and,

$$C_d = \widetilde{C}_p(\alpha)\mathrm{Cos}\alpha - \int_{-\pi/2}^{\pi/2} \sum_{n=o}^{\infty} A_n \mathrm{Cos}n\beta \mathrm{Cos}(\beta - \alpha)d\beta \tag{11}$$

Or,

$$C_\ell = -\widetilde{C}_p(\alpha)\mathrm{Sin}\alpha + \sum_{n=o}^{\infty} A_n \int_{-\pi/2}^{\pi/2} \mathrm{Cos}n\beta \mathrm{Sin}(\beta - \alpha)d\beta \tag{12}$$

Now

$$\int_{-\pi/2}^{\pi/2} \mathrm{Cos}n\beta \mathrm{Sin}(\beta - \alpha)d\beta = 2\left(\frac{(-1)^{n/2}}{n^2 - 1}\right)\mathrm{Sin}\alpha + \pi/2(\mathrm{Sin}\alpha)$$

$(n \neq 1)$

$$\therefore \quad C_\ell = \left\{-\widetilde{C}_p + A_1\pi/2 + \sum_{n=o,2,..}^{\infty} A_n 2\left(\frac{(-1)^{n/2}}{n^2 - 1}\right)\right\} \mathrm{Sin}\alpha \tag{13}$$

Similarly,

$$C_d = \left\{ C_p - A_1\pi/2 - \sum_{n=o,2\ldots}^{\infty} 2A_n \frac{(-1)^{n/2}}{n^2 - 1} \right\} \cos\alpha \qquad (14)$$

i.e.

$$-C_\ell = C_d \tan\alpha \qquad (15)$$

Consider now a D - Section elastically mounted at zero angle of attack. When the cylinder is vibrating, there is an aerodynamic force , F_v, acting parallel to the flat upstream surface

From appendix D, (assuming a two dimensional cylinder),

$$C_{F_v} = (C_\ell + C_d \tan\alpha)\sec\alpha$$

Thus if p_w is constant or symmetrical,for $\alpha > 0$,

$$C_{F_v} = 0$$

and $$dC_{F_v}/d\alpha = 0$$

Conclusion

If the wake pressure is constant or symmetrical with respect to the upstream face for values of σ greater than zero, Den Hartog's criterion for instability states that the aerodynamic damping is exactly zero. Also, the lift can be expressed in terms of the drag, i.e.,

$$-C_\ell = C_d \tan\alpha$$

APPENDIX F

Aerodynamic Coefficients for the Rectangular Cylinder

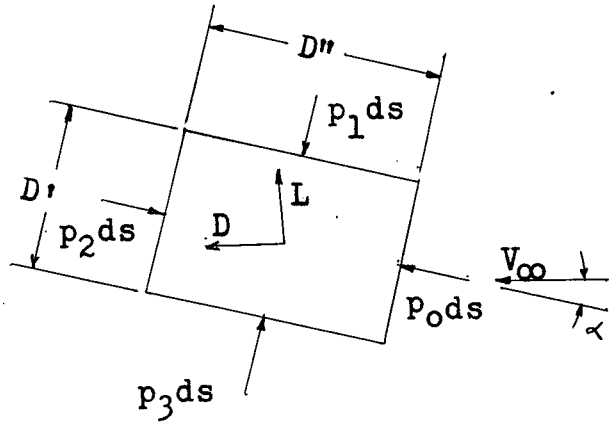

Forces and velocities are positive as shown

From the diagram

$$C_\ell = \frac{1}{D'}\int_0^{D'}(C_{po} - C_{p2})\mathrm{Sin}\alpha ds + \frac{1}{D'}\int_0^{D''}(C_{p3} - C_{p1})\mathrm{Cos}\alpha ds$$

and,

$$C_d = \frac{1}{D'}\int_0^{D'}(C_{po} - C_{p2})\mathrm{Cos}\alpha ds - \frac{1}{D'}\int_0^{D''}(C_{p3} - C_{p1})\mathrm{Sin}\alpha ds$$

If the wake pressure is constant or symmetrical with respect to the chord(D'), then,

$$C_{F_V} = 0$$

and

$$C_\ell = - C_d \mathrm{Tan}\alpha$$

REFERENCES

1. Hoerner, S.F., Fluid dynamic drag, p. 3-28, 1958.

2. Lanchester, F.W., Aerodynamics, A.Constable & Co. Ltd., London, pp.44-45.

3. von Karman, T., Flussigkeits-u-Luftwiderstand, Phys. Zeit., v. 13, p.49, 1911.

4. Fage, A., and Johannsen, F., Flow behind a flat plate, Proc. Royal Society, v. 116, 1927.

5. Fage, A., and Johannsen, F., The structure of vortex sheets, R & M #1143, British ARC 1927.

6. Steinman, D.B., Problems of aerodynamic and hydrodynamic stability, Univ. of Iowa, Studies in Engineering Bulletin 31, 1947.

7. Den Hartog, J.P., Mechanical vibrations, McGraw-Hill, pp. 299 - 309, 1956.

8. Pankhurst, R.C., and Holder, D.W., Wind tunnel technique, Pitman, 1948.

9. Dryden and Kuethe, Hydrodynamics, Dover, 1956.

10. Benedict, R.R., Introduction to Industrial Electronics, Prentice Hall, E.E. Series, pp. 151-154.

11. Parkinson, G.V., and Brooks, P.N., On the aeroelastic instability of bluff cylinders. (Unpublished) 1960.

12. Steinman, D.B., Suspension Bridges - the aerodynamic problem and its solution, Int. Assn. of Bridge and Structural Engineer, Publications, 1953-54, p.209.

13. Strouhal, V., Uber eine besondere Art der Tonerregung, Ann. Phys. Chem. N.F. Bd. 5, Heft 10, October 1878, pp.216-251.

14. Kuethe and Schetzer, Foundations of aerodynamics, Wiley New York, p.40, 67, 1950.

15. Cheers, F., A note on galloping conductors, N.R.C. Report MT-14, June 1950.

16. Harris, G.O., Galloping conductors II, Feb. 1, 1948 to August 1, 1948. Report to Utilities Research Commission. Univ. of Notre Dame.

17. Roshko, A., On the drag and shedding frequencies of two-dimensional bluff bodies, NACA TN 3169, 1954.

18. Cowdrey, C.F., and Lawes, J.A., Force measurements on squares and dodecagonal sectional cylinders at high NR, NPL/Aero/351, 1959.

19. Scruton, C., and Walshe, D.E., A means of avoiding wind-excited oscillations of structures with circular or near circular cross-section. Report NPL/Aero/335, 1959.

20. Kirchhoff, G., Zur Theorie freier Flüssigkeitsstrahlen, Crelles Journal, v. 70, 1869.

SUPPLEMENTARY BIBLIOGRAPHY

Dickey, W.L., and Woodruff, G.B., Vibration of Steel Stacks, Proc. ASCE, #540, Nov. 1954.

Dockstader, E.A., The Vibration of Steel Stacks at the Moss Landing Plant of the Pacific Gas and Electric Co., ASCE Separate #511, Sept. 1954.

Dockstader, E.A., Swiger, W.F., and Ireland, E., Resonant Vibration of Steel Stacks, Proc. ASCE #541, 1954.

Fujino et al, The Dynamic Behavior of Tall Stacks under the action of the Wind, Proc. 7th Nat. Congr. Appl. Mech., Tokyo 1957, pp.387-392.

Omori, F., Wind Pressure on Tall Chimneys, Engineering, v. 106, 1918, pp.334-336.

Ozker, M.S., and Smith, J.O., Factors influencing the Dynamic Behavior of Tall Stacks under the action of the Wind, ASME paper #55-A-69.

Penzien, J., Wind induced vibration of Cylindrical Structures, ASCE, Eng. Mech. Div. Proc. Paper #1141, Jan. 1957.

Price, P., Suppression of fluid induced Vibration of Circular Cylinders, ASCE Proc. 1030 v.82, July 6, 1956.

Scruton, C.S., Wind excited oscillations of tall stacks, The Engineer, June 10, 1955.

Scruton, C.S., and Walshe, D.E., The aerodynamic investigation for the Crystal Palace T.V. Tower, Report NPL/Aero/298, 1958.

Scruton, C.S., and Walshe, D.E., and Woodgate, L., The aerodynamic investigation for the east chimney stack of the Rugeley Generating Station, NPL/Aero/352, 1959.

Scruton, C.S., Note on the aerodynamic stability of truncated circular cones and tapered stacks. Report NPL/Aero/305, 1958.

Walshe, D.E., and Whitbread, R.E., The aero investigation for a stack for the Canada India Reactor Project. Report NPL/Aero/395, 1959.

Woodgate, L., and Maybrey, J.F., Use of Helical Strakes to avoid vortex induced vibration of circular cylinders. Report NPL/Aero/381, 1959.

Blyumina, L., & Zakharov, Y. G., Vibrations of cylindrical bodies in an air flow, Referativnoii Zhurnal Mekhaniki, #10, 1958, Rev. 10987.

Kerr, Shannon, & Arnold, The problem of the singing propeller, Inst. Mech. Engineers, Proceedings, 144, 54, 1940.

Reudy, R., Vibration of power lines in a steady wind, Canadian Journal of Research, October 1935.

Smirnov, L.P., & Pavlihina, M.A., Vortical traces for flow around vibrating cylinders, Izv. Akad. Nauk, Otd. Tekh. Nauk, #8 124-127, Aug. 1958.

Ammann, von Karman, & Woodruff, The failure of the Tacoma Narrows Bridge, a report to the Federal Works Agency, March 28, 1941.

Farquharson, P., Aerodynamic stability of suspension bridges, the Tacoma Narrows Bridge, Univ. Washington, Engin. Exp. Sta. Bull. #116, part 3.

Frazer, R. A., The Severn Bridge aero research, Nature, v. 163 p. 7, Jan. 1, 1949.

Maher, F., Frederick, D., & Estes, E.R. & Steinman, D., Bulletin #69, Engineering Experimental Station Series, Virginia Polytechnic Institute.

Scruton, C.S., An experimental investigation of the aerodynamic stability of suspension bridges. Preliminary publication of the 3rd Congress I. A. for B & S.E., 1948.

Bleich, McCullough, Rosecrans & Vincent, Mathematical theory of vibration in suspension bridges, Bureau of Public Roads, U.S. Dept. of Commerce, Government Printing Office.

Schacter & Eskinazi, An analysis of the vortex sheet generated in a viscous fluid, Journal of Fluid Mechanics, v. 6#2, pp 241 - 260, August 1959.

Steinman, D.B., Aerodynamic theory of bridge oscillations, Trans. ASCE, v. 115, 1950 p. 1180.

Bingham, H.H., Weimer, D.K., Griffeth, W., The cylinder and semicylinder in subsonic flow, Princeton University, Dept. of Physics, Techn. Report 11-13, 1952.

Commetta, C., An investigation of the unsteady flow pattern in the wake of cylinders and spheres using a hot wire probe. Tech. Report W721, October 1957, Brown University.

Kovasznay, L., An investigation of the wake behind cylinders at low Reynolds numbers, Proc. Royal Society, v. 198, pp. 174-190, 1949.

Relf, E.F., & Simmonds, L.F.G., The frequency of the eddies generated by the motion of circular cylinders through a fluid. R. & M. 917, British ARC 1924.

Rosenhead, L., Vortex systems in wakes, Naval Contract, N-S ori-76-Project 22, 1950.

Roshko, A., A new hodograph for free streamline theory, NACA TN 3168, 1954.

Roshko, A., On the wake and drag of bluff bodies, Journal of Aero-Sciences, v. 22#2, 1955, pp. 124-133.

Sherlock, R.H., & Stalker, A study of flow phenomena in the wake of smoke stacks, Engineering Research Bulletin, #29, University of Michigan, 1941.

Taneda, S., Downstream developments of the wakes behind cylinders, Journal of the Physical Society of Japan, v. 14, June 1959.

Tyler, E., Vortex formation behind obstacles of various sections, Phil. Mag., 1931, v. 11, p.849.

Tyler, E., Vortices behind airfoil sections and rotating cylinders, Phil. Mag., 1928, v. 7, p.449.

Drescher, H., Measurement of the time variable pressures exerted on a cylinder with cross flow, Z. Flugwissenschaft, v. 4 #1/2, pp. 17-21, Jan/Feb. 1956.

Fage, A., The airflow around a circular cylinder in the region where the boundary layer separates from the surface, R. & M. #1174, British ARC 1928.

McGregor, D., & Etkin, B., Investigation of the fluctuating pressures on a circular cylinder in an airstream, Physics of Fluids, March/April 1958.

Prendergast, V., Measurement of two point correlations of the surface pressure on a circular cylinder, UTIA TN15, 1958.

Delany, N.K., & Sorenson, N.E., Low speed drag of cylinders of various shapes, NACA TN 3038, 1953.

Weiselsberger, C., Further information on the laws of fluid

resistance, N.A.C.A. TN 121, 1922.

von Karman, T., & Rubach, H., Mechanism of fluid resistance, N.A.C.A. TR 24-50, 1918.

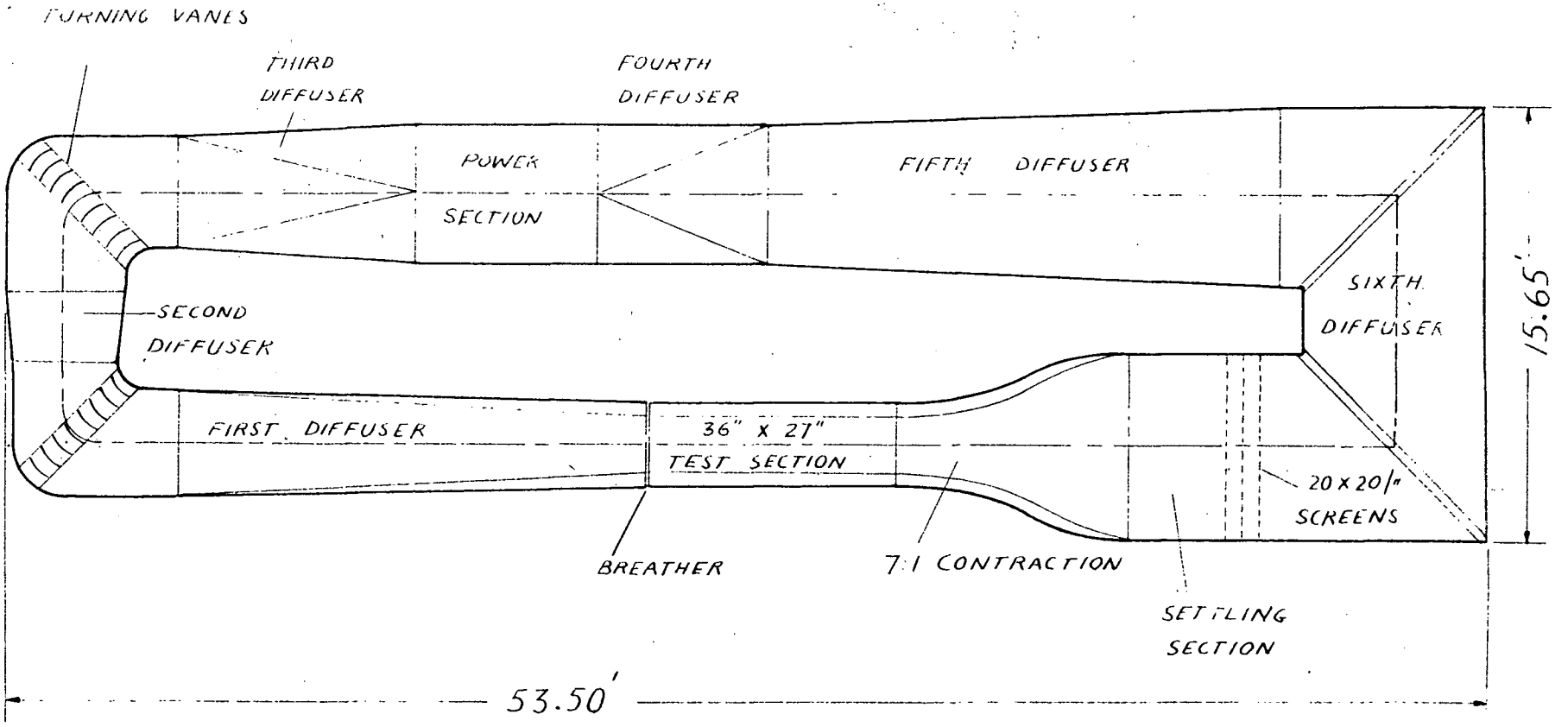

FIGURE 1 - WIND TUNNEL AERODYNAMIC OUTLINE

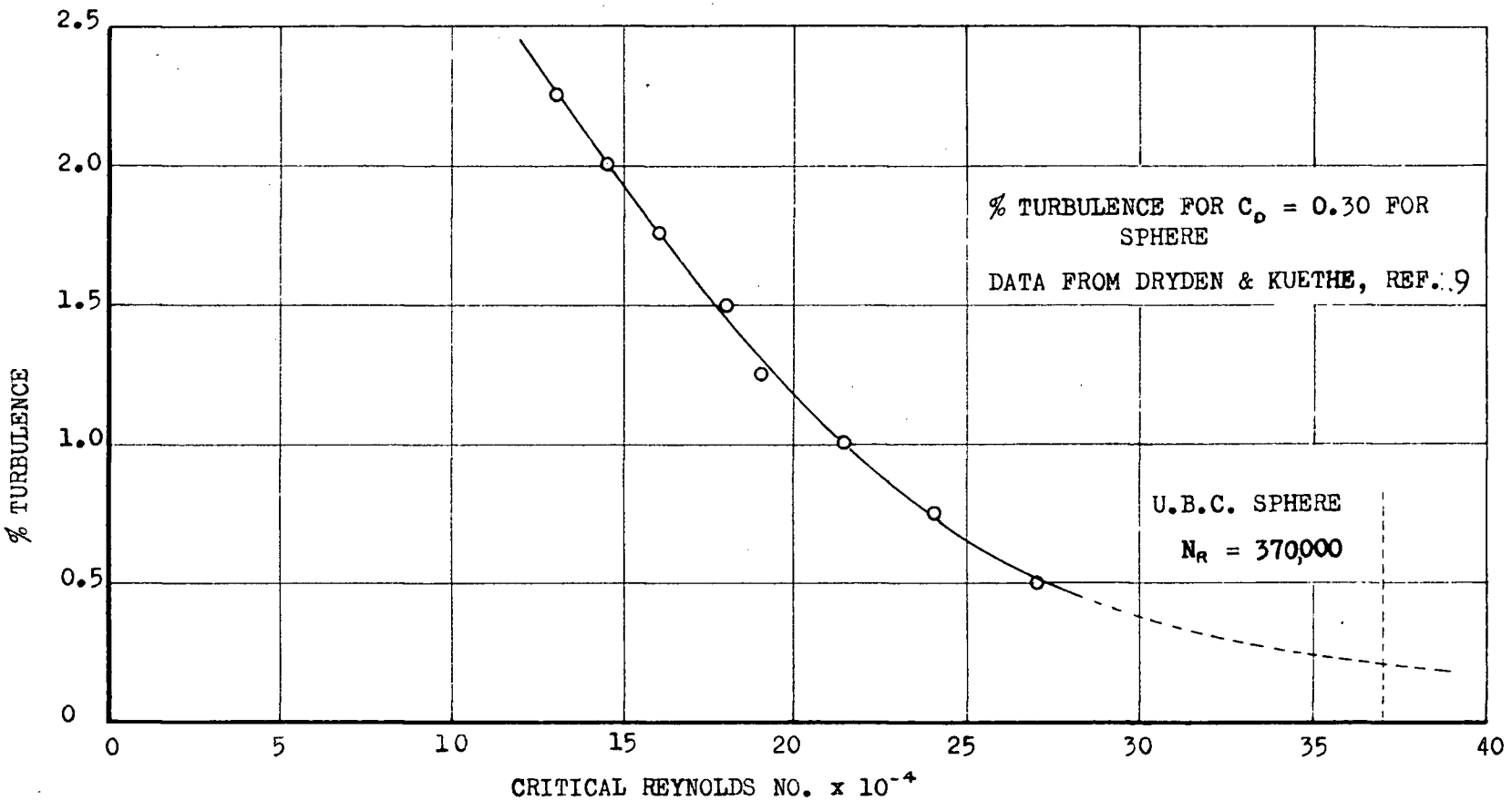

FIGURE 2 - ESTIMATION OF TEST SECTION TURBULENCE LEVEL

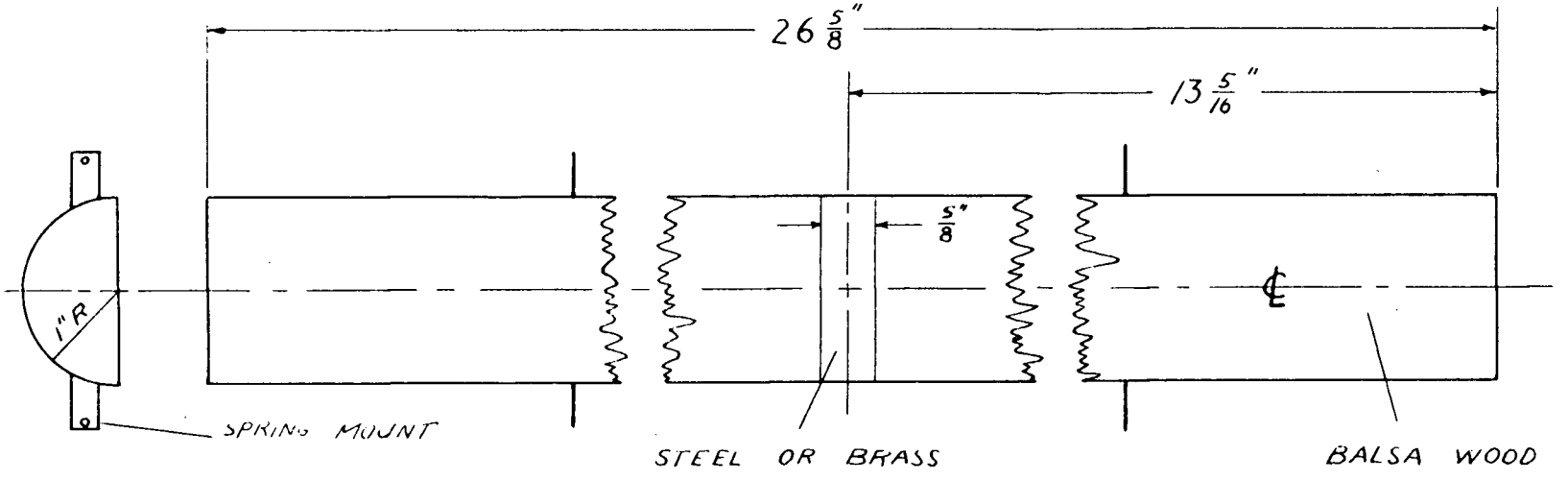

FIGURE 3 - TYPICAL DYNAMIC MODEL.

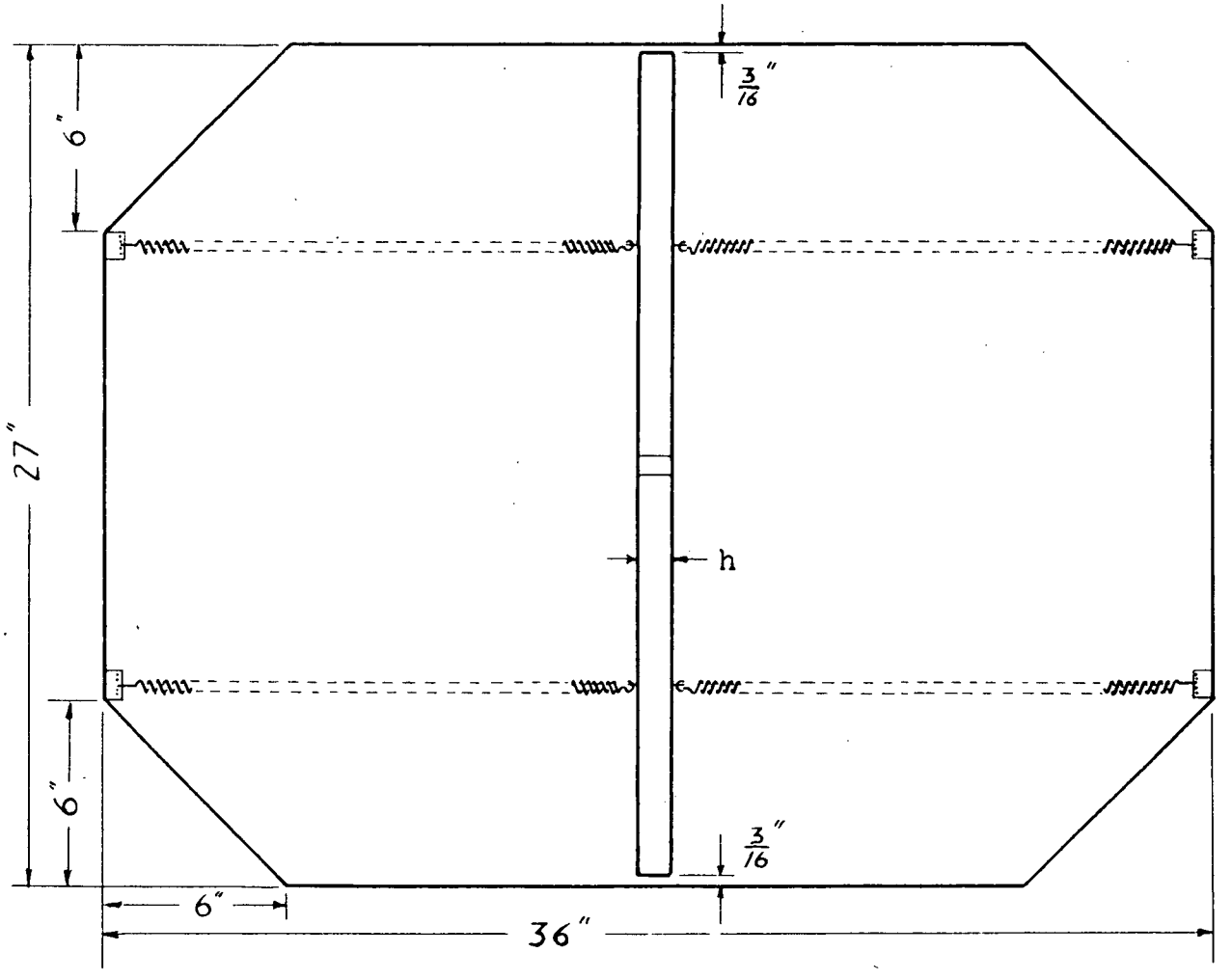

FIGURE 4a- MOUNTING OF DYNAMIC MODEL

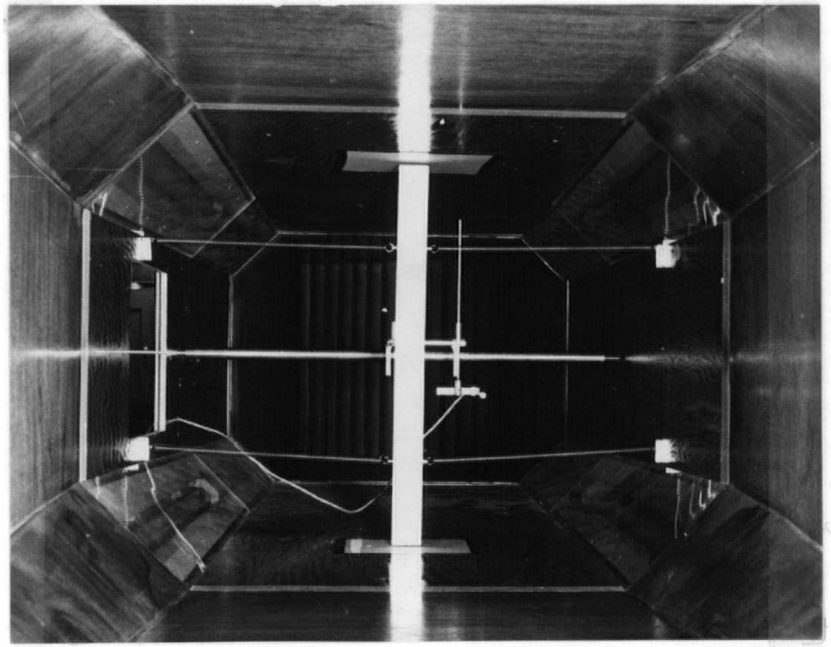

FIGURE 4b - MOUNTING OF DYNAMIC MODEL

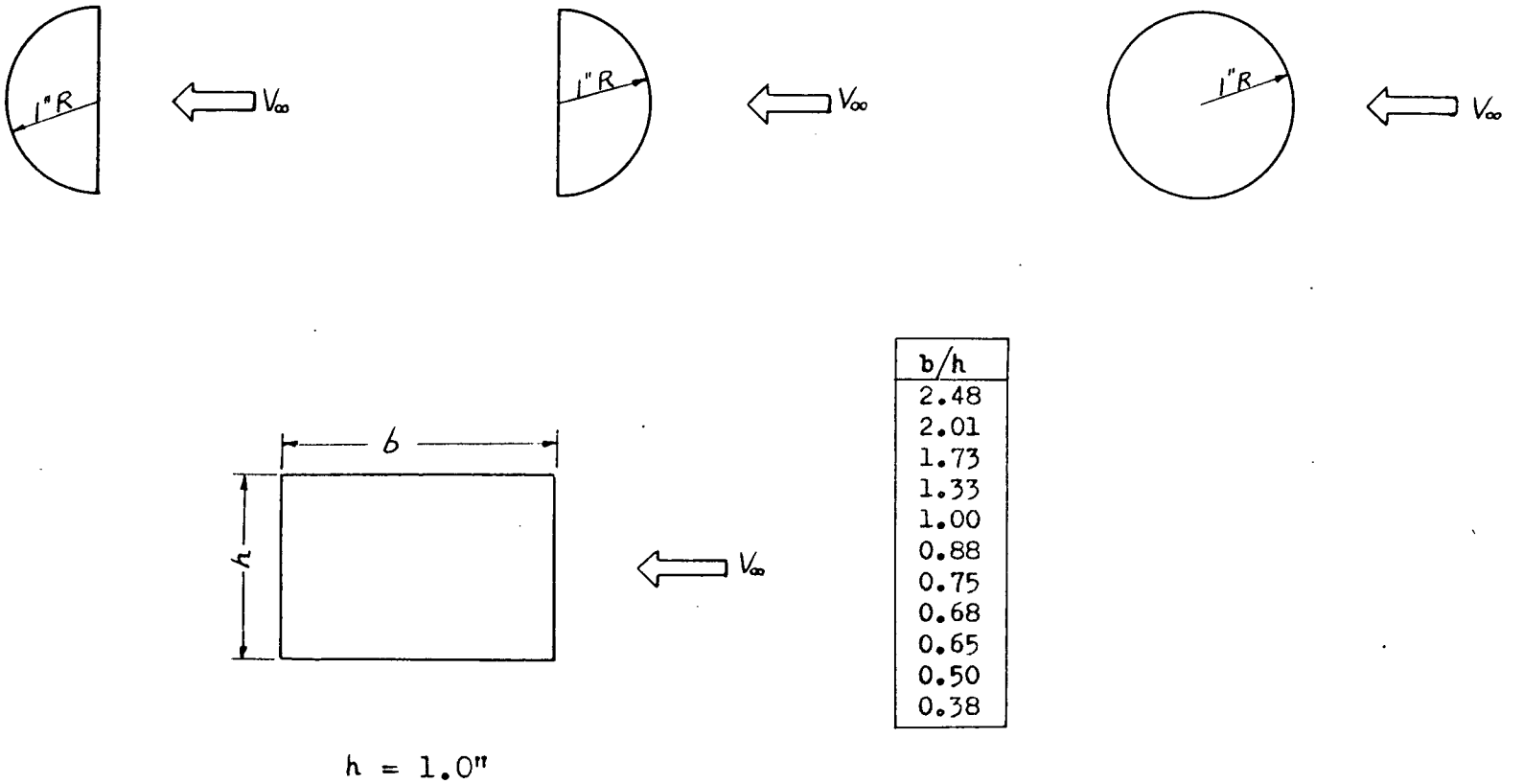

b/h
2.48
2.01
1.73
1.33
1.00
0.88
0.75
0.68
0.65
0.50
0.38

FIGURE 5 - CROSS SECTIONS OF DYNAMIC MODELS

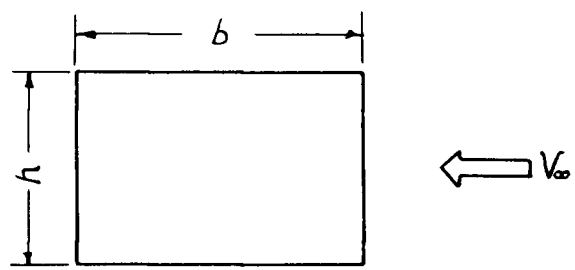

$h = 1.5''$

b/h
4.45
3.97
3.64
3.23
3.09
2.81
2.73
2.54
2.40
2.31
2.04
1.73
1.38
1.00

FIGURE 6 - MODELS FOR WAKE WIDTH MEASUREMENTS.

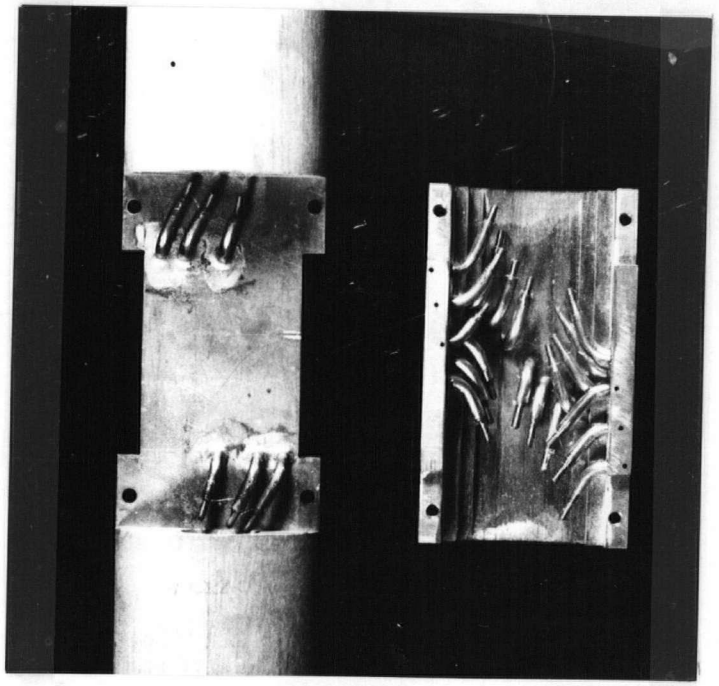

FIGURE 7 - D-SECTION PRESSURE MODEL

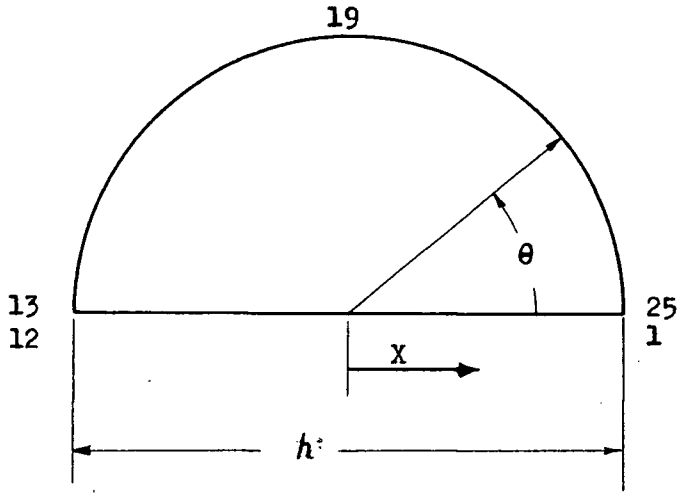

NO.	POSITION x/h'	NO.	POSITION θ DEG.
1	0.4625	13	170.0
2	0.4425	14	159.0
3	0.4175	15	148.5
4	0.3000	16	134.0
5	0.1875	17	118.5
6	0.0025	18	104.0
7	- 0.0100	19	88.0
8	- 0.1950	20	73.5
9	- 0.3150	21	59.0
10	- 0.4160	22	45.0
11	- 0.4500	23	30.0
12	- 0.4790	24	21.0
		25	10.5

FIGURE 8 - LOCATION OF PRESSURE TAPS ON D-SECTION PRESSURE MODEL

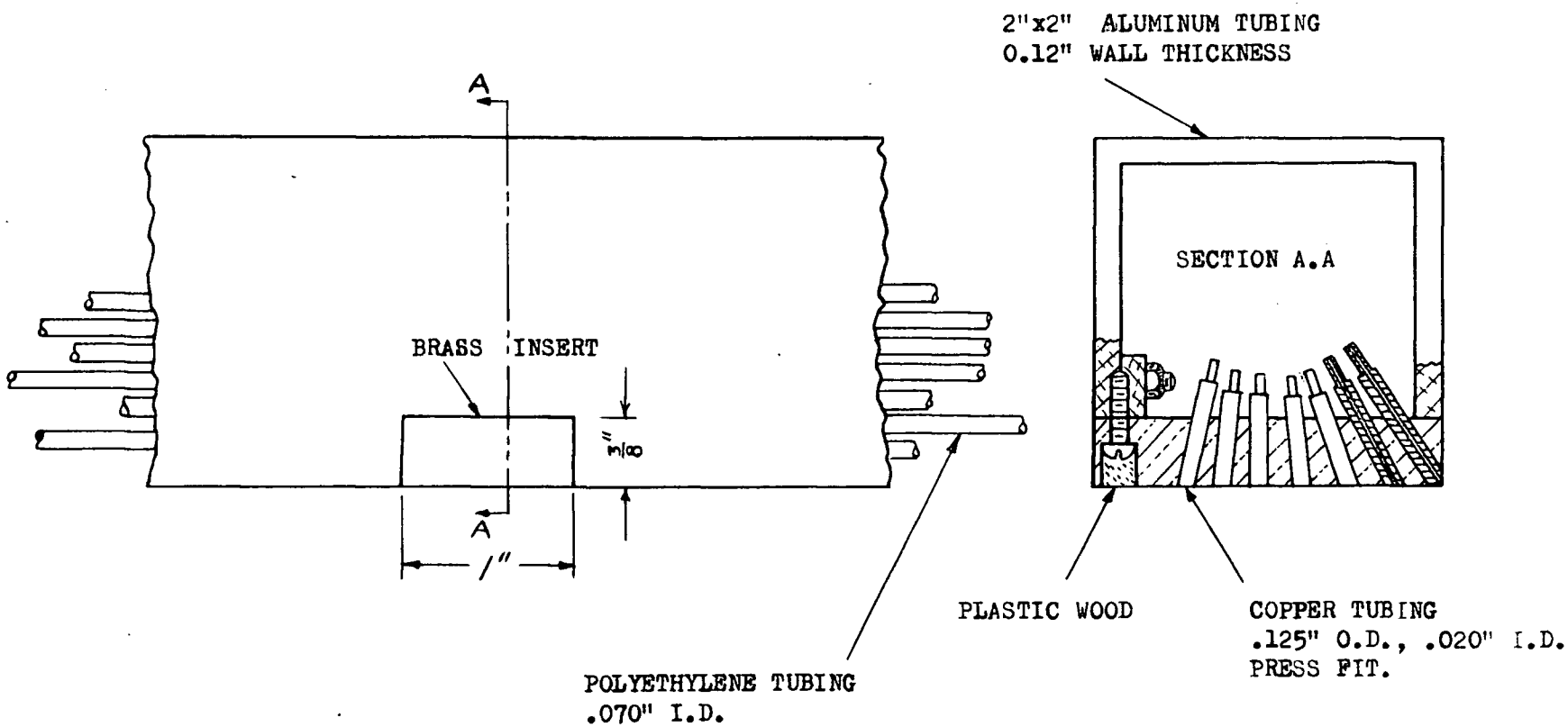

FIGURE 9 - DETAILS OF PRESSURE MODEL.

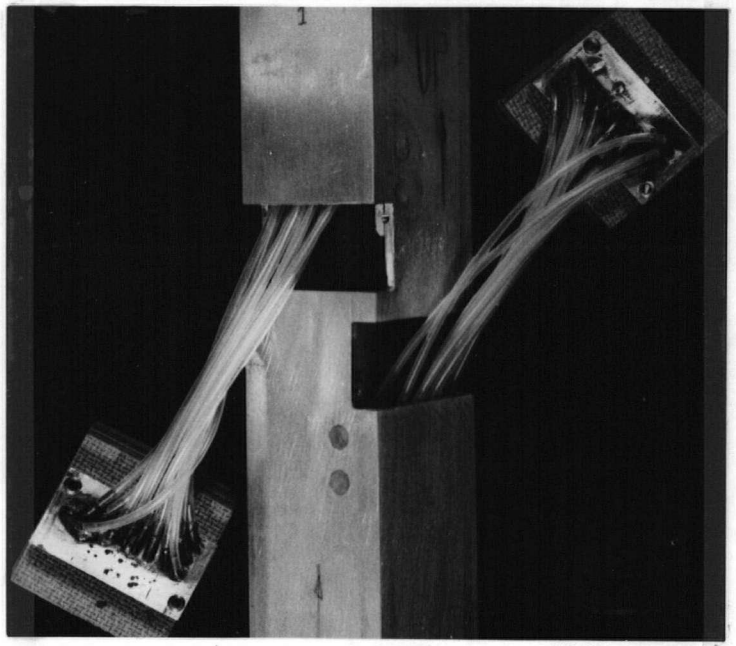

FIGURE 10 - SQUARE SECTION PRESSURE MODEL

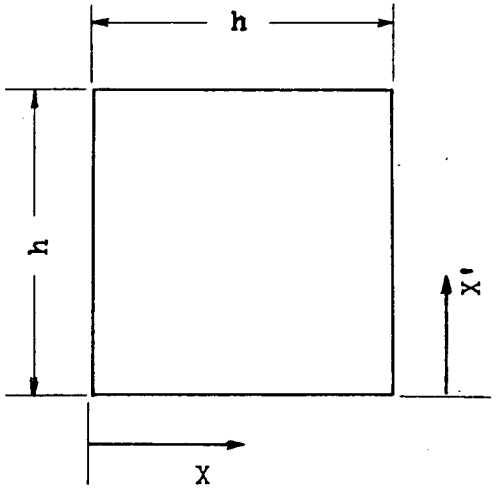

NO.	X/h	NO.	X'/h
1	0.034	11	0.014
2	0.094	12	0.050
3	0.216	13	0.076
4	0.340	14	0.246
5	0.430	15	0.368
6	0.504	16	0.500
7	0.600	17	0.690
8	0.732	18	0.816
9	0.858 0	19	0.942
10	0.936	20	0.960

FIGURE 11 - LOCATION OF PRESSURE TAPS ON SQUARE SECTION MODEL

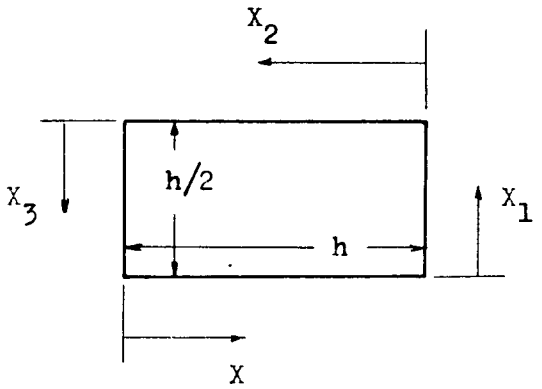

NO.	X/h	NO.	X_1/h	NO.	X_2/h	NO.	X_3/h
1	0.055	11	0.035	18	0.065	28	0.010
2	0.065	12	0.065	19	0.155	29	0.050
3	0.190	13	0.140	20	0.270	30	0.065
4	0.313	14	0.240	21	0.400	31	0.150
5	0.500	15	0.340	22	0.495	32	0.240
6	0.630	16	0.420	23	0.565	33	0.349
7	0.760	17	0.450	24	0.650	34	0.410
8	0.920			25	0.780	35	0.470
9	0.940			26	0.900	36	0.480
10	0.970			27	0.960		

FIGURE 12 - LOCATION OF PRESSURE TAPS ON RECTANGULAR SECTION MODEL

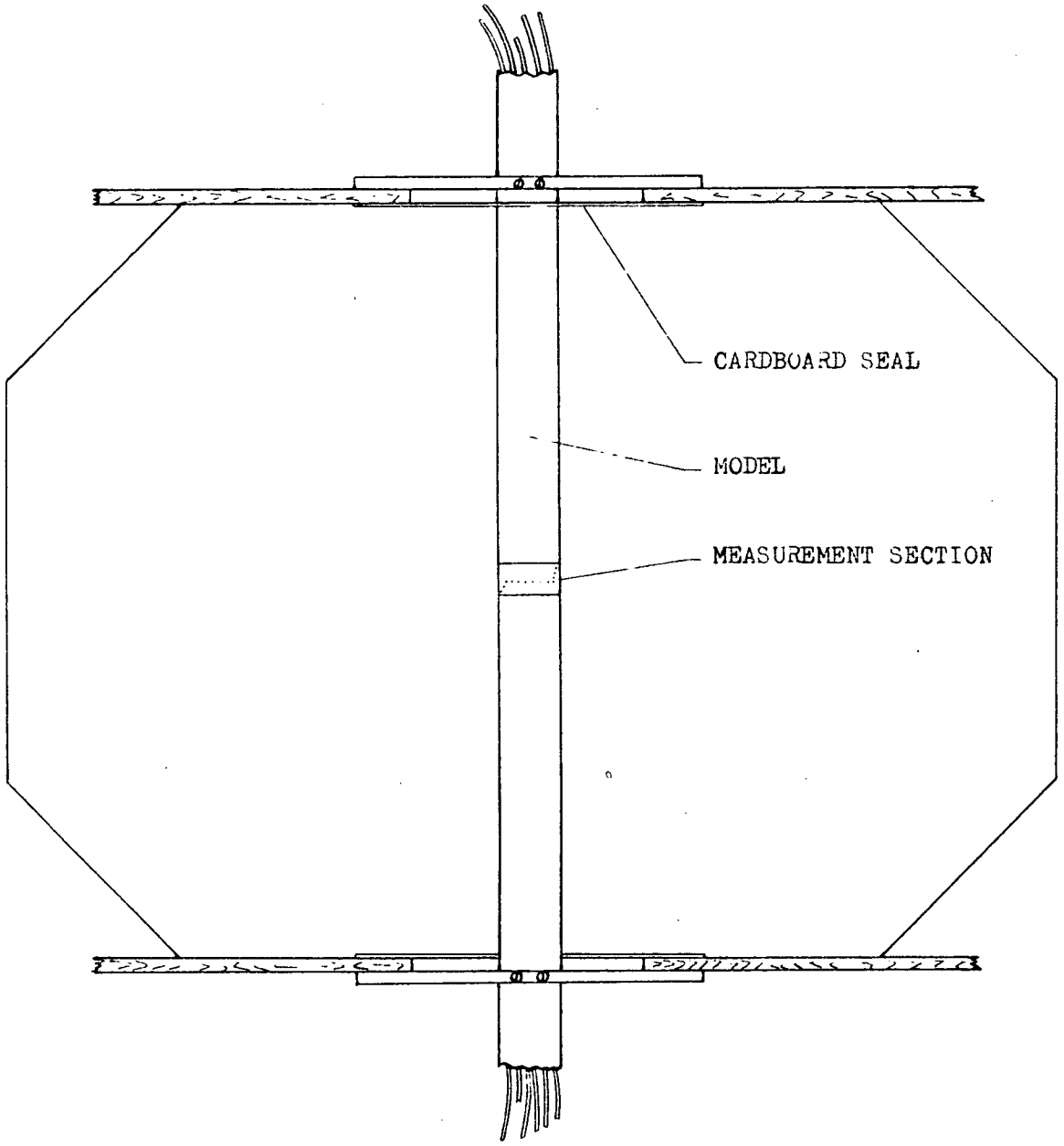

FIGURE 13 - MOUNTING OF PRESSURE MODEL

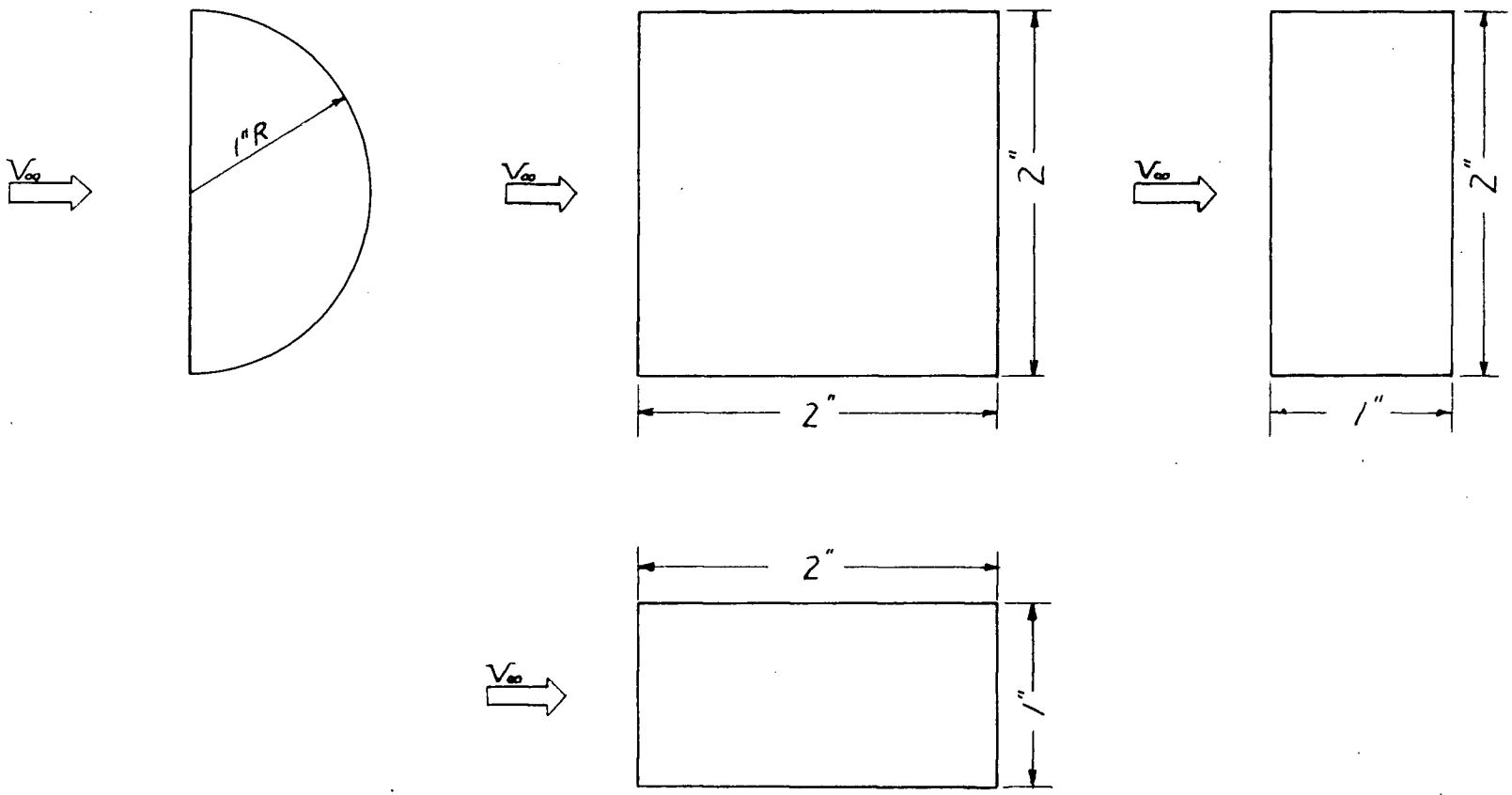

FIGURE 14 - CROSS SECTIONS OF PRESSURE MODELS.

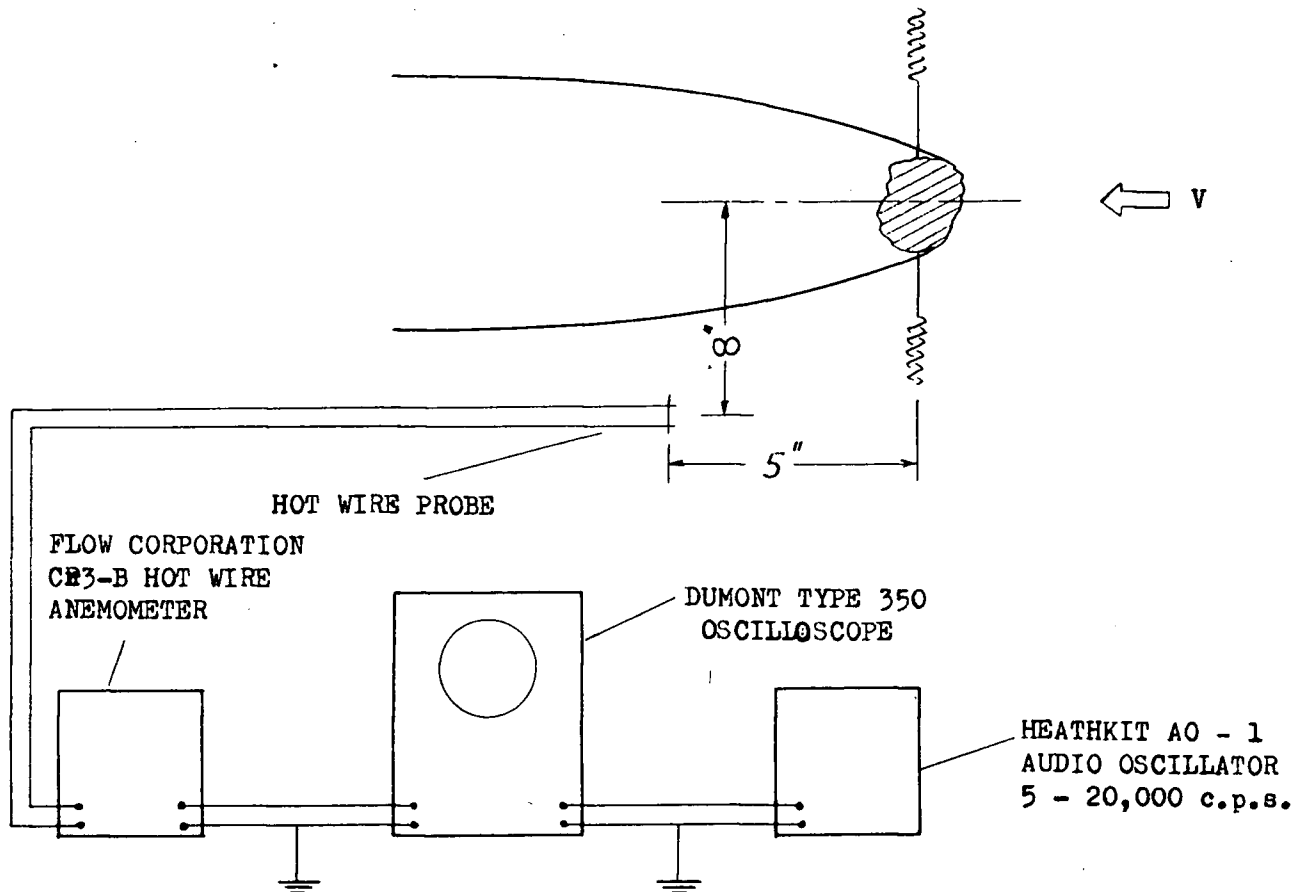

FIGURE 15 - MEASUREMENT OF SHEDDING FREQUENCY.

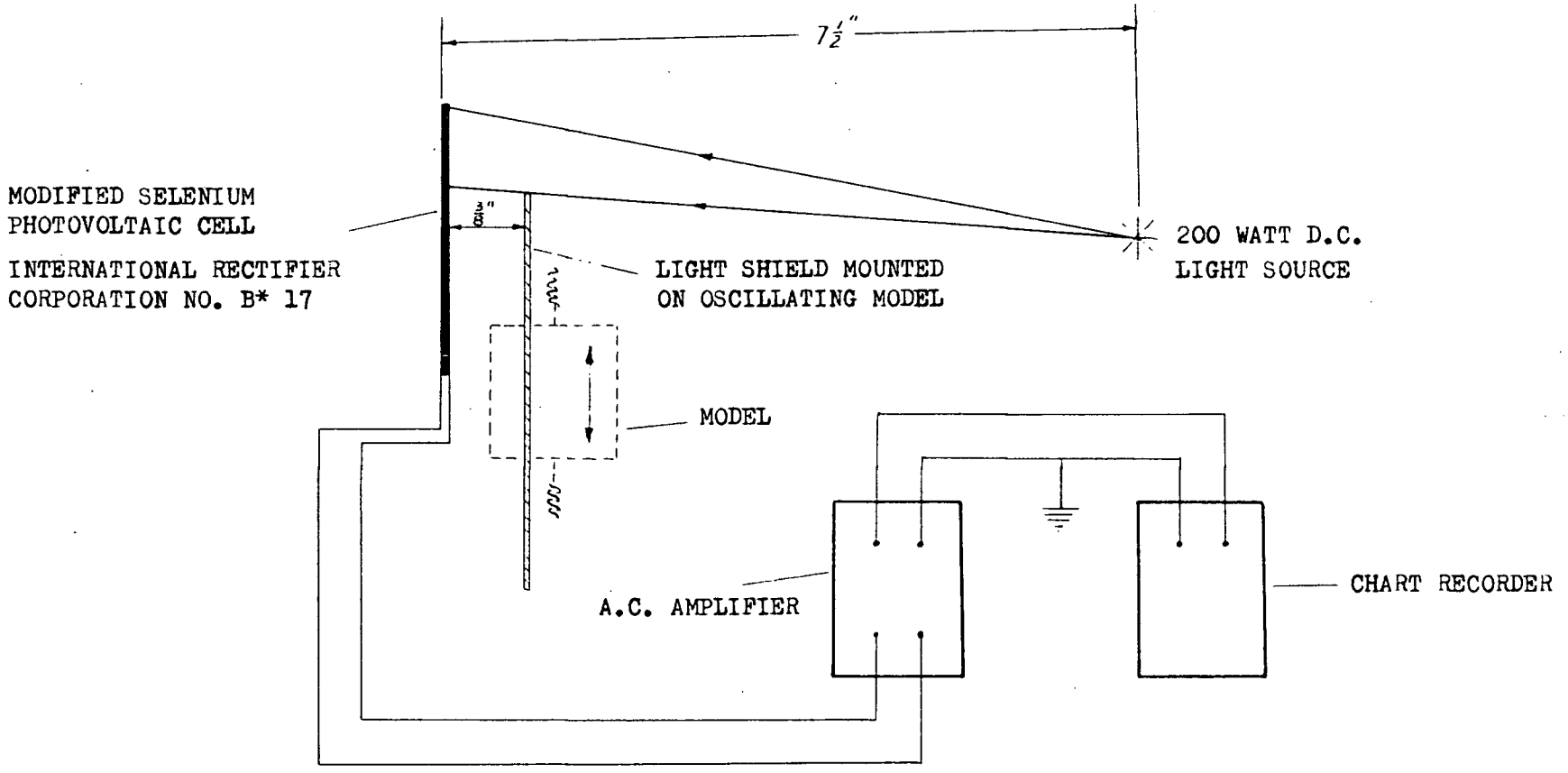

FIGURE 16 - MEASUREMENT OF AMPLITUDE BUILD-UP WITH TIME.

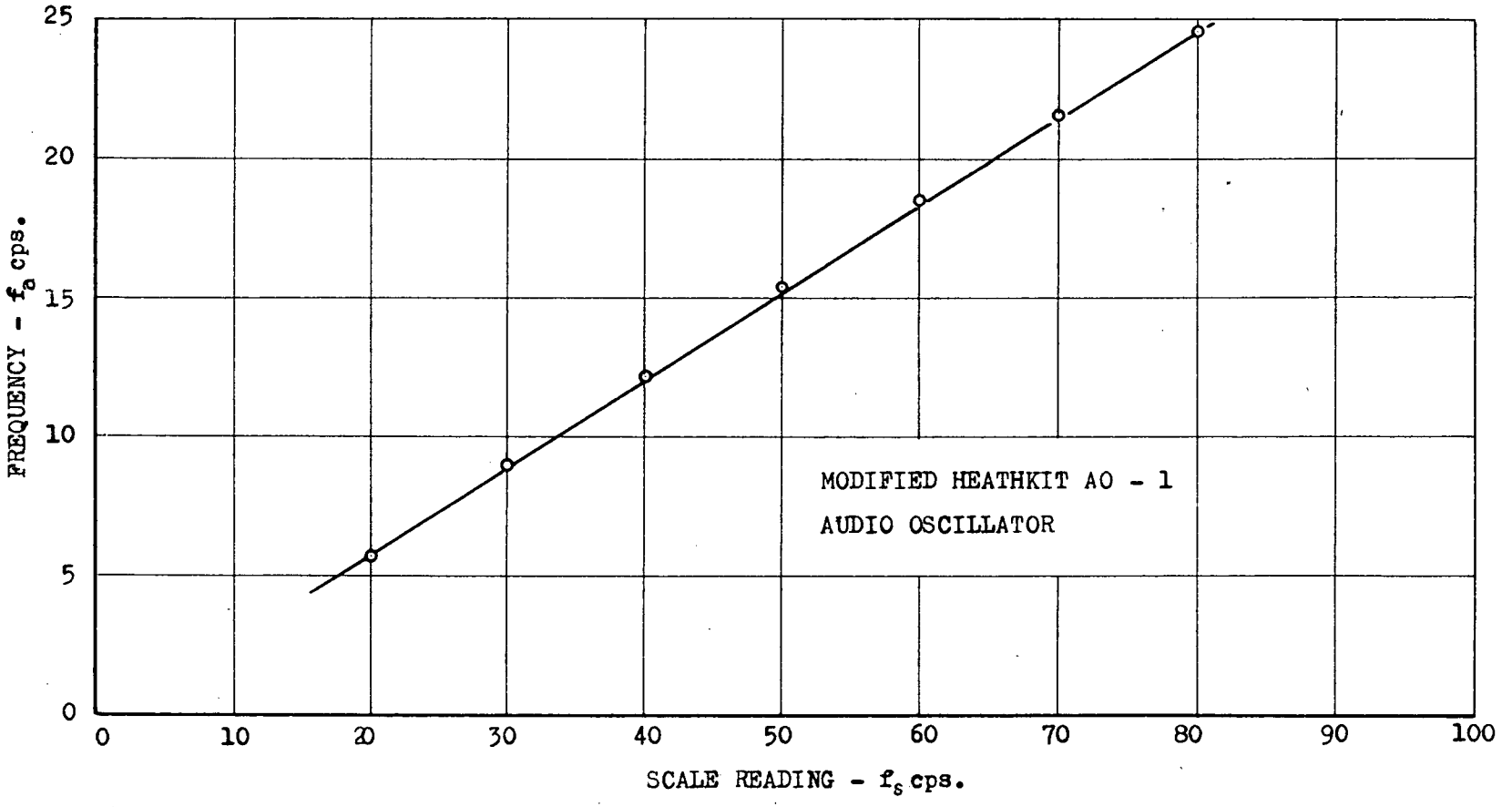

FIGURE 17 - CALIBRATION OF AUDIO OSCILLATOR.

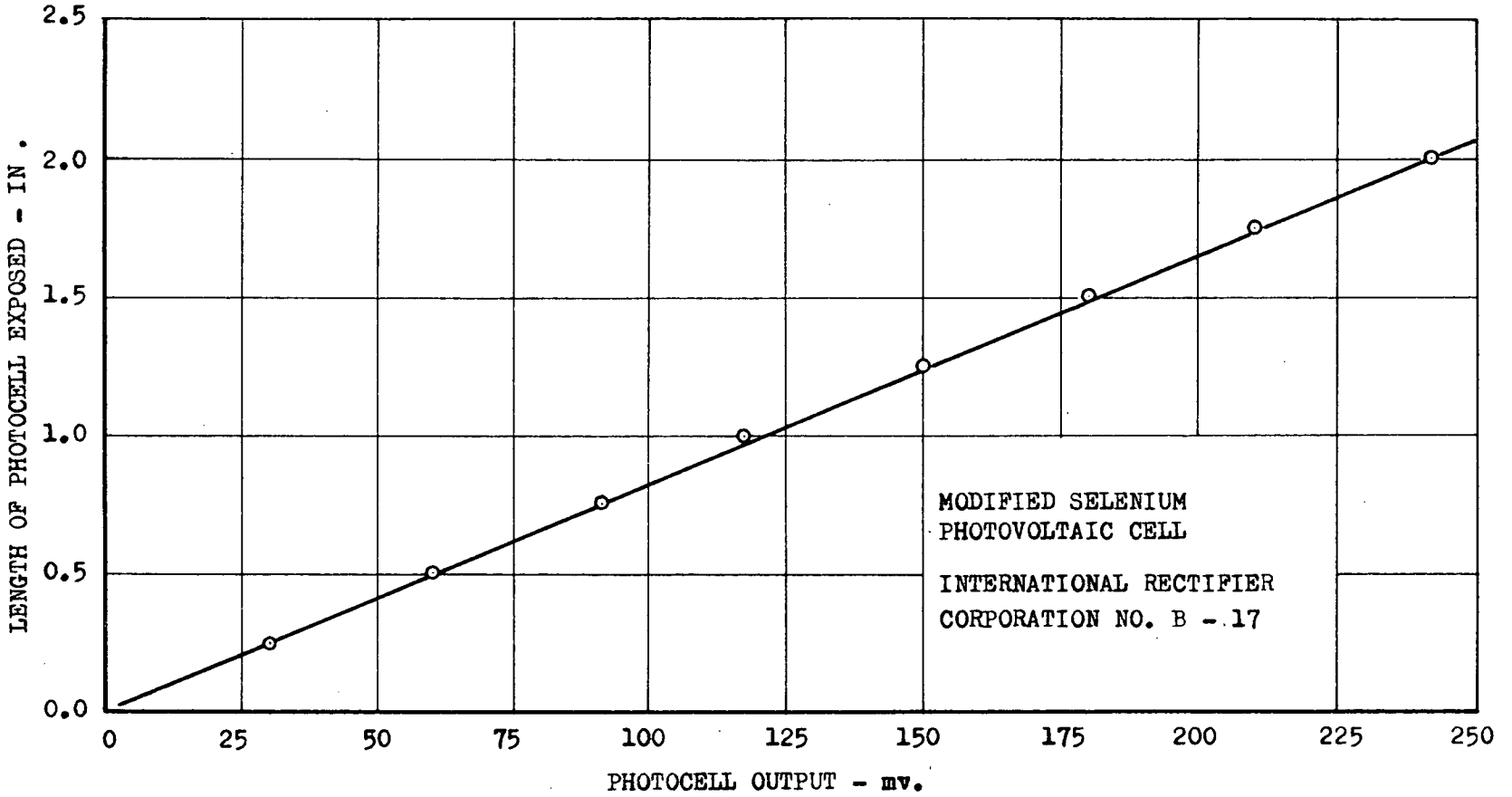

FIGURE 18 - CALIBRATION OF PHOTOCELL.

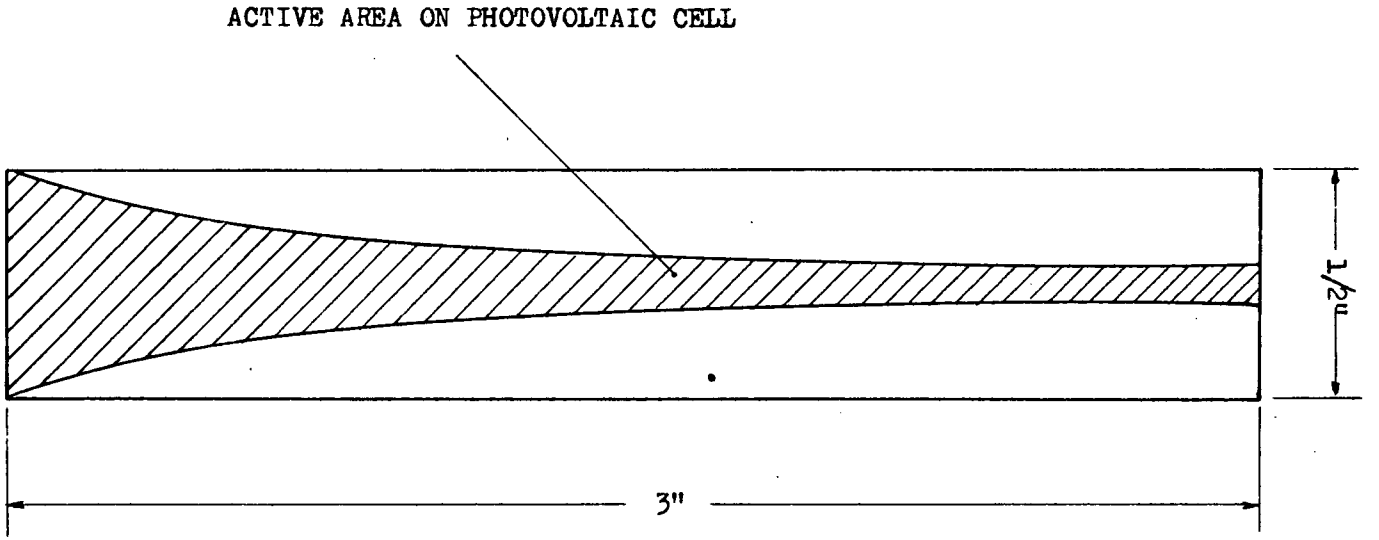

FIGURE 19 - SHAPE OF PHOTOVOLTAIC CELL USED FOR AMPLITUDE MEASUREMENT

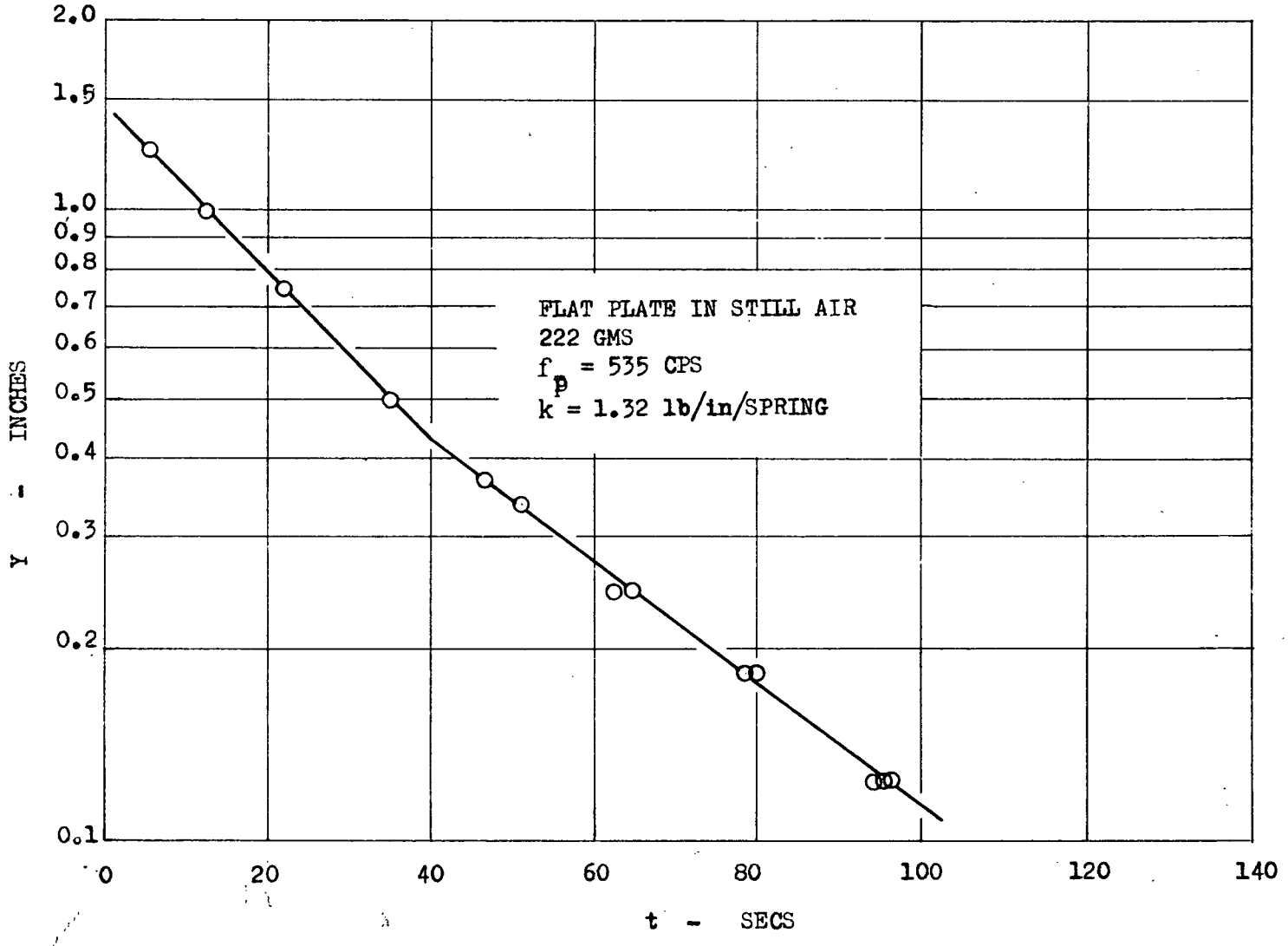

FIGURE 20 - NON-AERODYNAMIC DAMPING FOR DYNAMIC TESTS

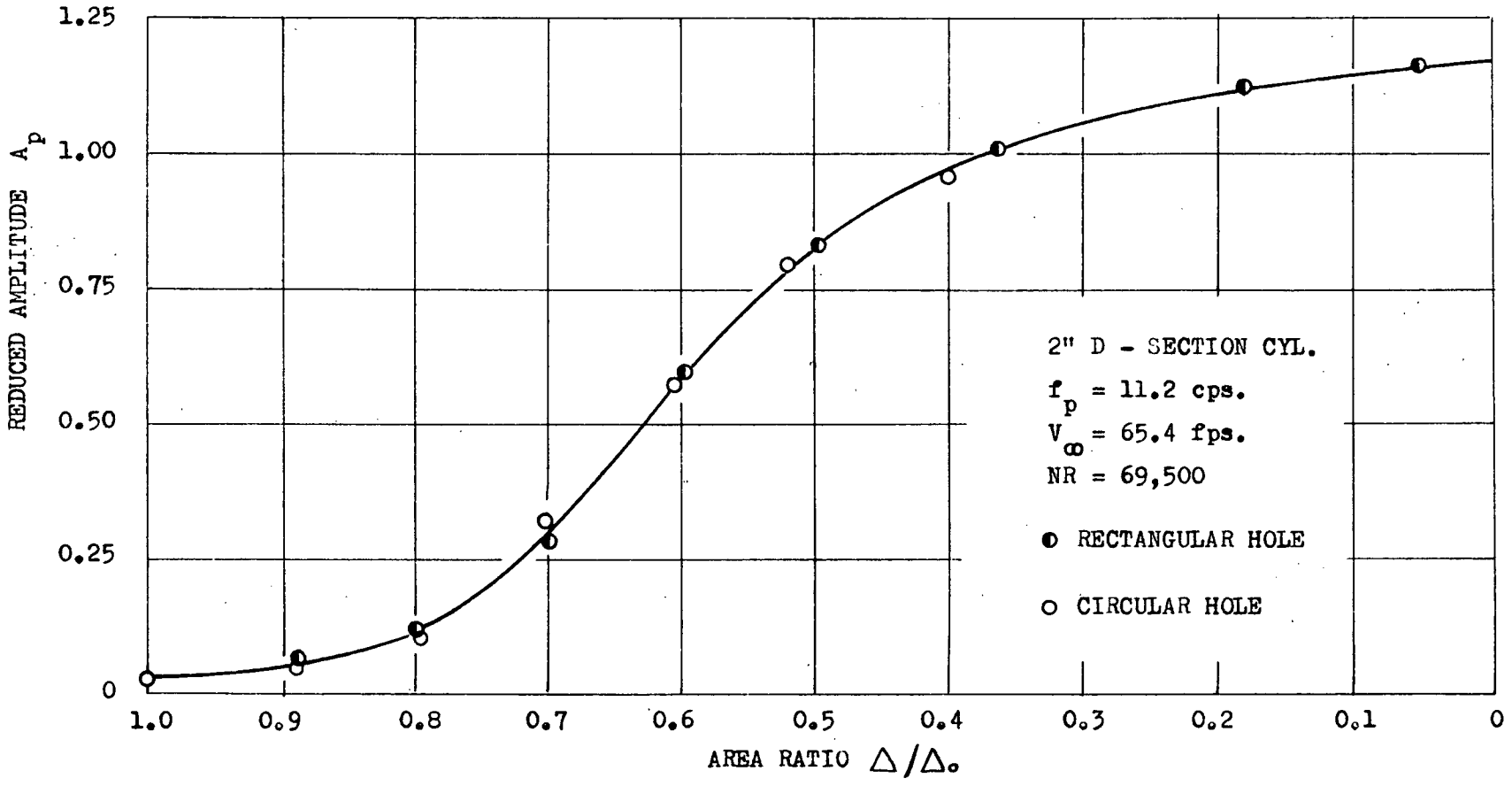

FIGURE 21 - EFFECT OF STREAMWISE POSITION IN HOLE ON AMPLITUDE

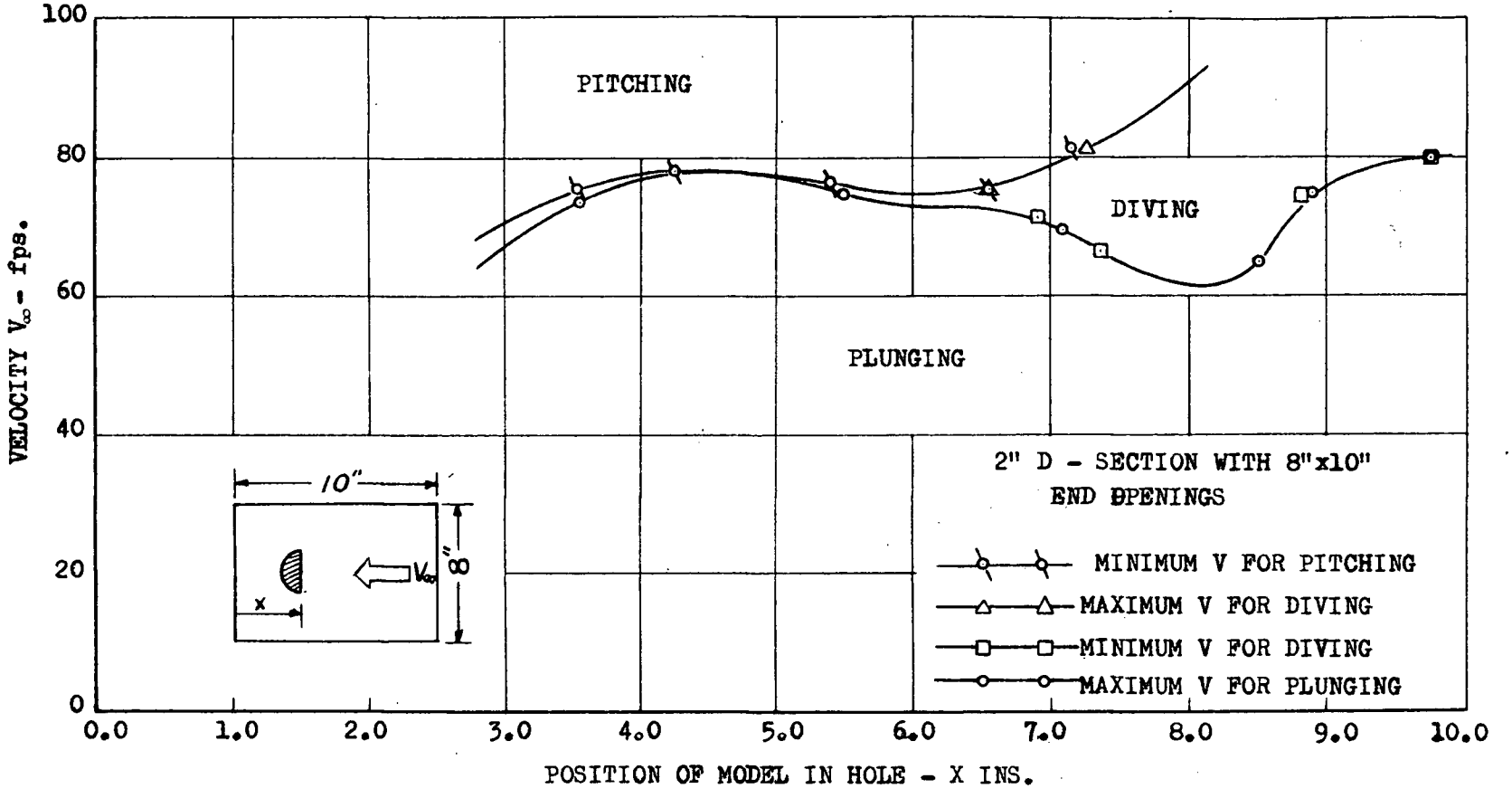

FIGURE 22 - ZONES OF INSTABILITY.

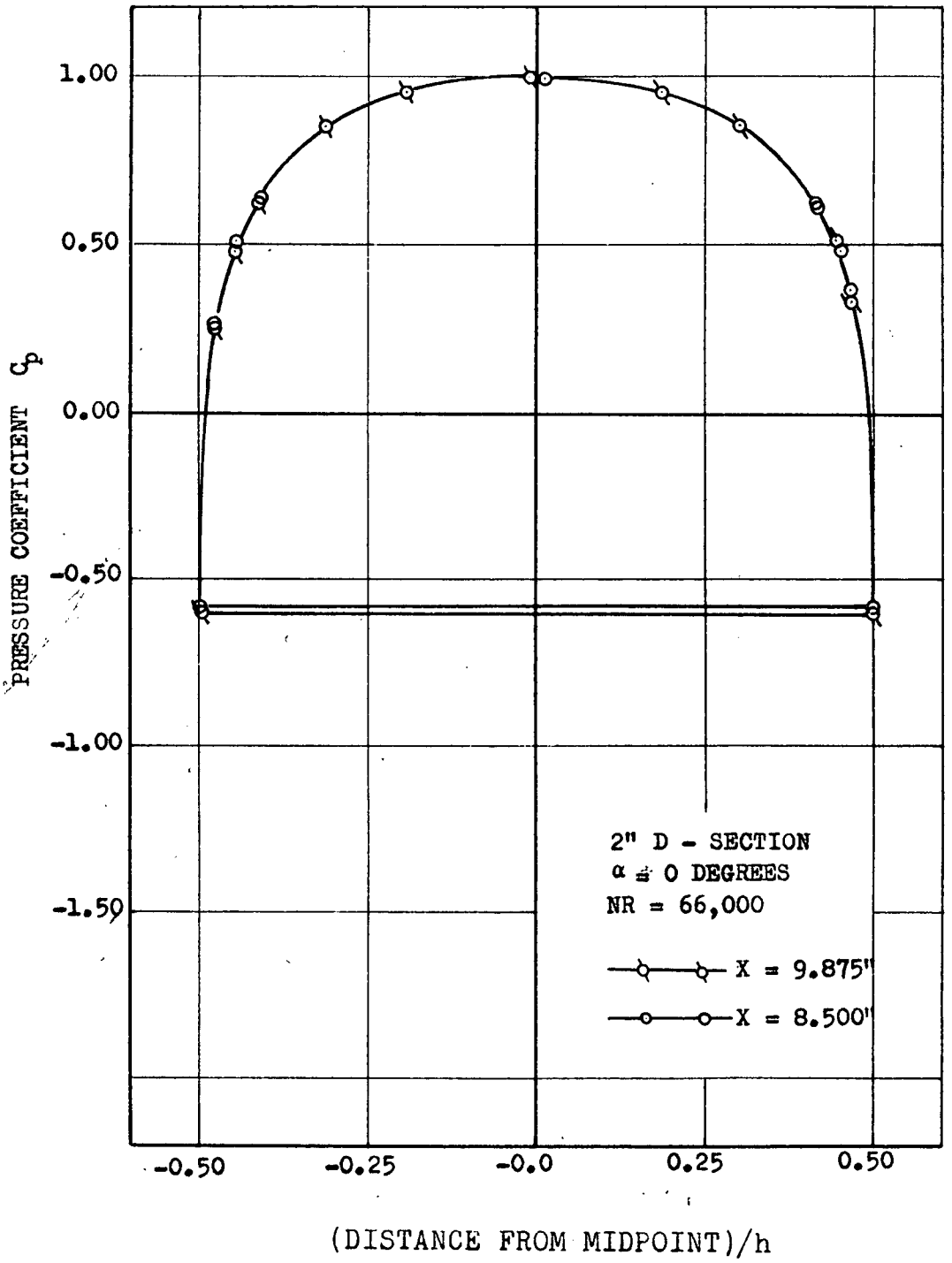

FIGURE 23 - PROJECTION OF C_p ON UPSTREAM SURFACE ($\alpha = 0^o$)

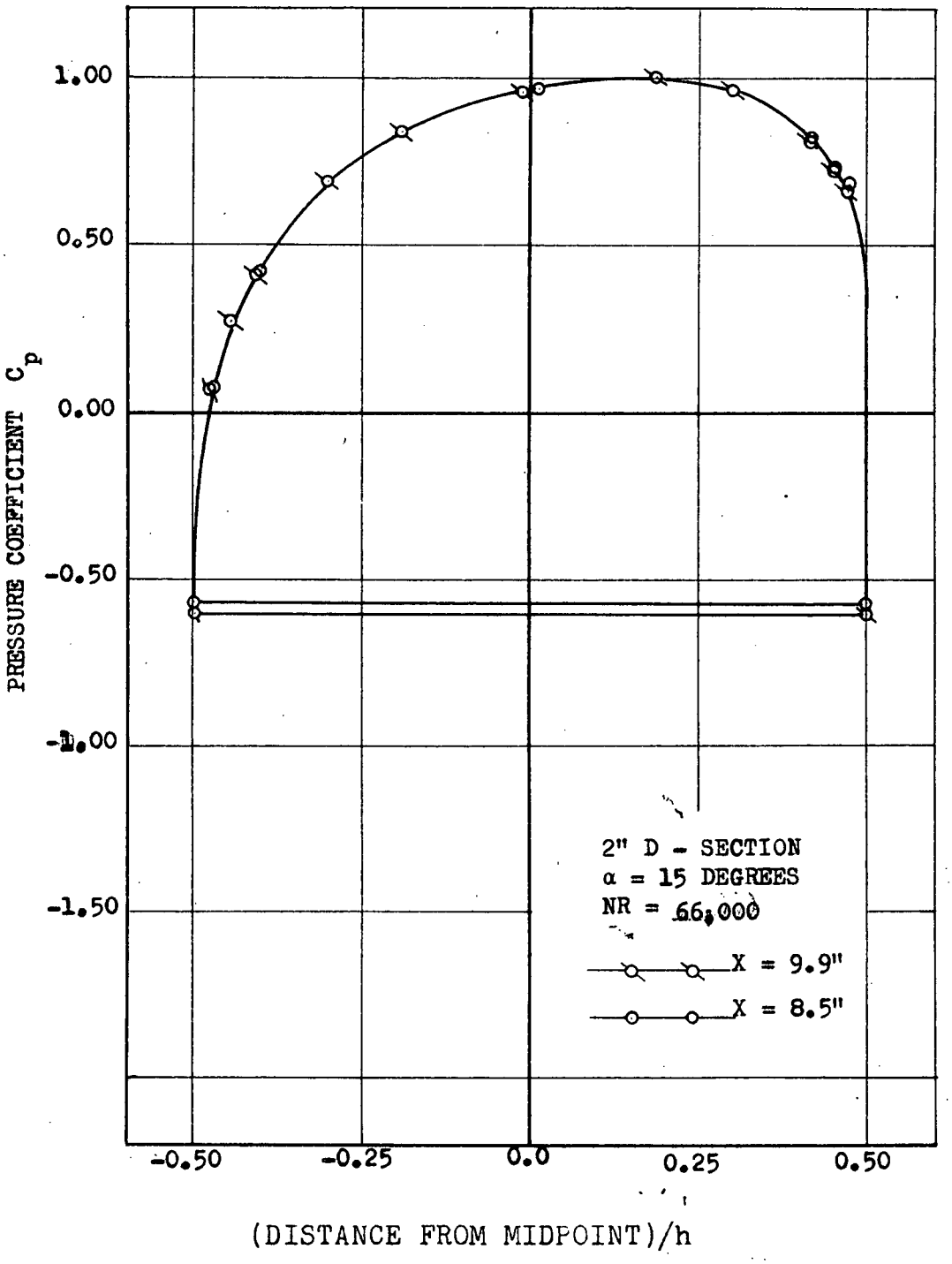

FIGURE 24 - PROJECTION OF C_p ON UPSTREAM SURFACE ($\alpha = 15^{\circ}$)

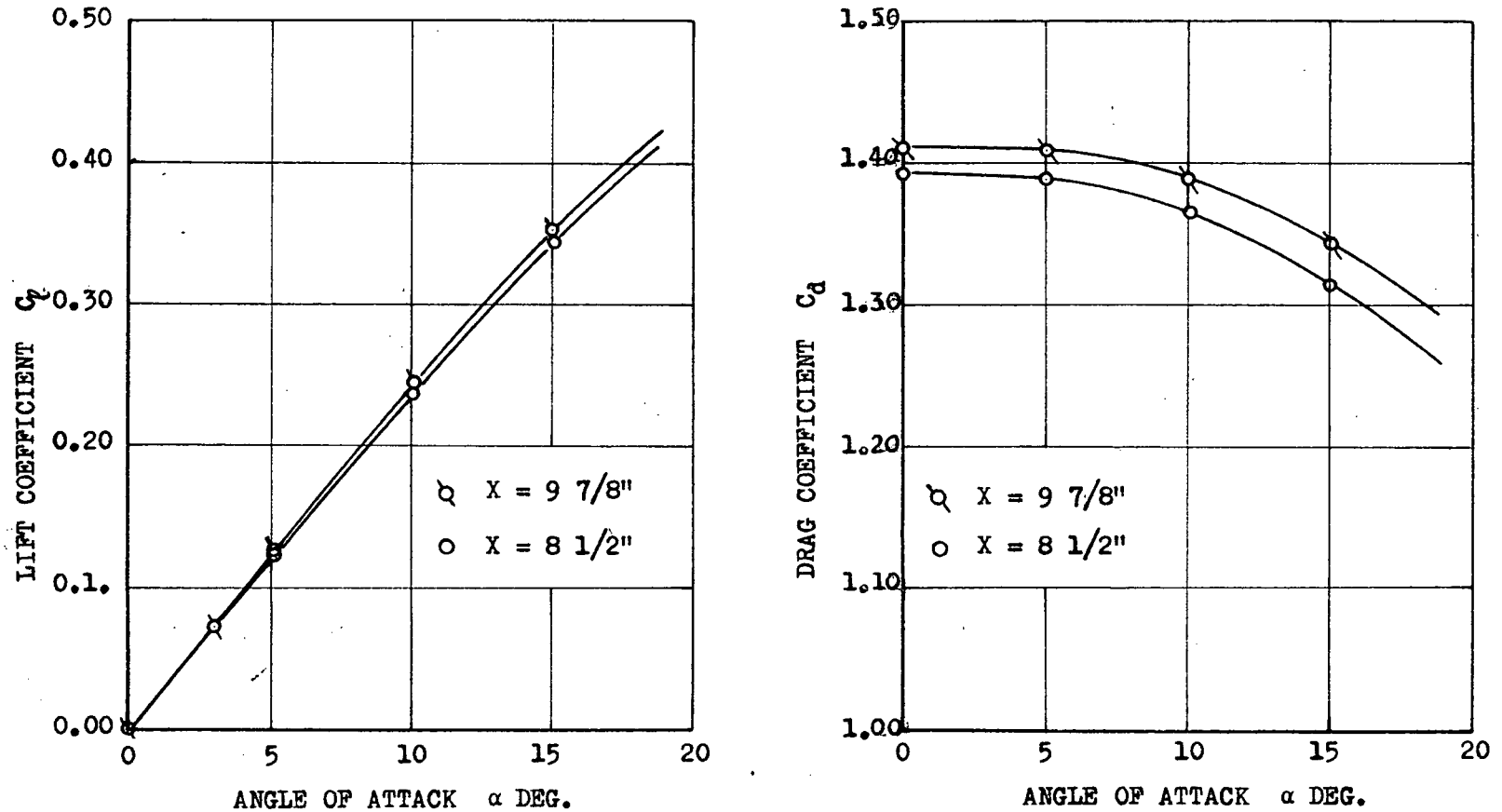

FIGURE 25 - MIDSPAN SECTIONAL COEFFICIENTS FOR D-SECTION NR = 66,000

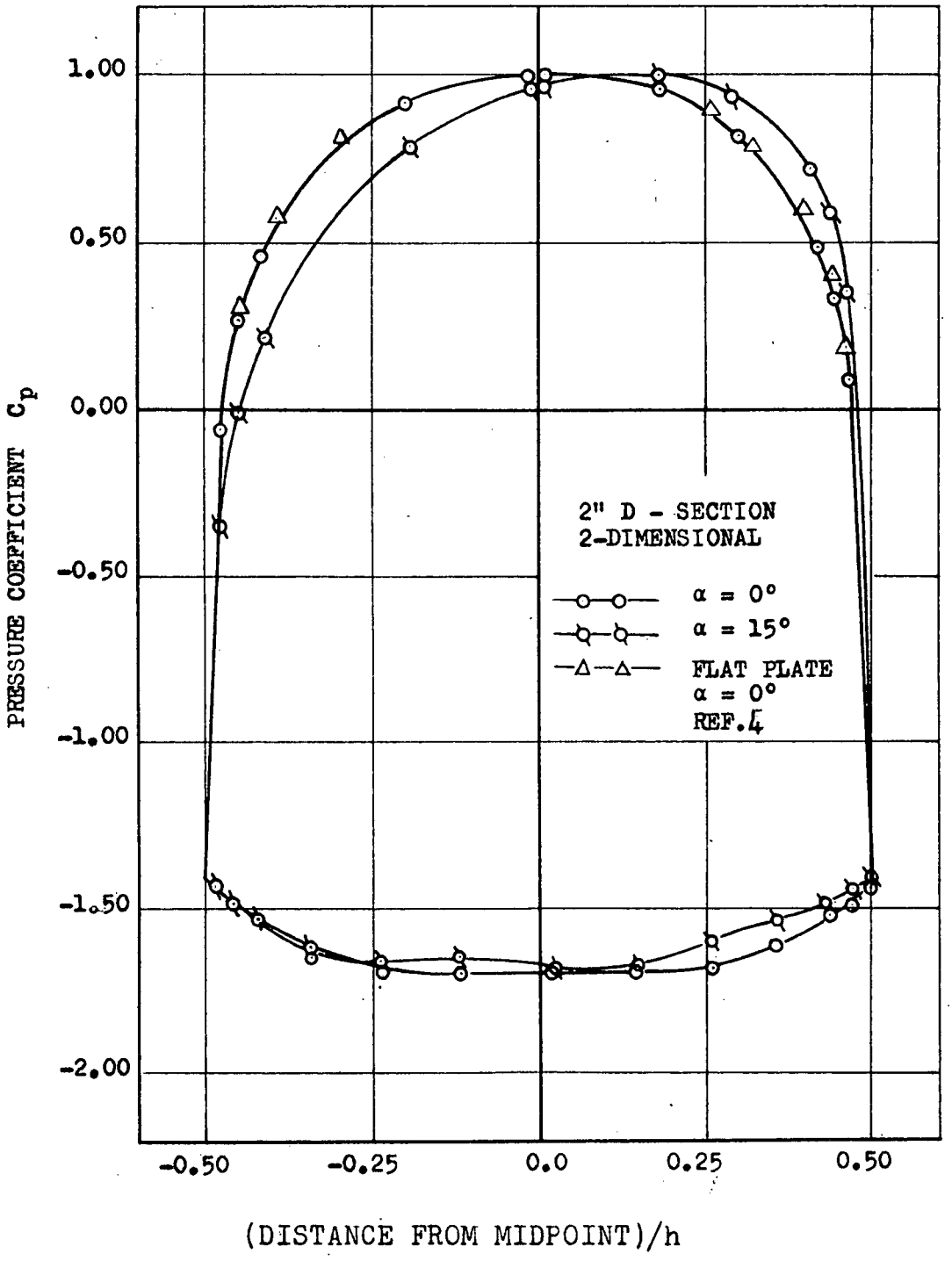

FIGURE 26 - PROJECTION OF C_p ON UPSTREAM SURFACE
TWO-DIMENSIONAL D-SECTION $\alpha = 0^\circ$ & 15°

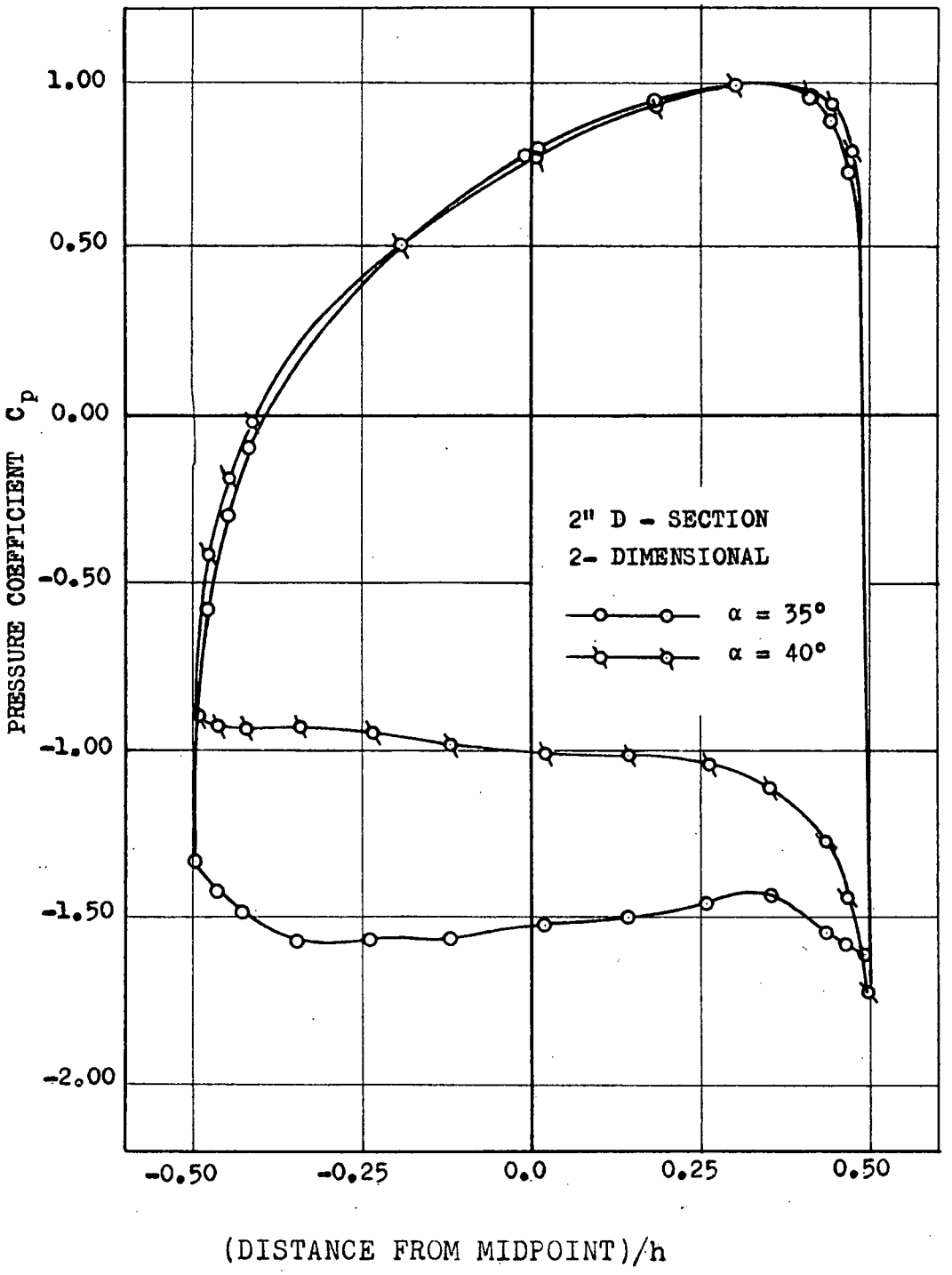

FIGURE 27 - PROJECTION OF C_p ON UPSTREAM SURFACE
TWO-DIMENSIONAL D-SECTION $\alpha = 35^\circ$ & 40°

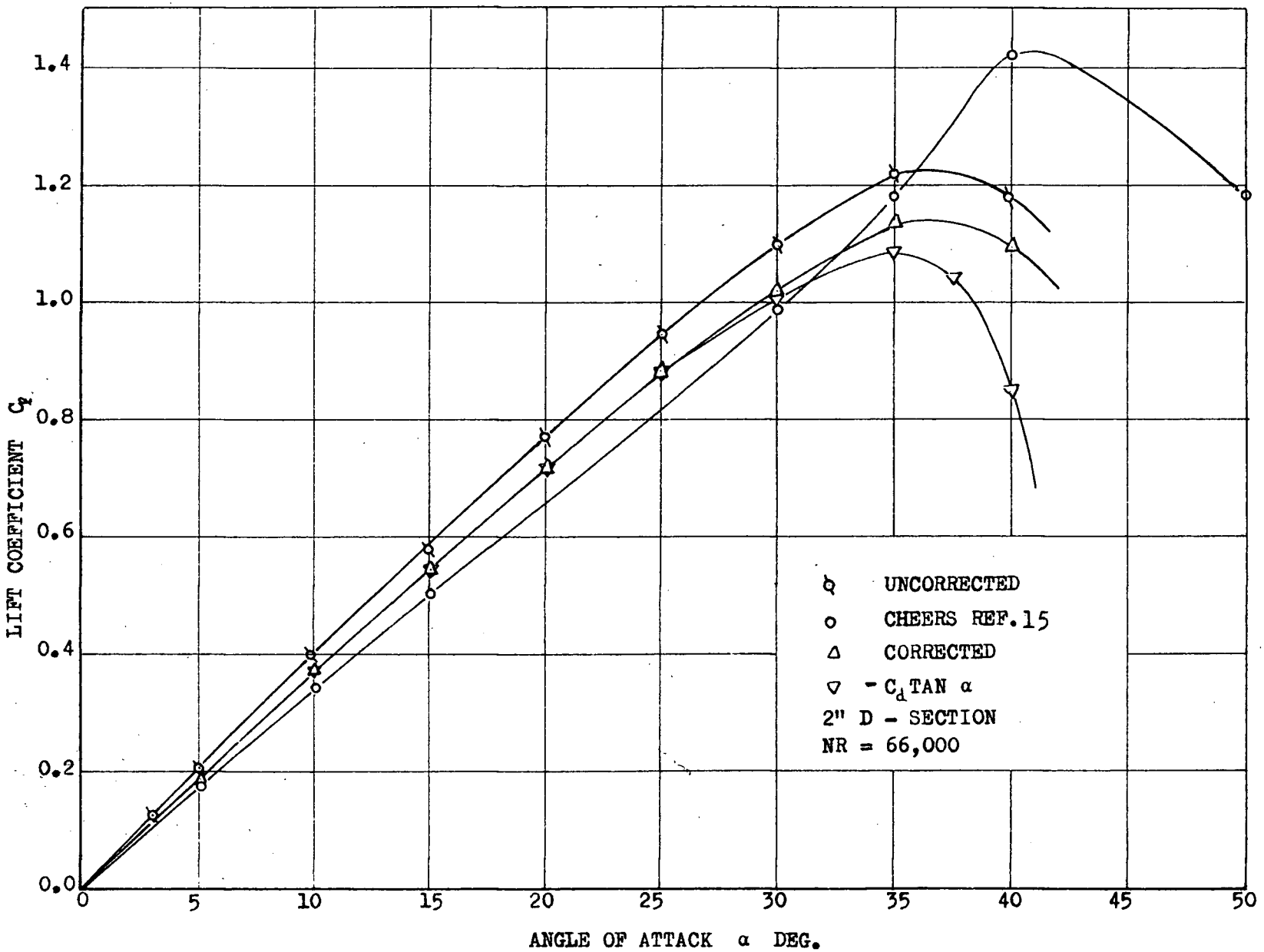

FIGURE 28 - SECTIONAL LIFT COEFFICIENT FOR 2 - DIMENSIONAL D - SECTION

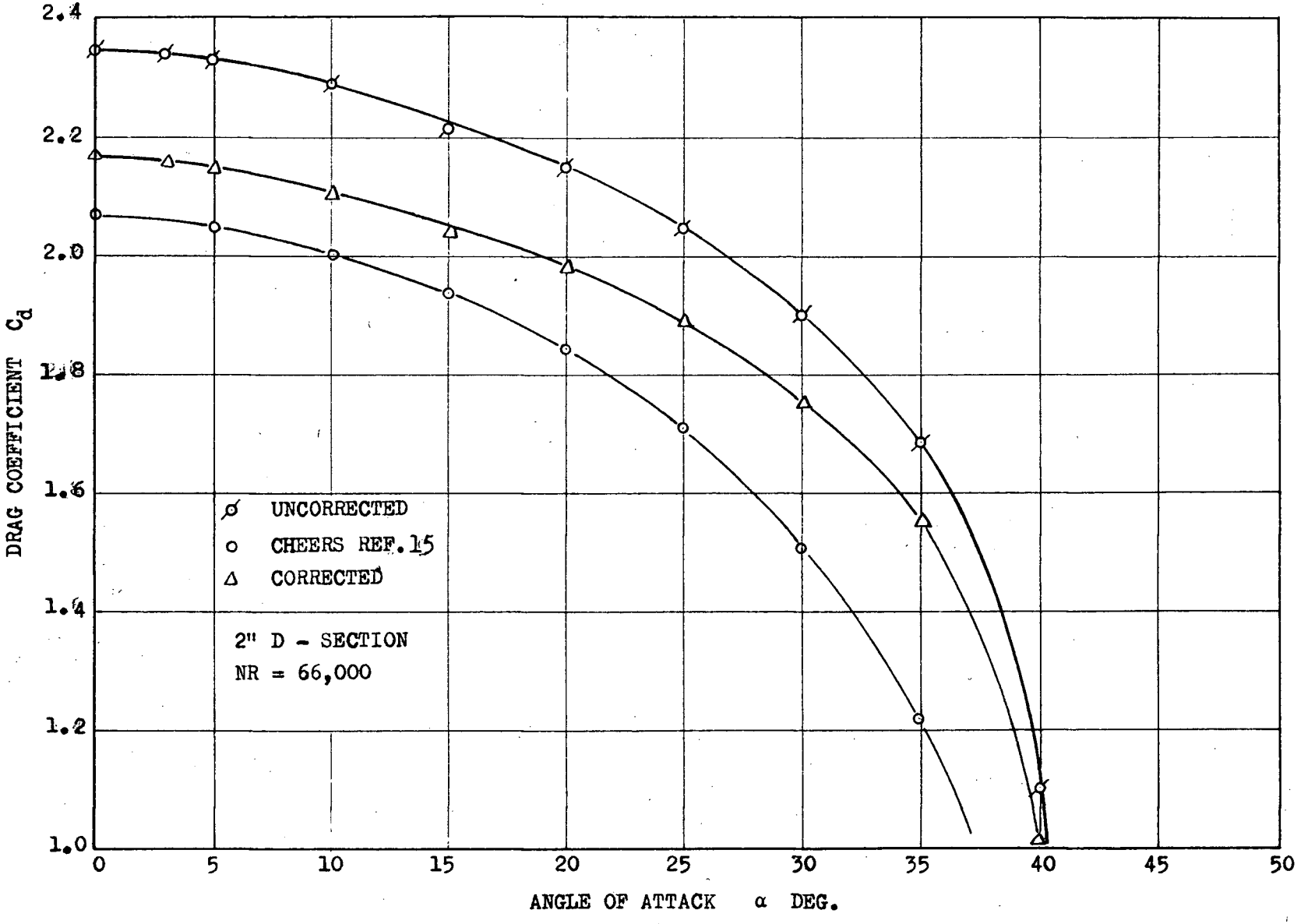

FIGURE 29 - SECTIONAL DRAG COEFFICIENT FOR 2 - DIMENSIONAL D - SECTION.

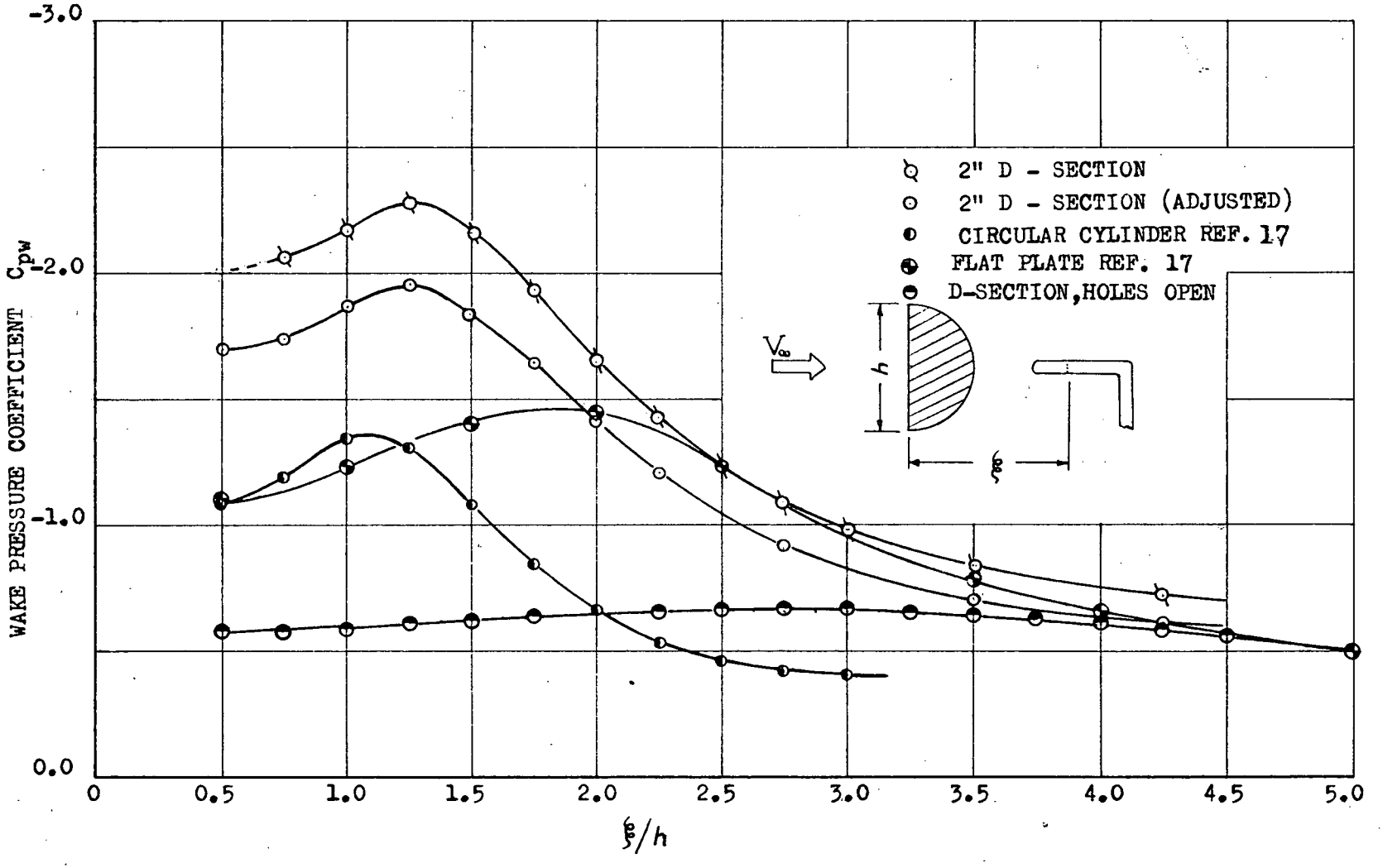

FIGURE 30 - PRESSURE ON CENTERLINE OF WAKE DOWNSTREAM OF VARIOUS CYLINDERS

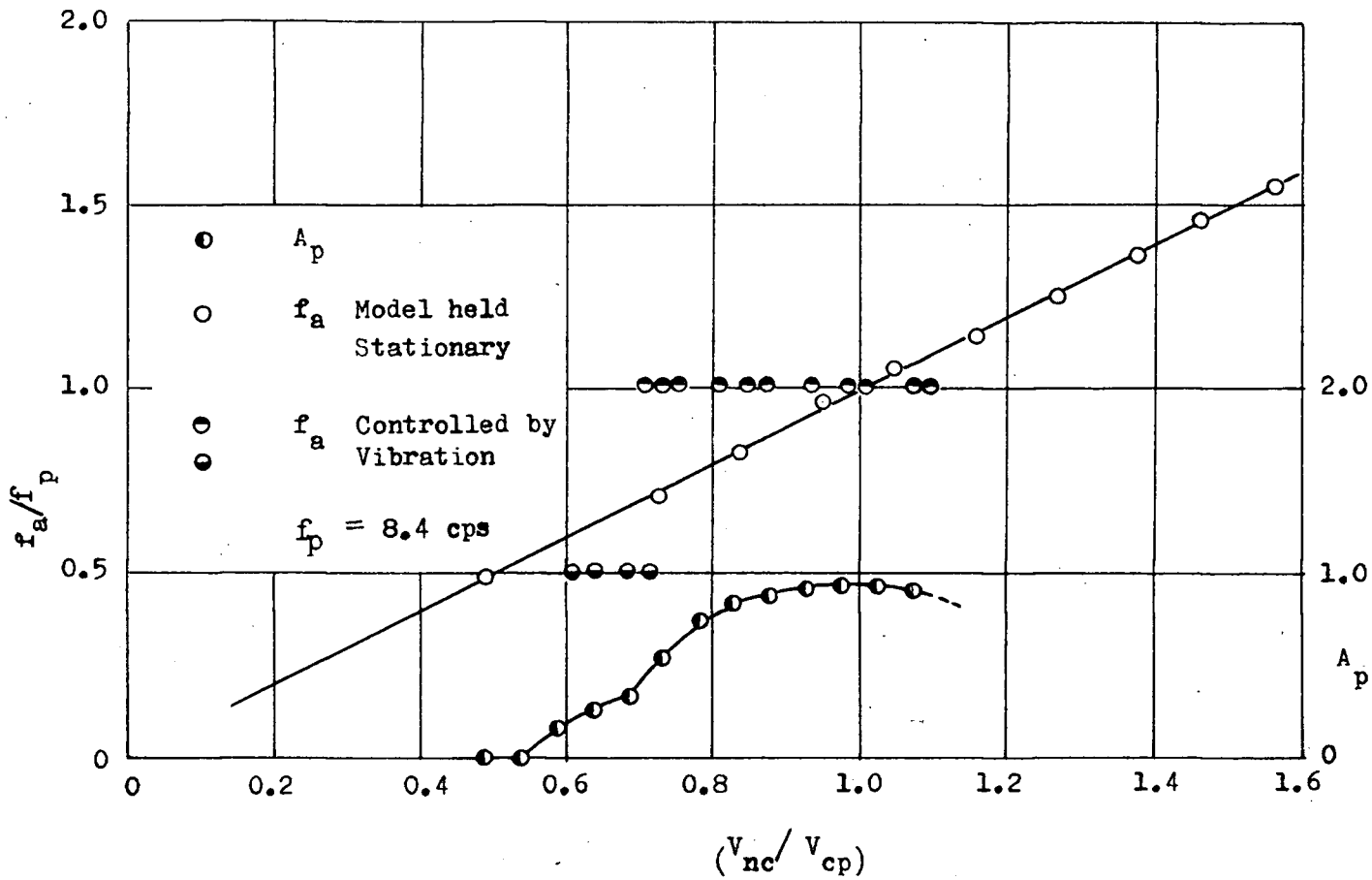

Figure 31 - AMPLITUDE AND VORTEX FREQUENCY OF D-SECTION - PLUNGING MODE

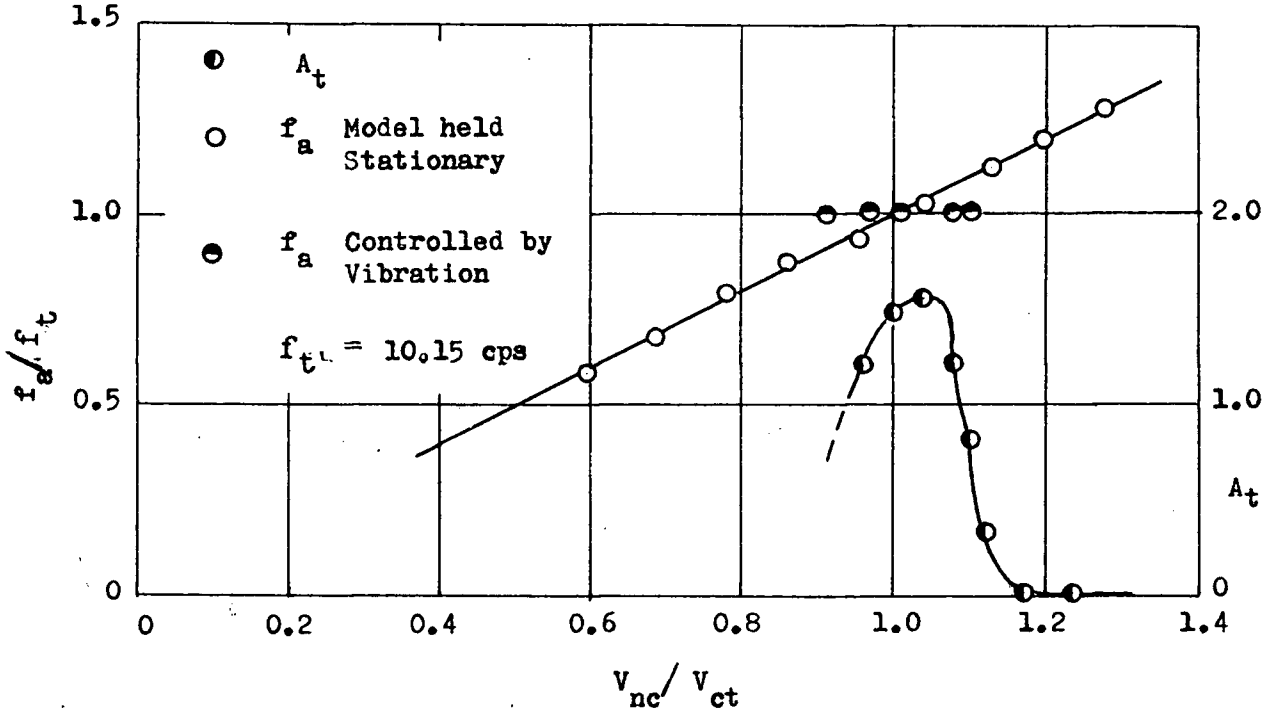

FIGURE 32 - AMPLITUDE AND VORTEX FREQUENCY OF D-SECTION - TORSIONAL MODE

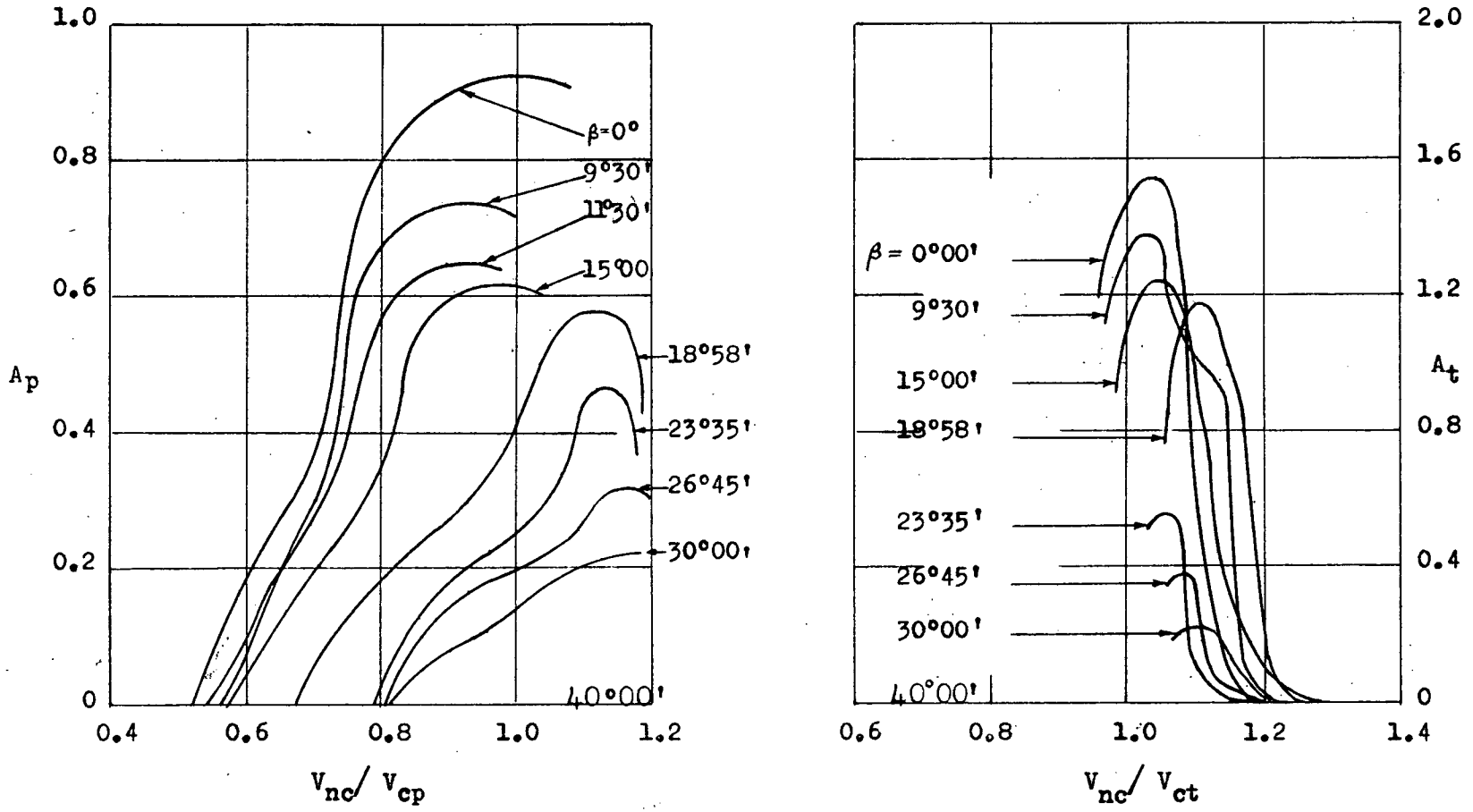

FIGURE 33 - PLUNGING AND TORSIONAL AMPLITUDES FOR D-SECTION AT VARIOUS ANGLES OF ATTACK (β)

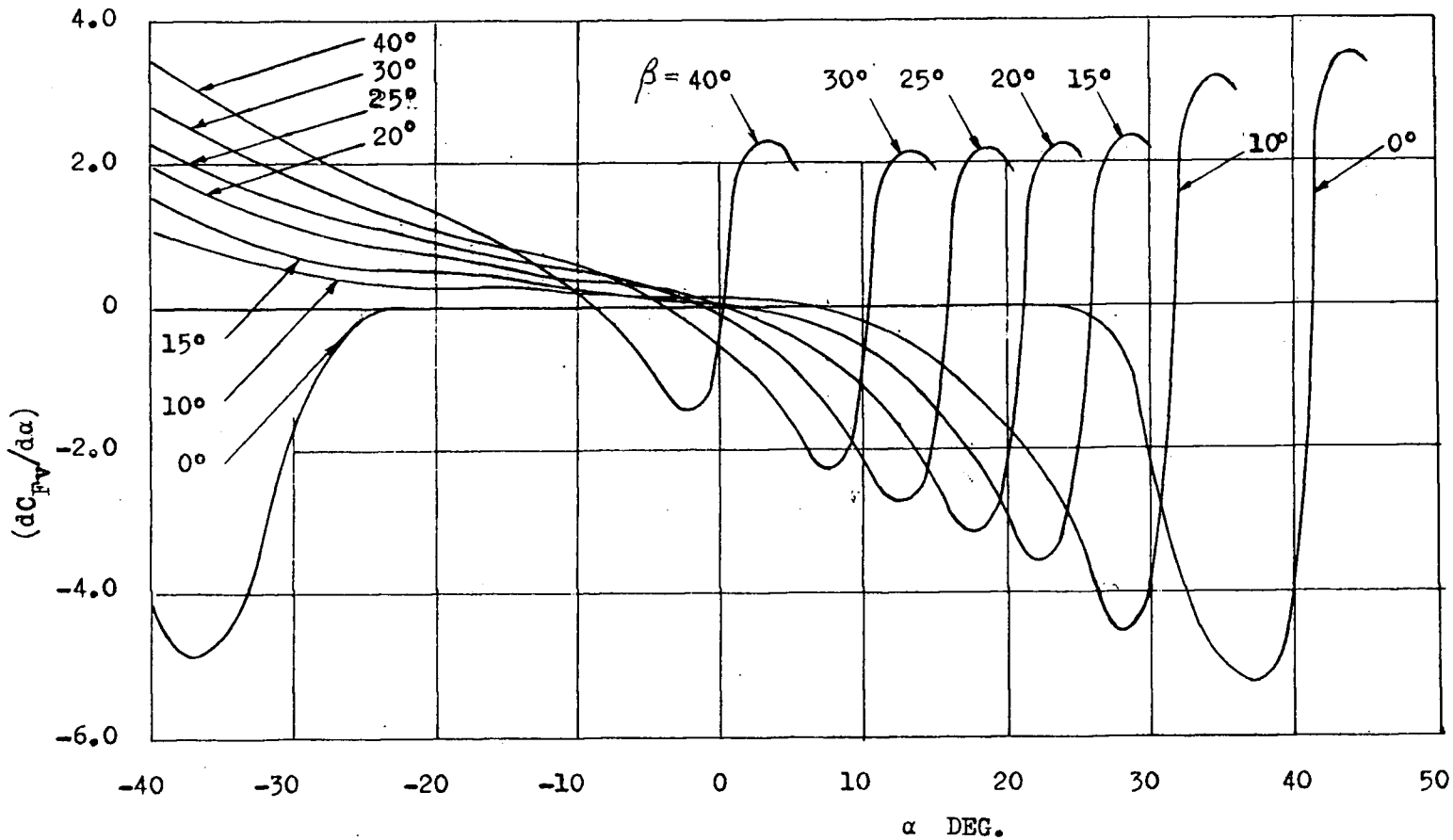

FIGURE 34 - $dC_{Fv}/d\alpha$ FOR D-SECTION CYLINDER

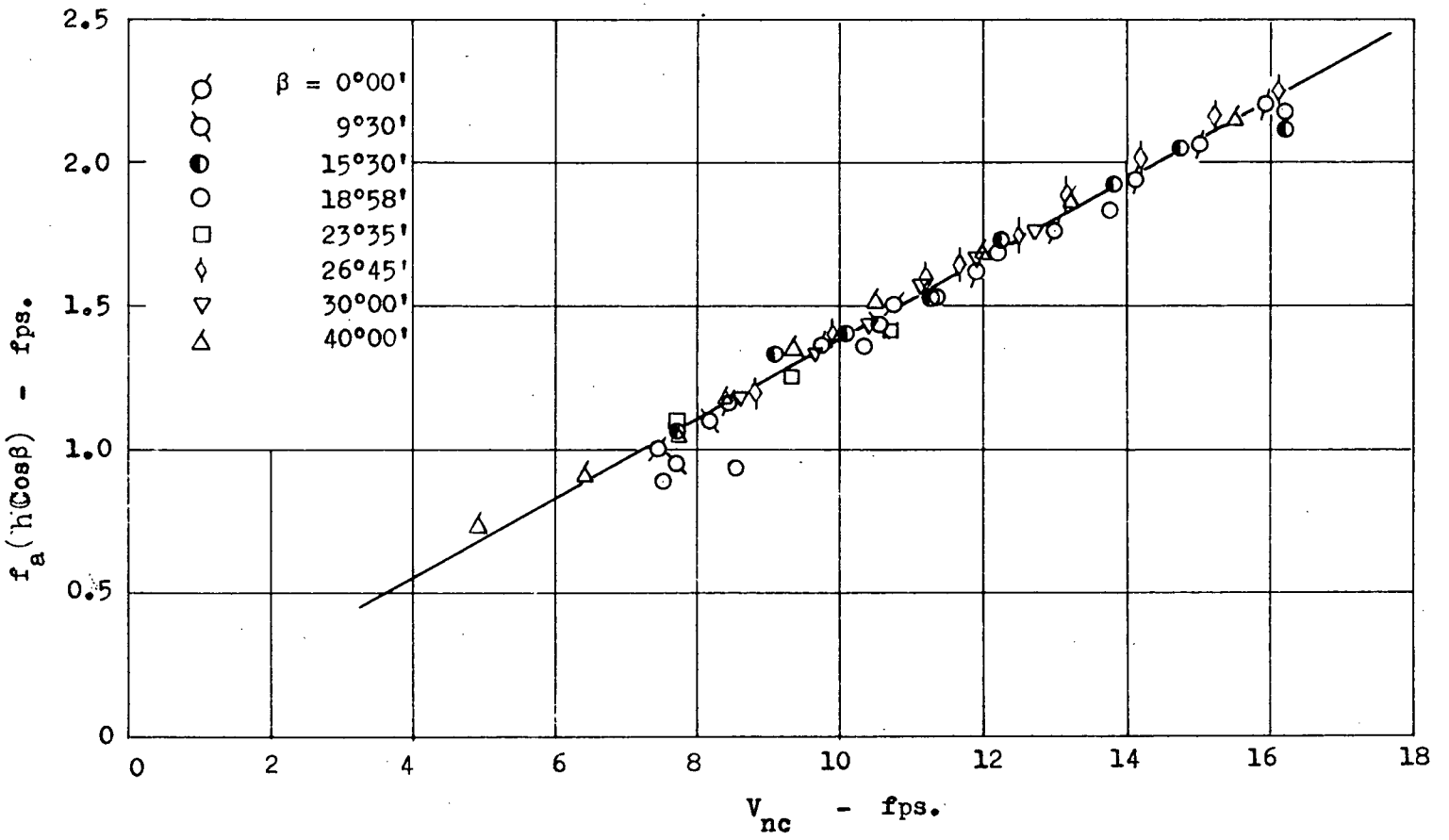

FIGURE 35 - STROUHAL NUMBER FOR D-SECTION CYLINDER AT VARIOUS β

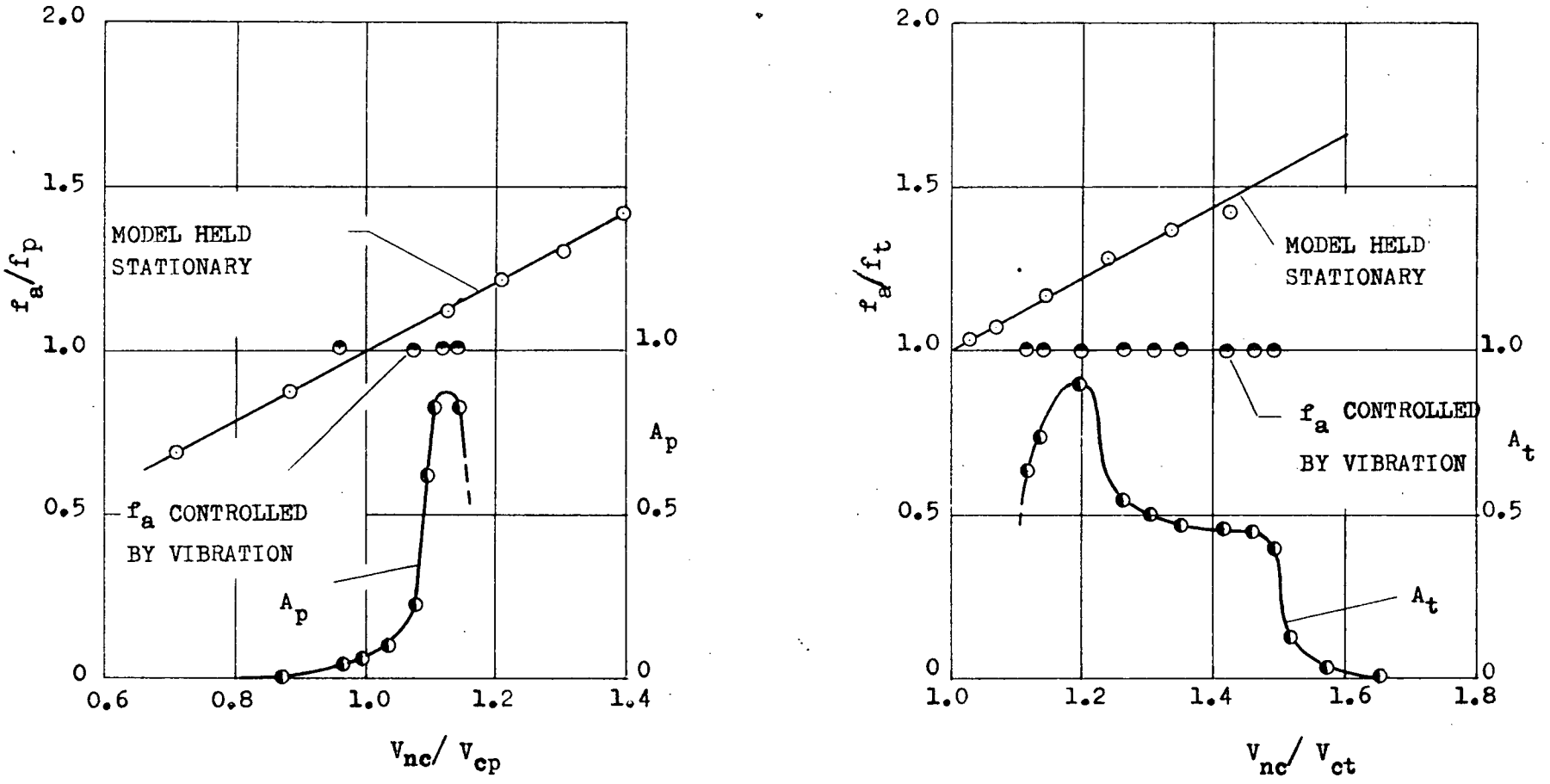

FIGURE 36 - PLUNGING AND TORSIONAL MODES FOR CIRCULAR CYLINDER

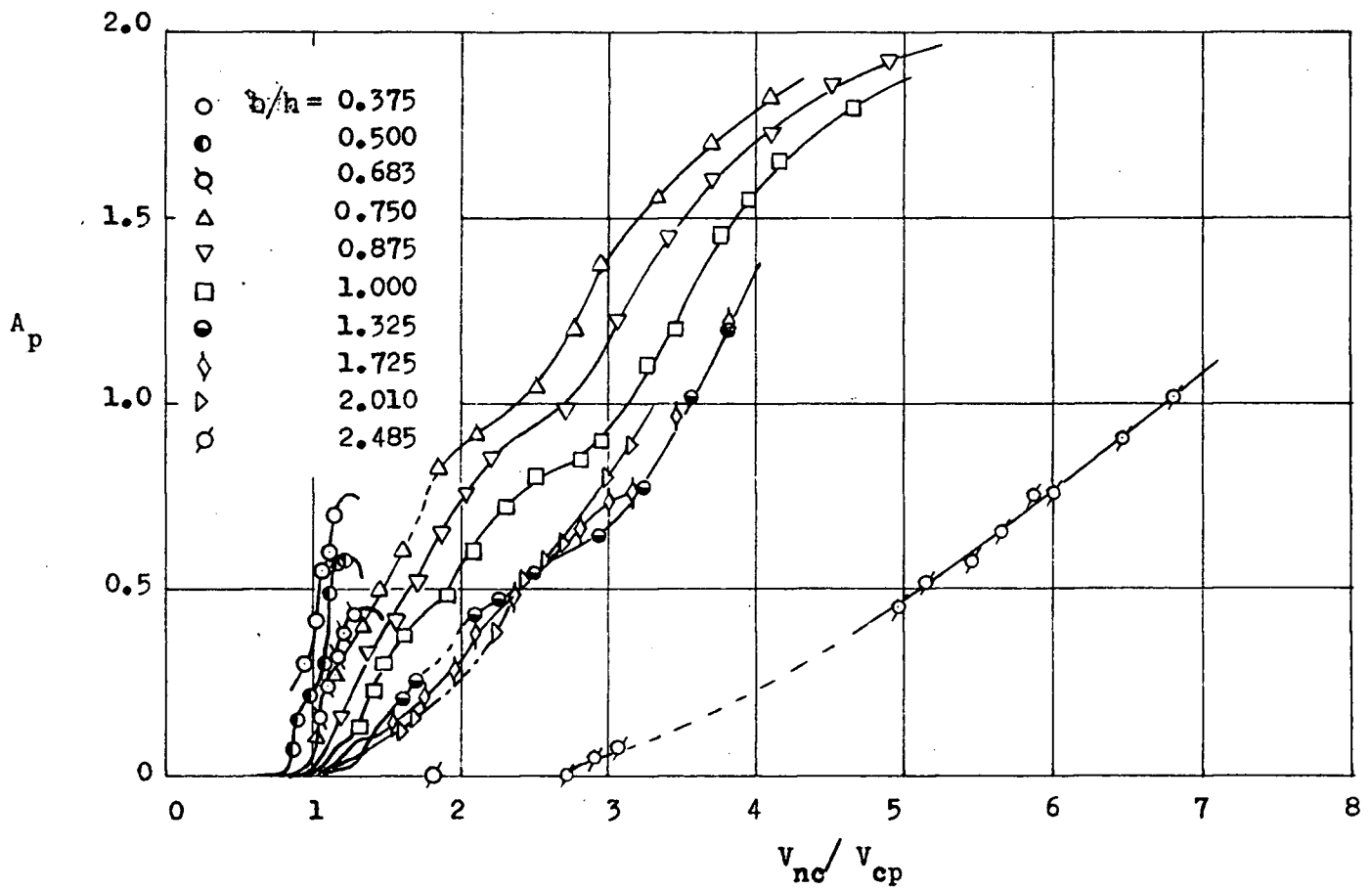

FIGURE 37 - AMPLITUDE VARIATION FOR RECTANGULAR CYLINDERS (PLUNGING MODE)

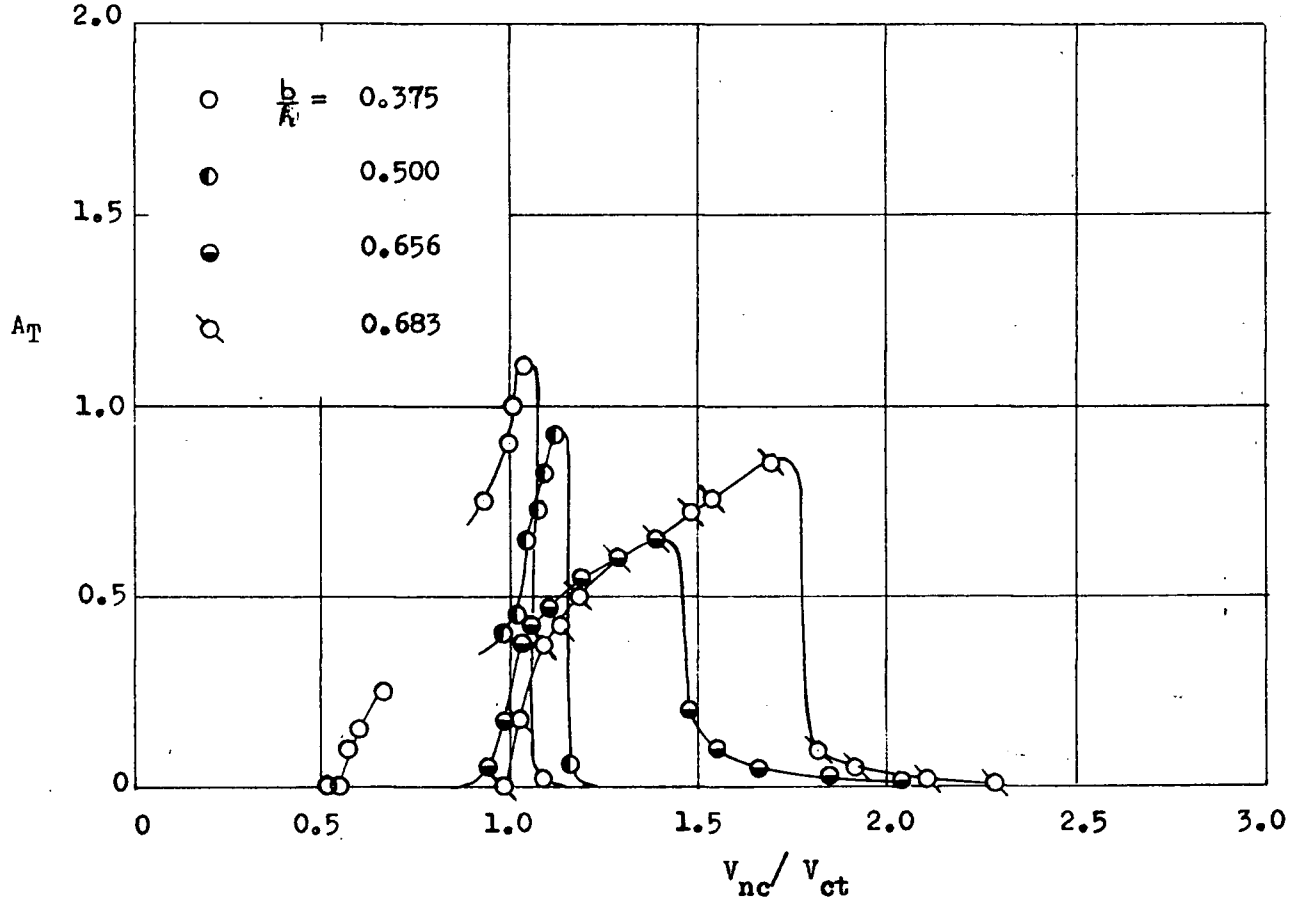

FIGURE 38 - AMPLITUDE VARIATION FOR RECTANGULAR CYLINDERS (TORSIONAL MODE)

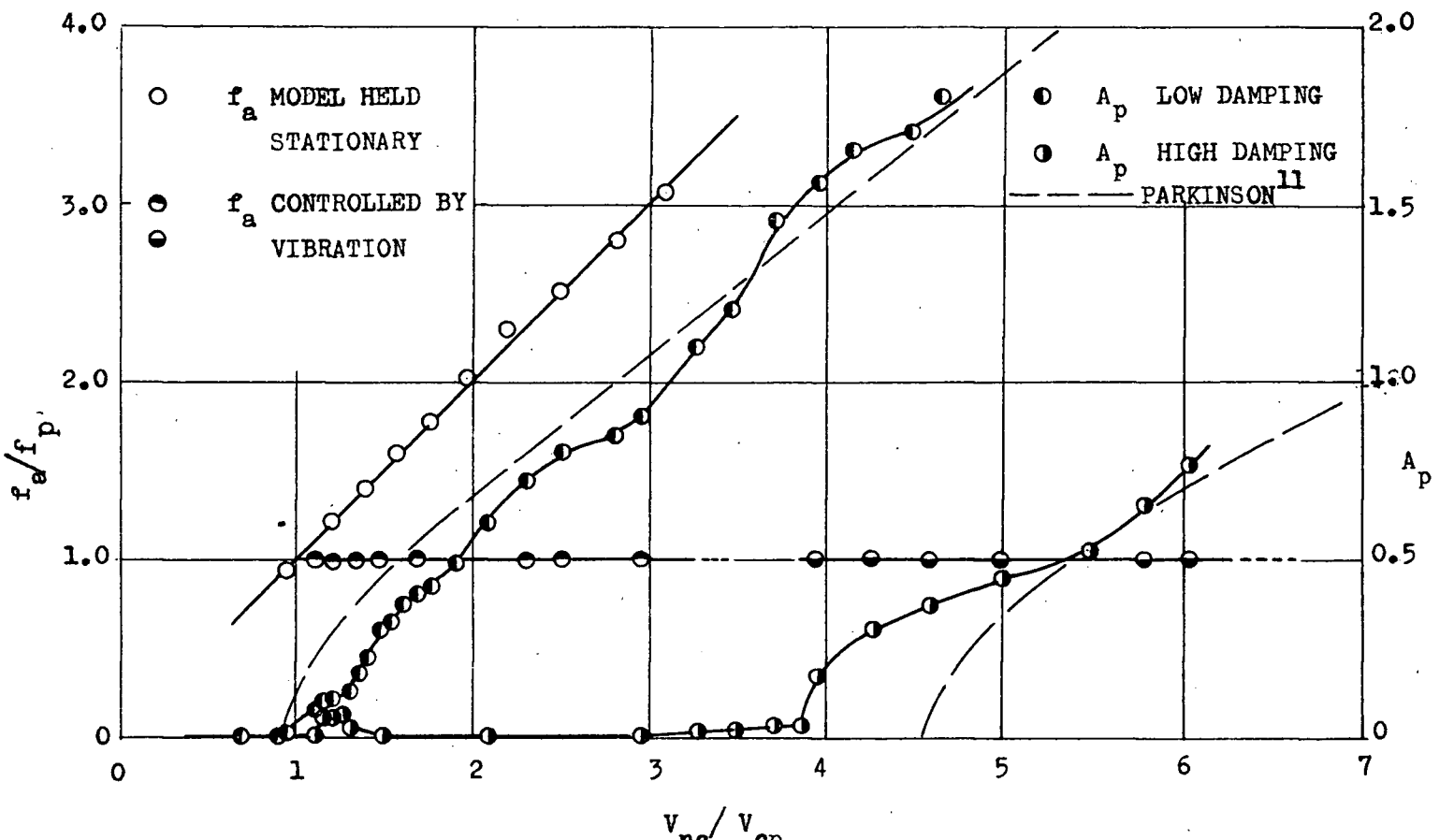

FIGURE 39 - AMPLITUDE AND VORTEX FREQUENCY FOR SQUARE SECTION - (PLUNGING MODE)

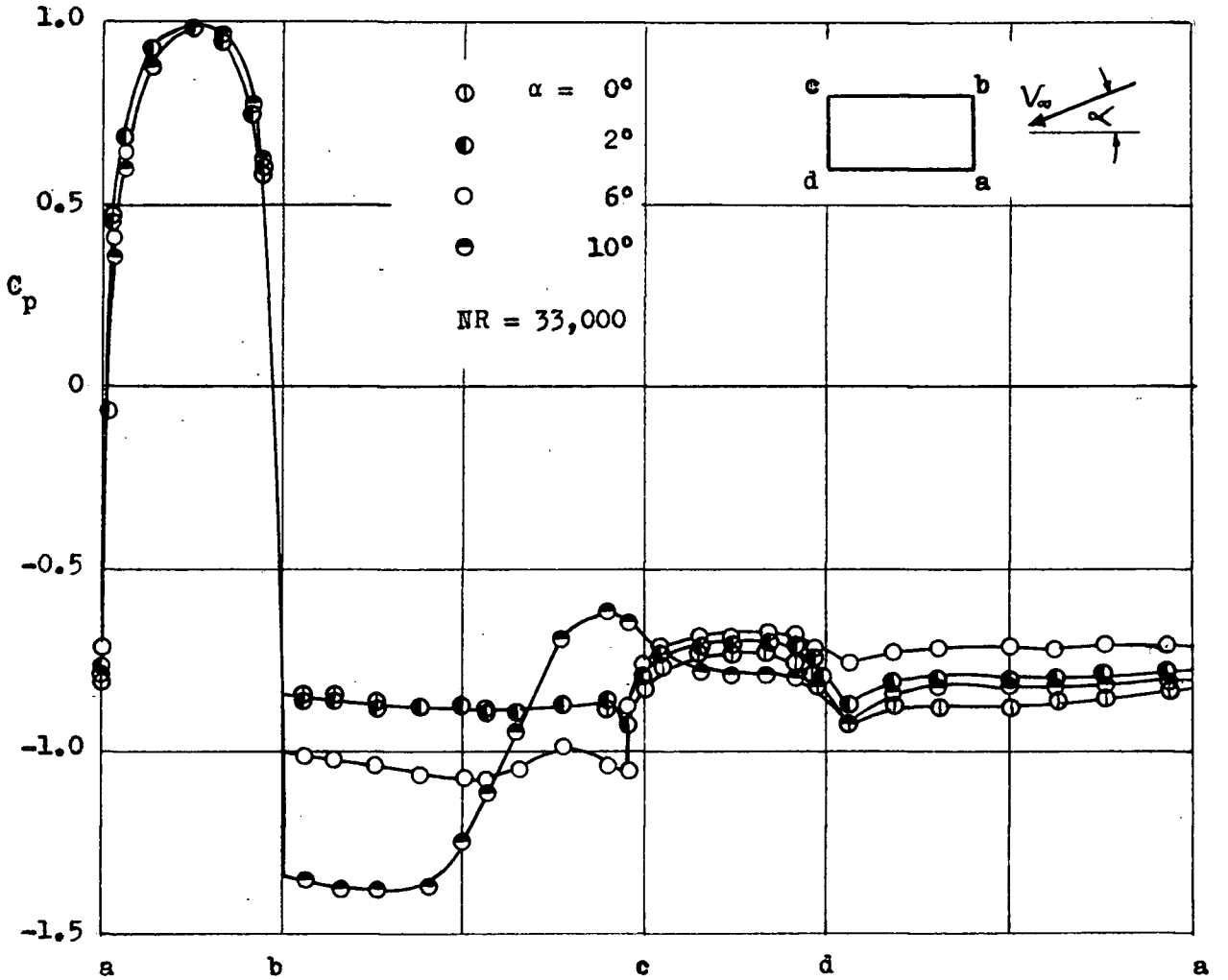

FIGURE 40 - C_p ON 2:1 RECTANGLE AT VARIOUS α

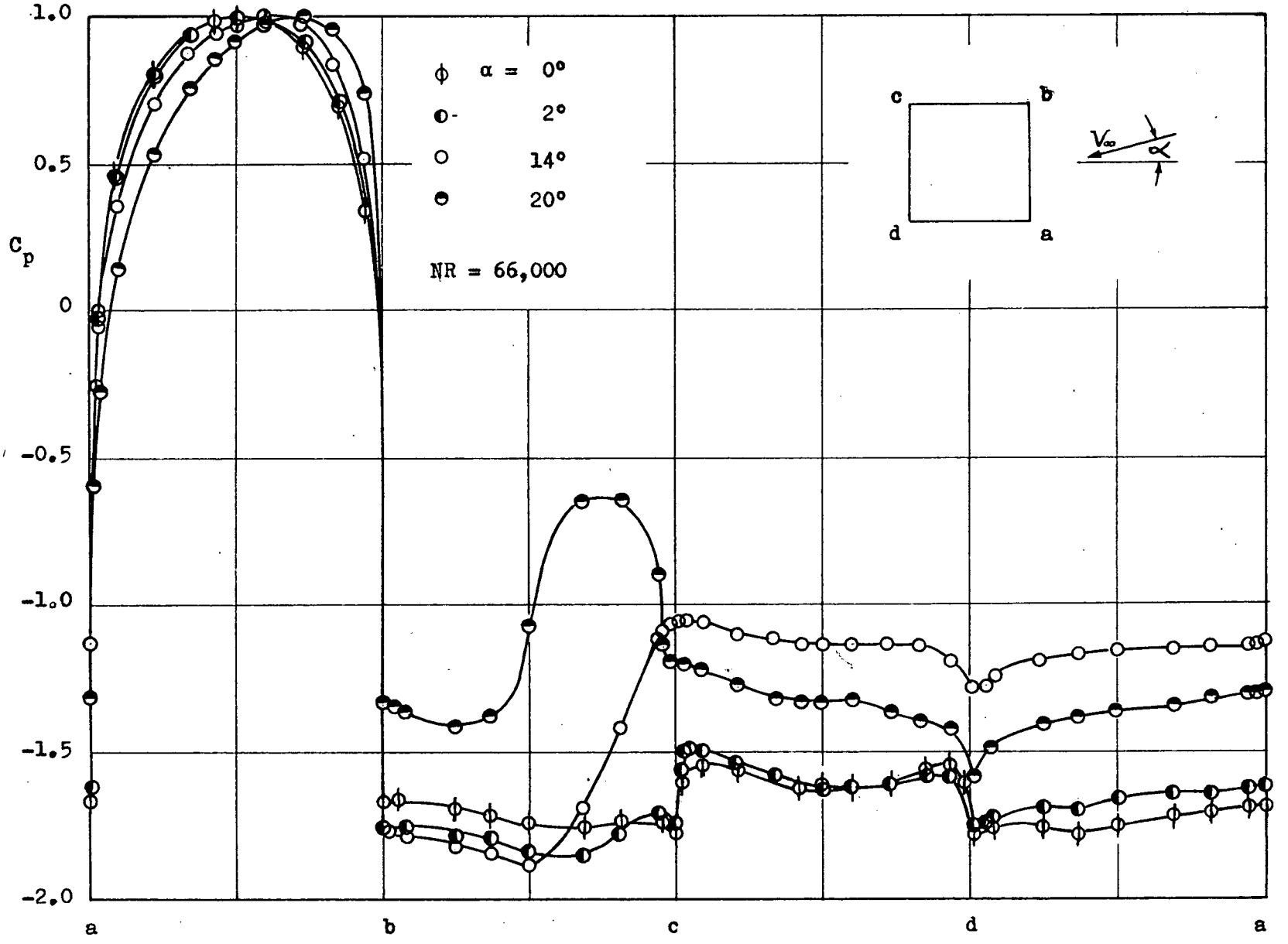

FIGURE 41 - C_p ON SQUARE CYLINDER FOR VARIOUS α

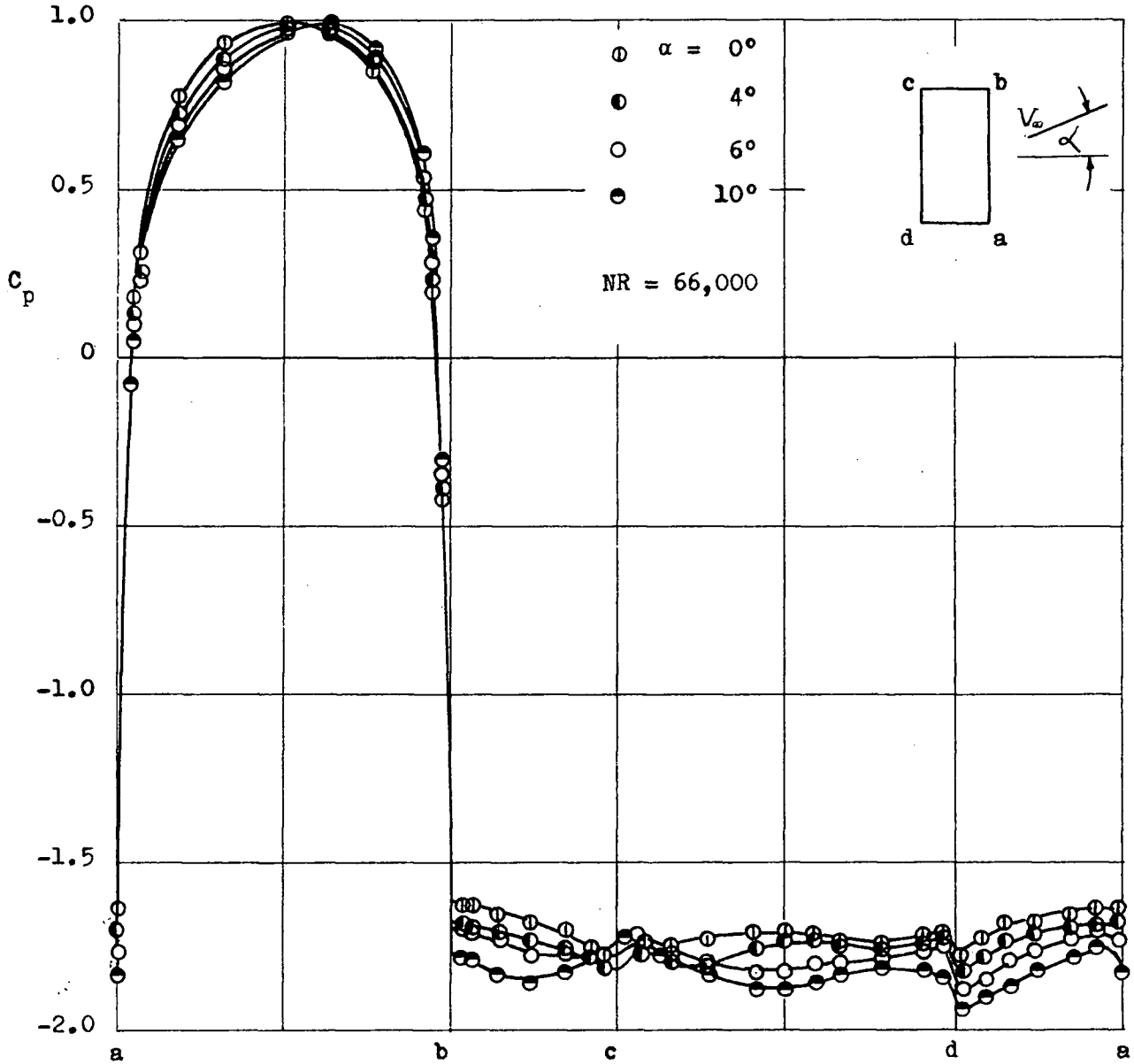

FIGURE 42 - C_p ON 1:2 RECTANGLE FOR VARIOUS α

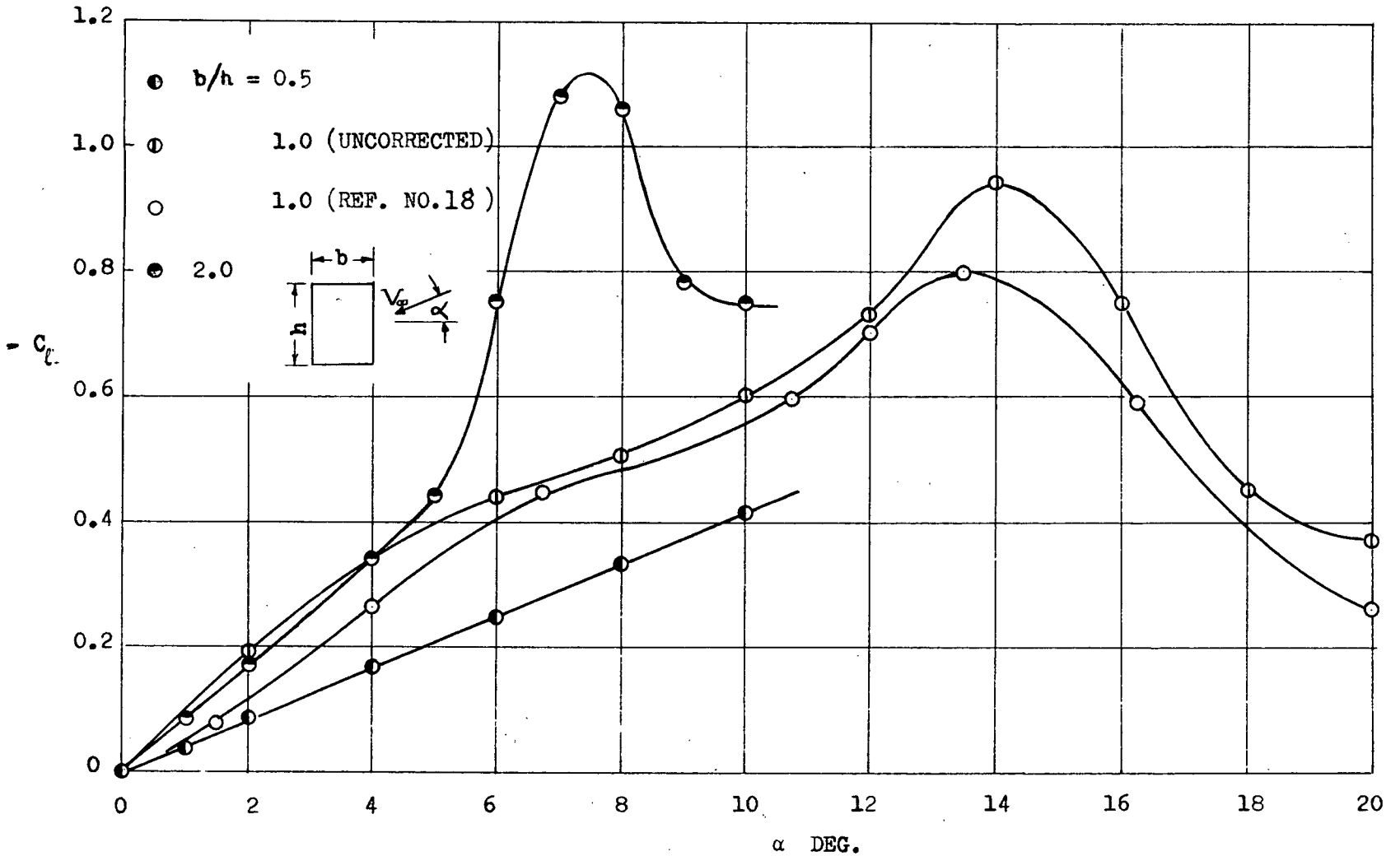

FIGURE 43- SECTIONAL LIFT COEFFICIENTS FOR RECTANGULAR CYLINDERS

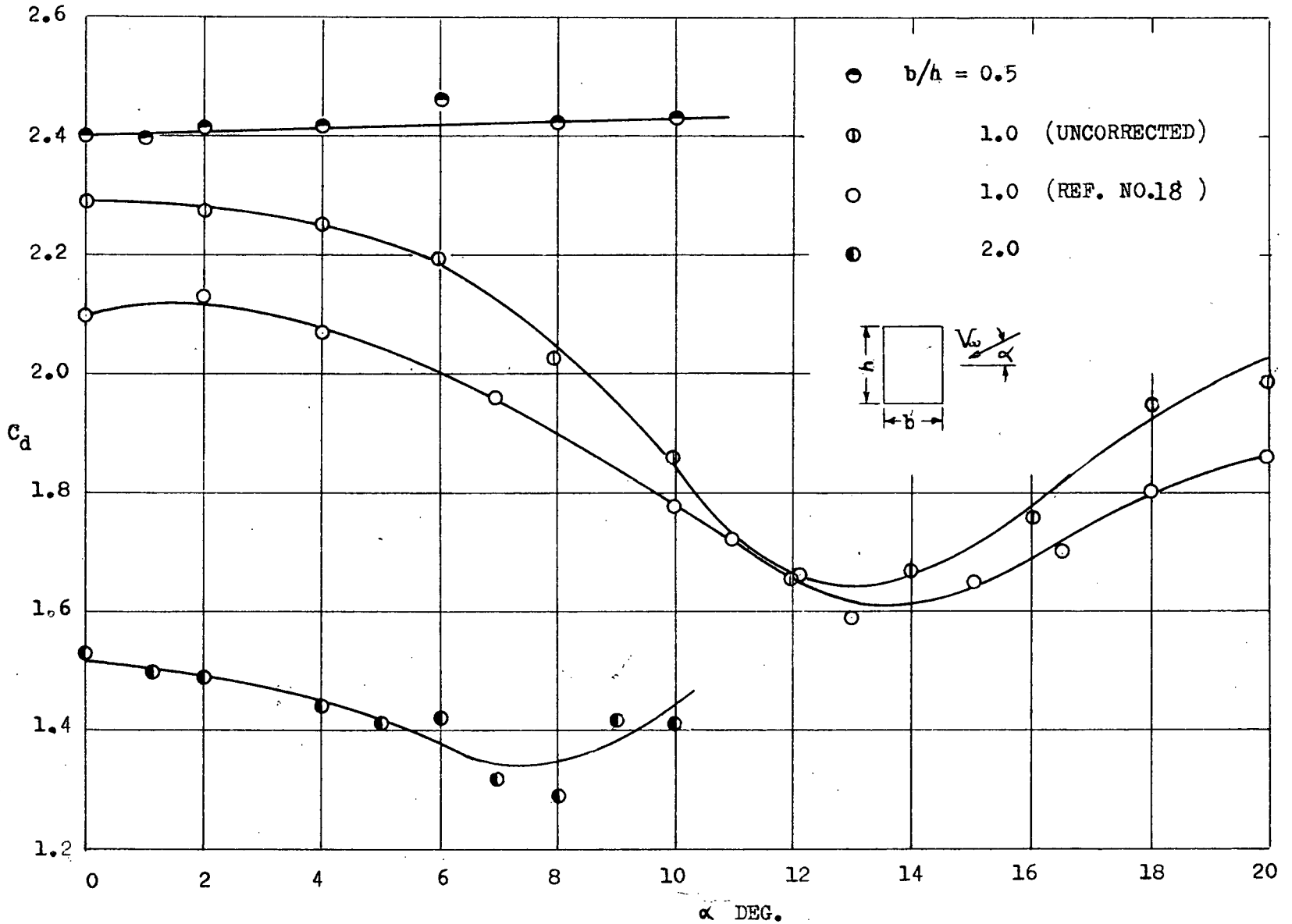

FIGURE 44 - SECTIONAL DRAG COEFFICIENTS FOR RECTANGULAR CYLINDERS

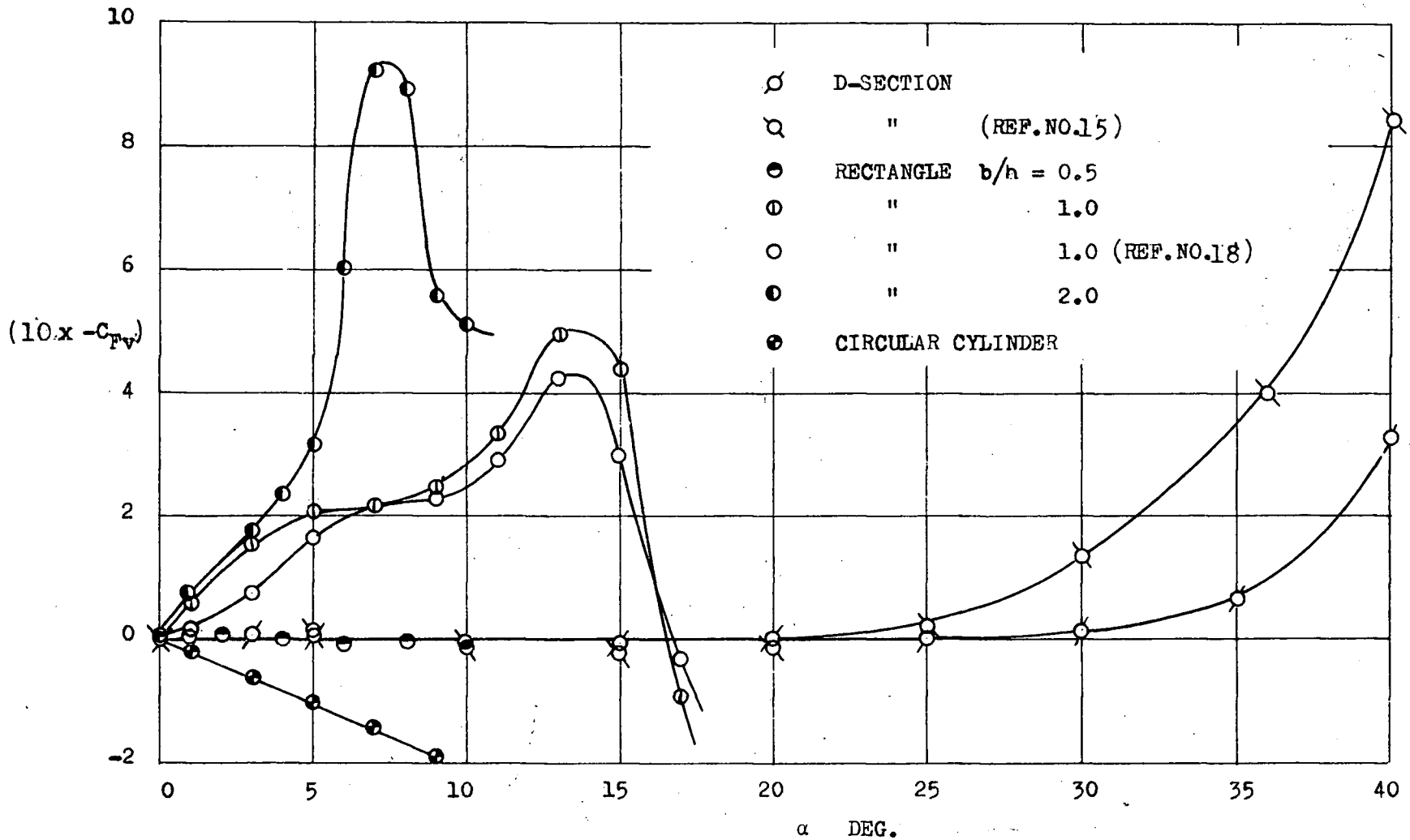

FIGURE 45- COMPARISON OF C_{F_V} FOR VARIOUS CYLINDER CROSS-SECTIONS

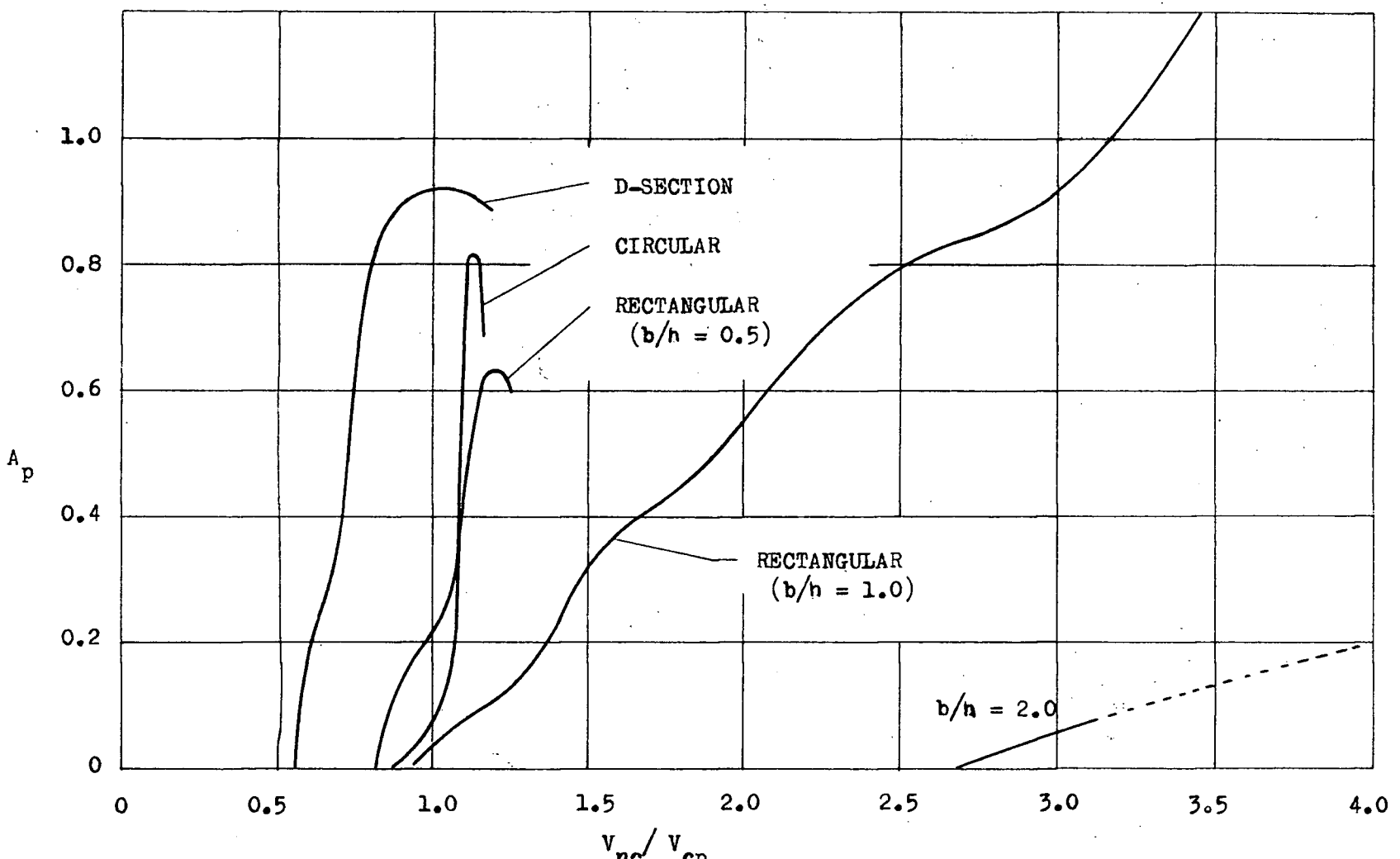

FIGURE 46 - COMPARISON OF VELOCITY - AMPLITUDE CHARACTERISTICS

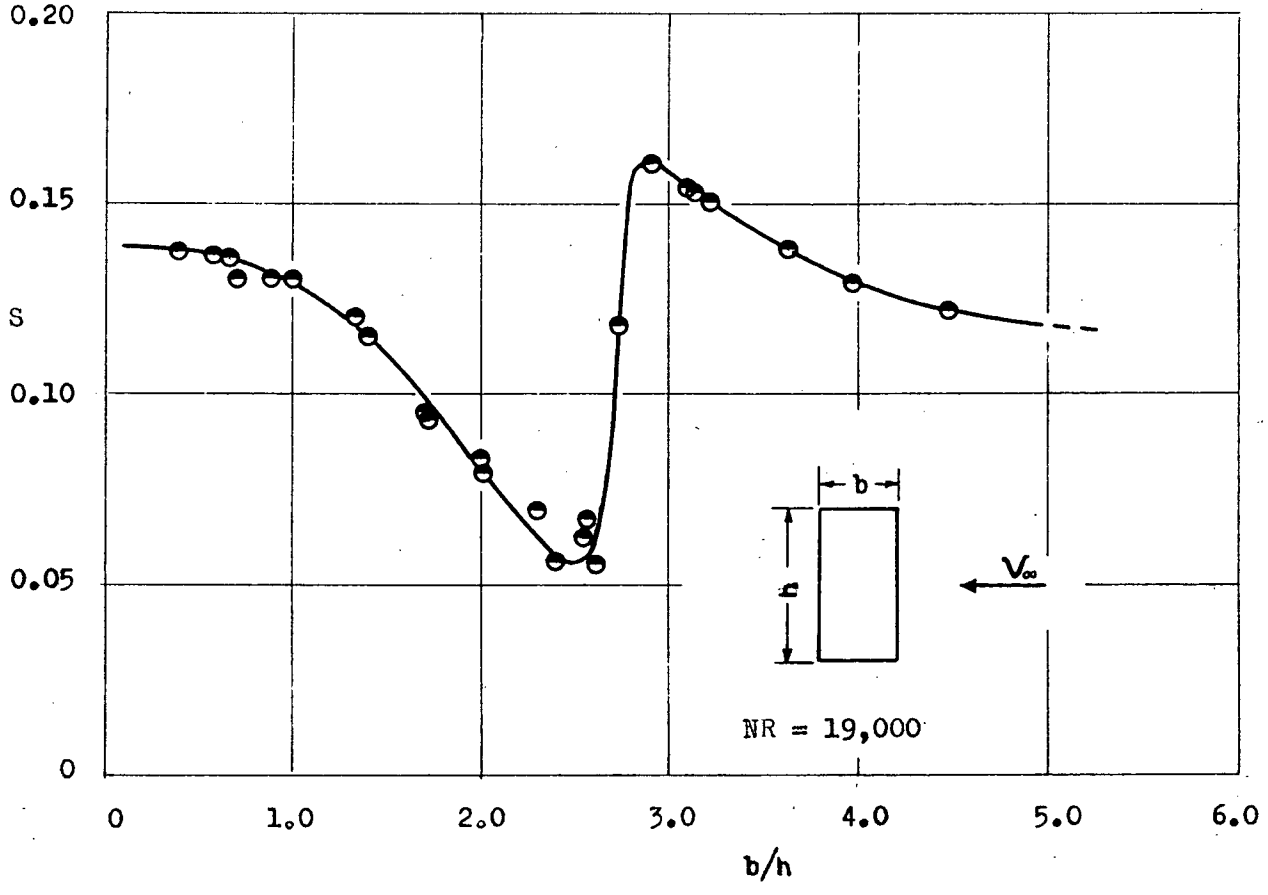

FIGURE 47 - VARIATION OF STROUHAL NUMBER WITH DEPTH OF RECTANGLE

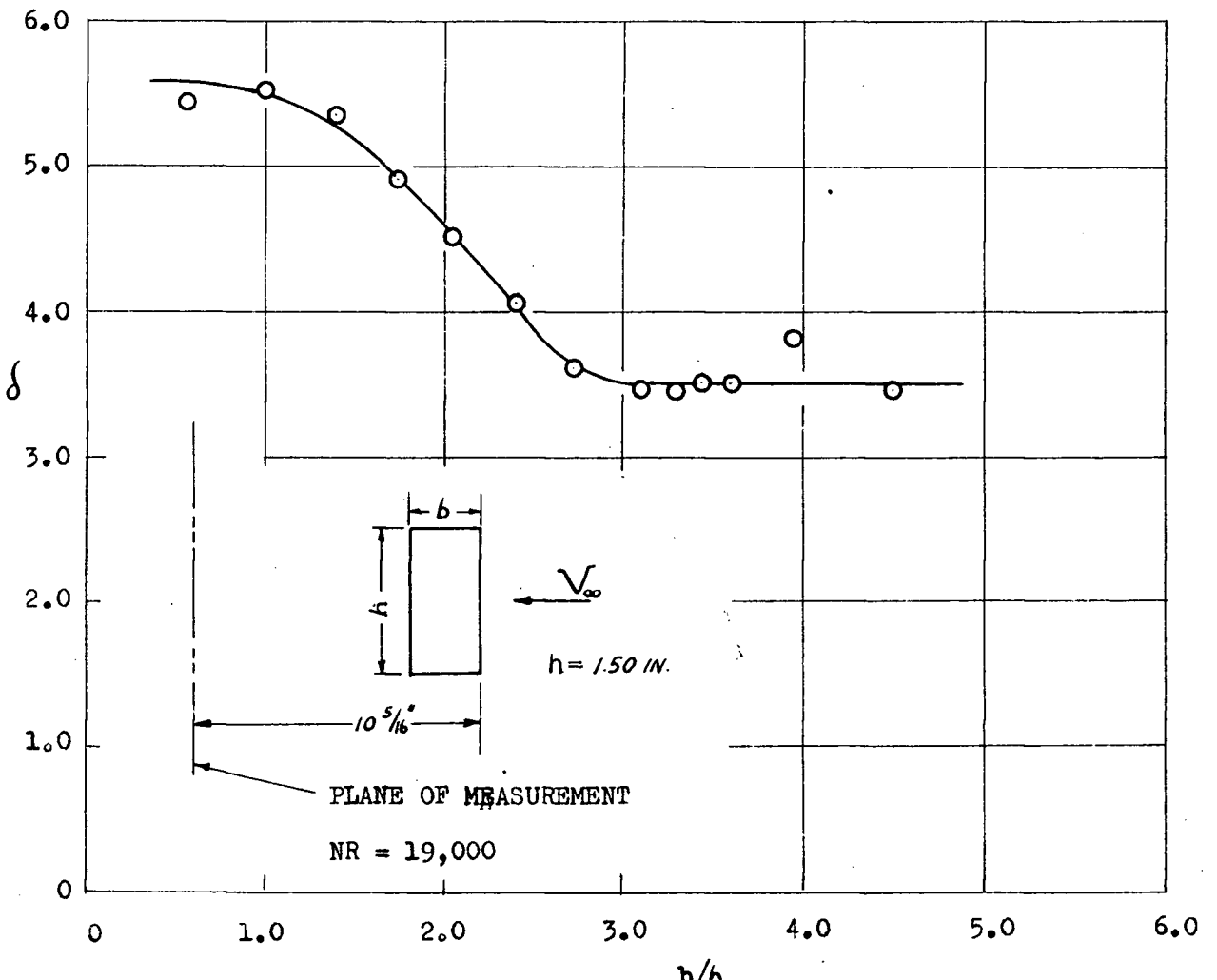

FIGURE 48 - VARIATION OF WAKE WIDTH WITH DEPTH OF RECTANGLE

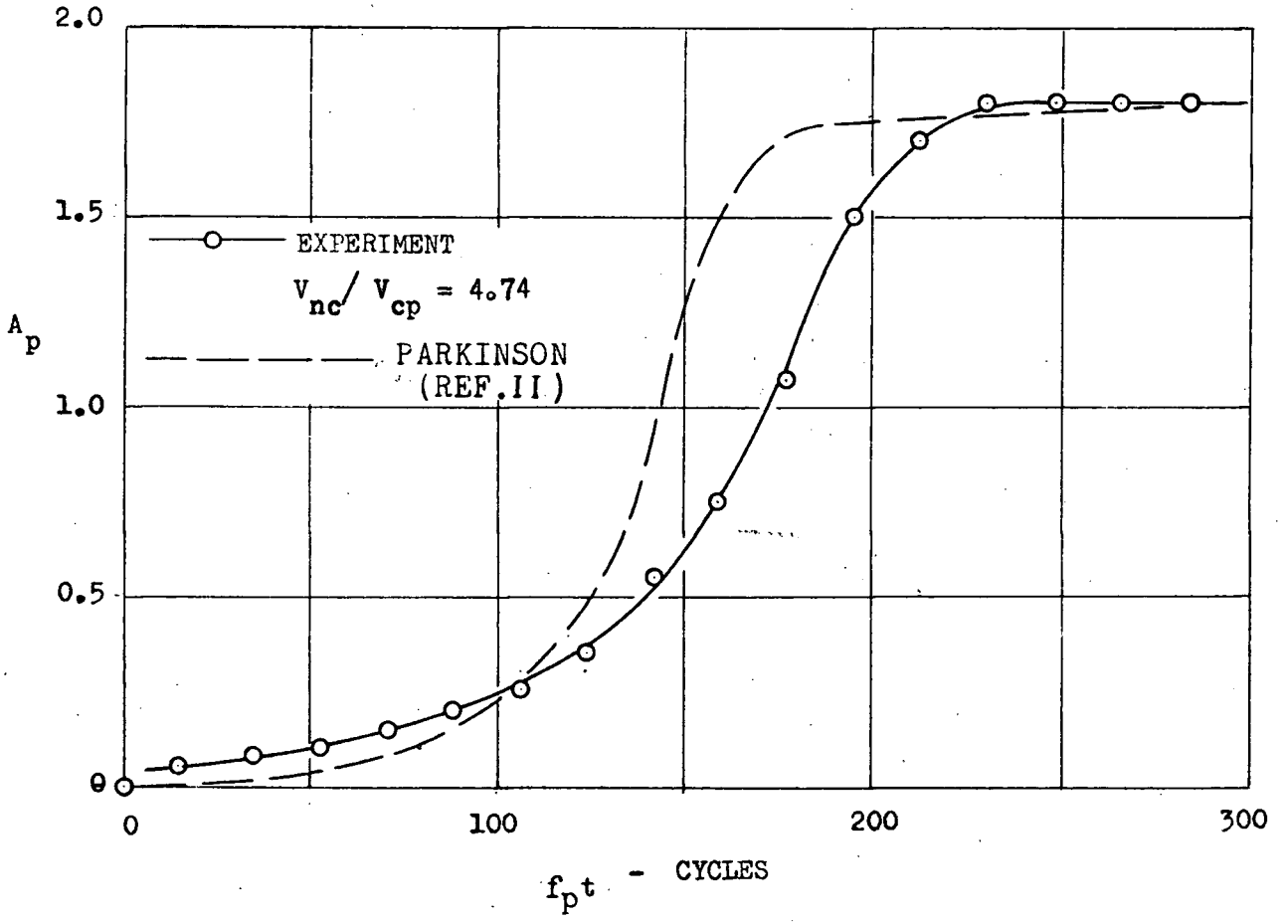

FIGURE 49 - TYPICAL TIME-AMPLITUDE CURVE FOR 1" SQUARE SECTION (f_p = 8.9 cps)

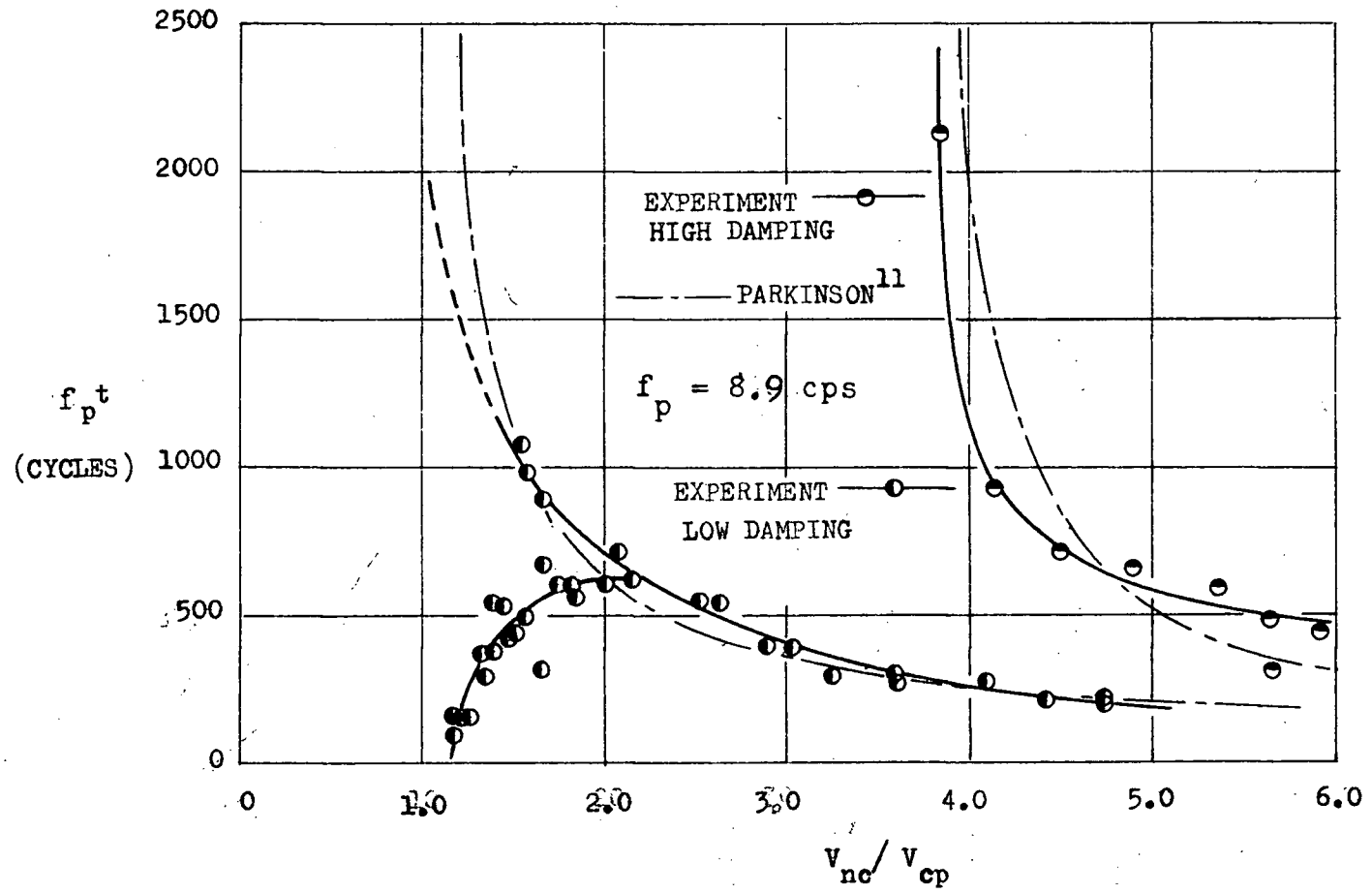

FIGURE 50 - NUMBER OF CYCLES TO MAXIMUM AMPLITUDE (b/h = 1.0)

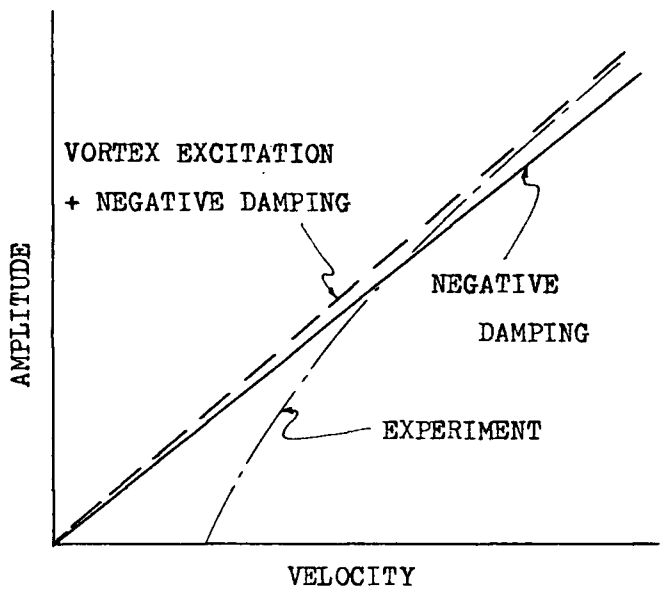

FIGURE 51

DYNAMIC RESPONSE -- GALLOPING

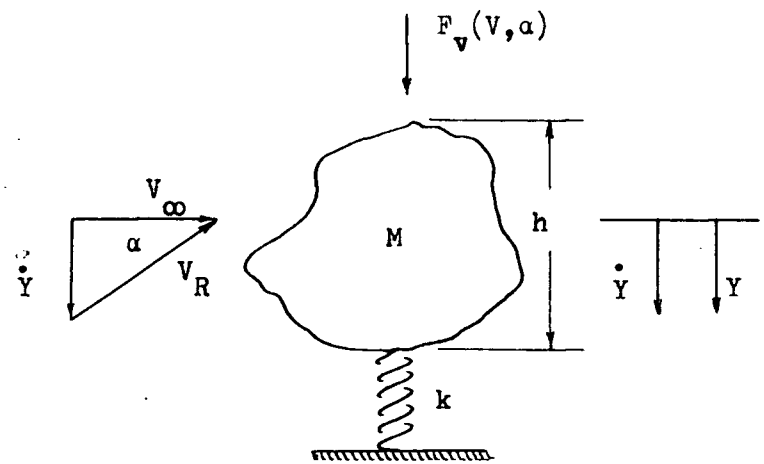

FIGURE 52

SPRING-MASS SYSTEM FOR ENERGY THEORY

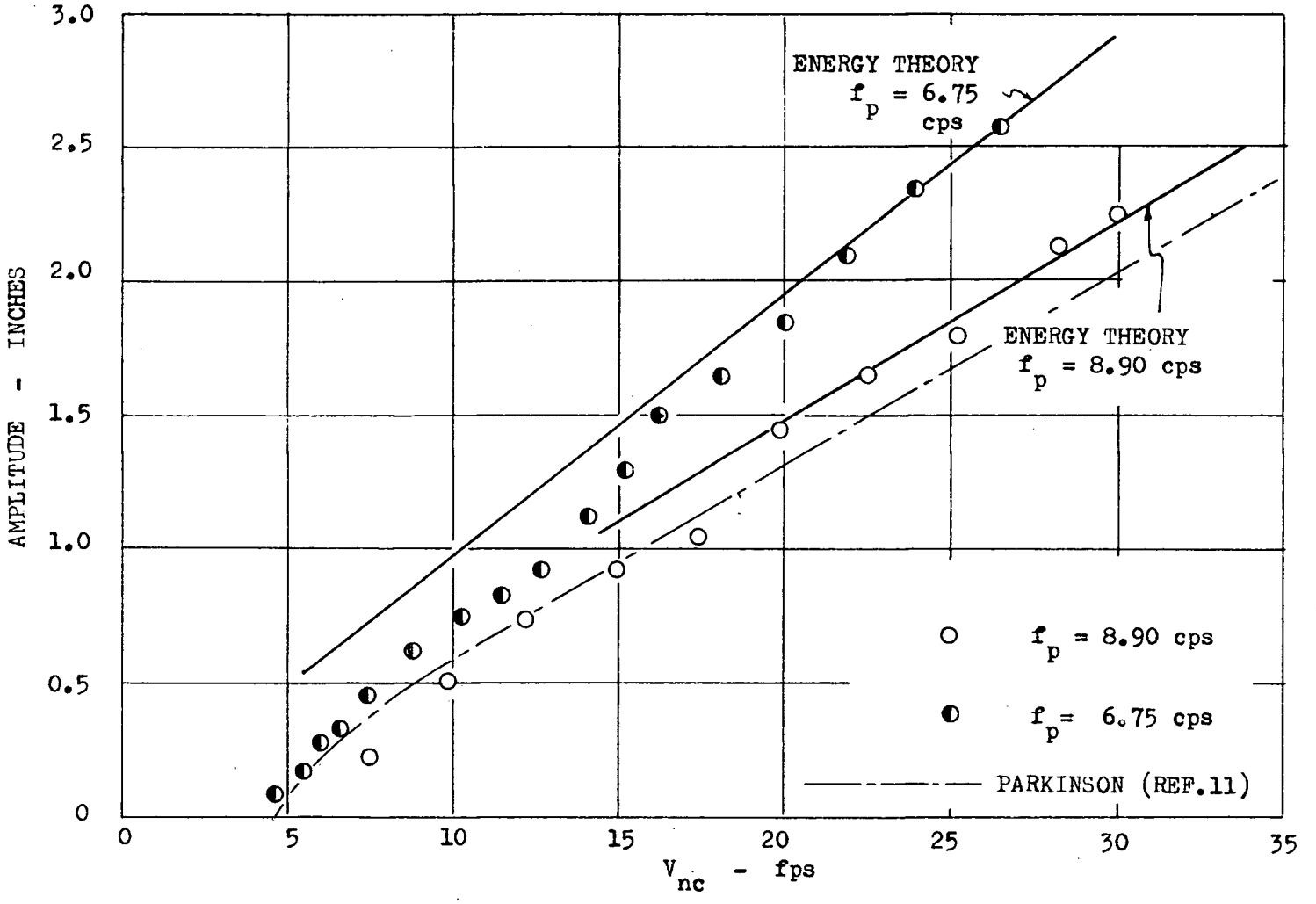

FIGURE 53 - AMPLITUDE RESPONSE FOR 1.0" SQUARE SECTION CYLINDERS

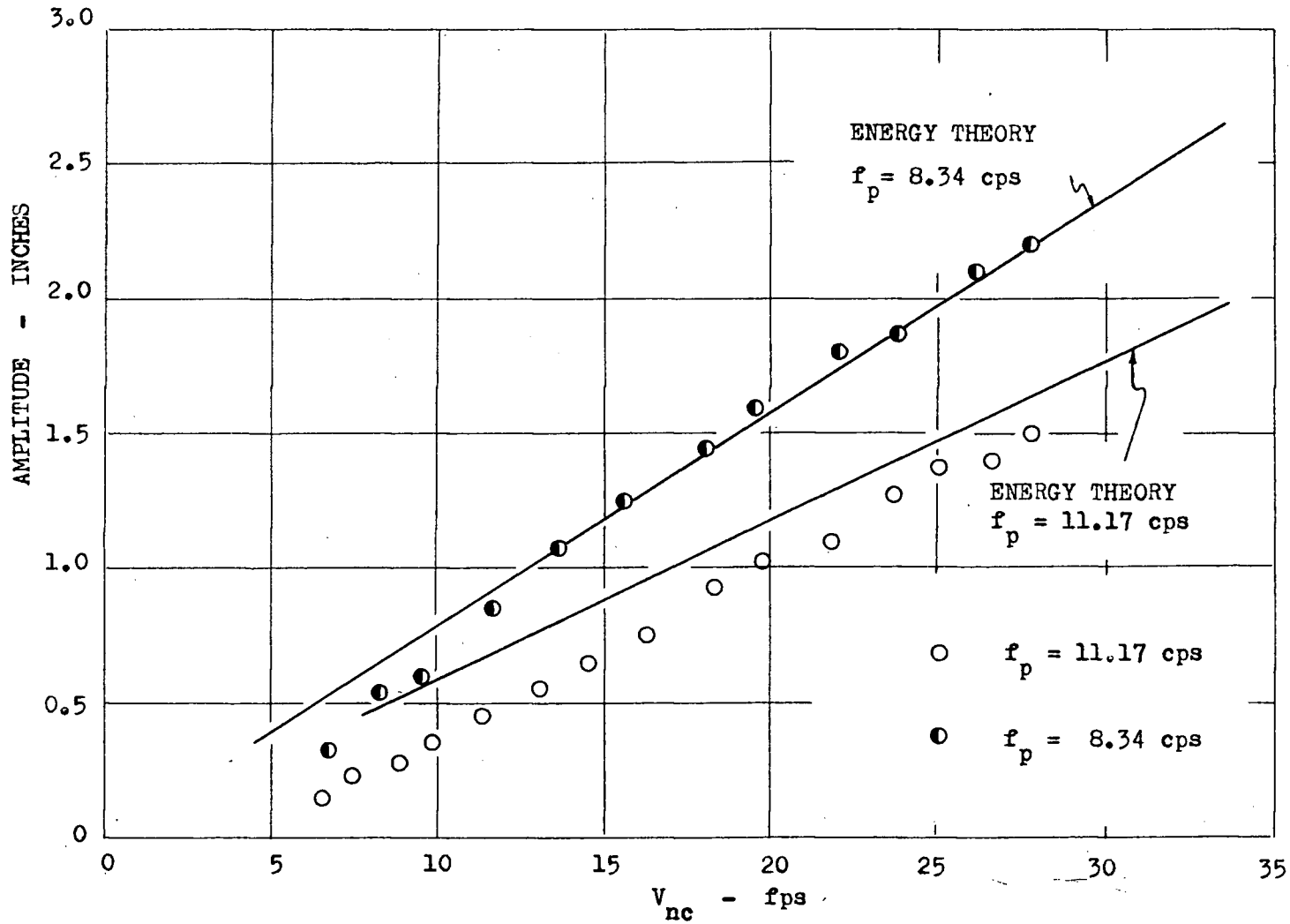

FIGURE 54 - AMPLITUDE RESPONSE FOR 0.75 " SQUARE SECTION CYLINDER

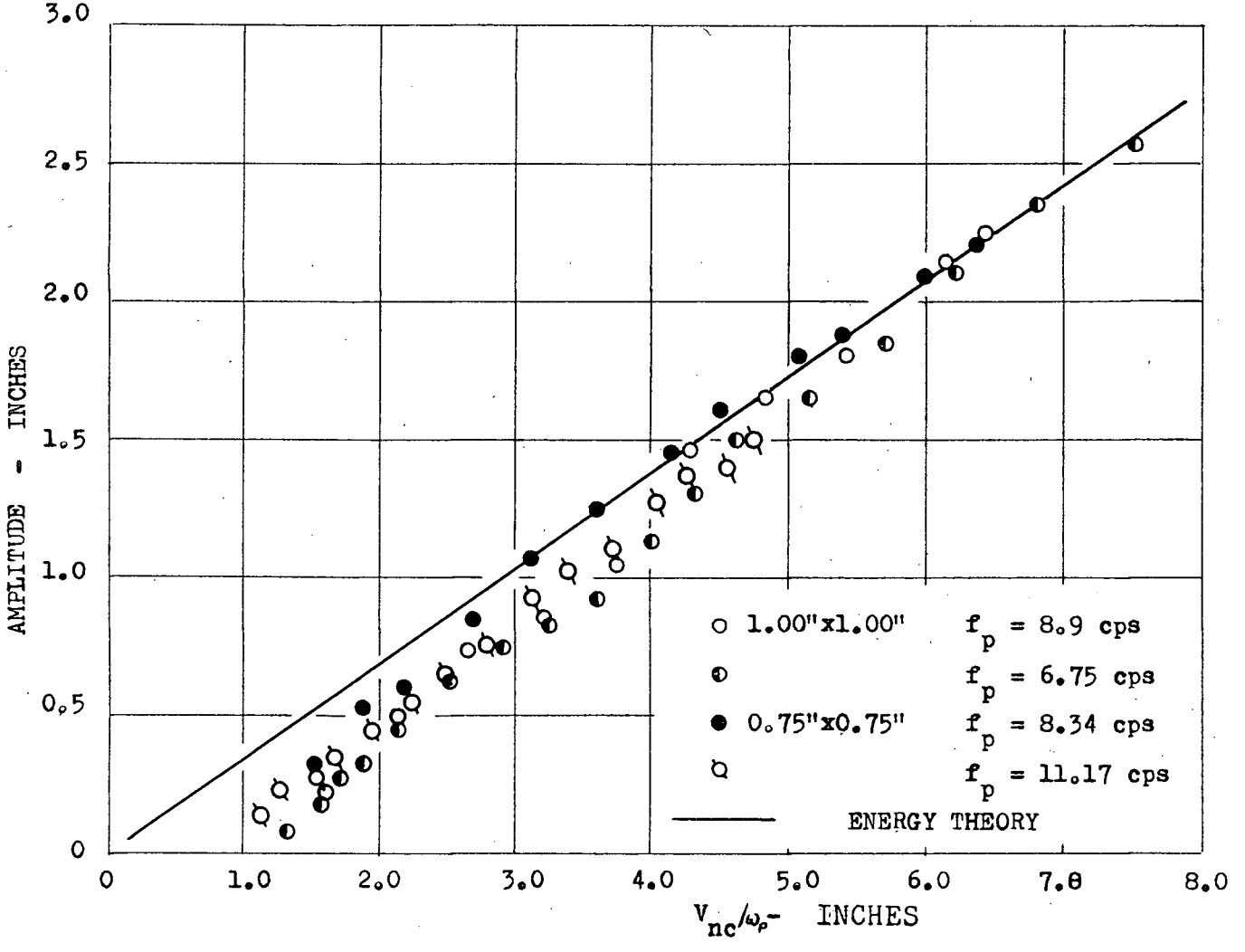

FIGURE 55 - AMPLITUDE RESPONSE FOR SEVERAL SQUARE SECTION CYLINDERS

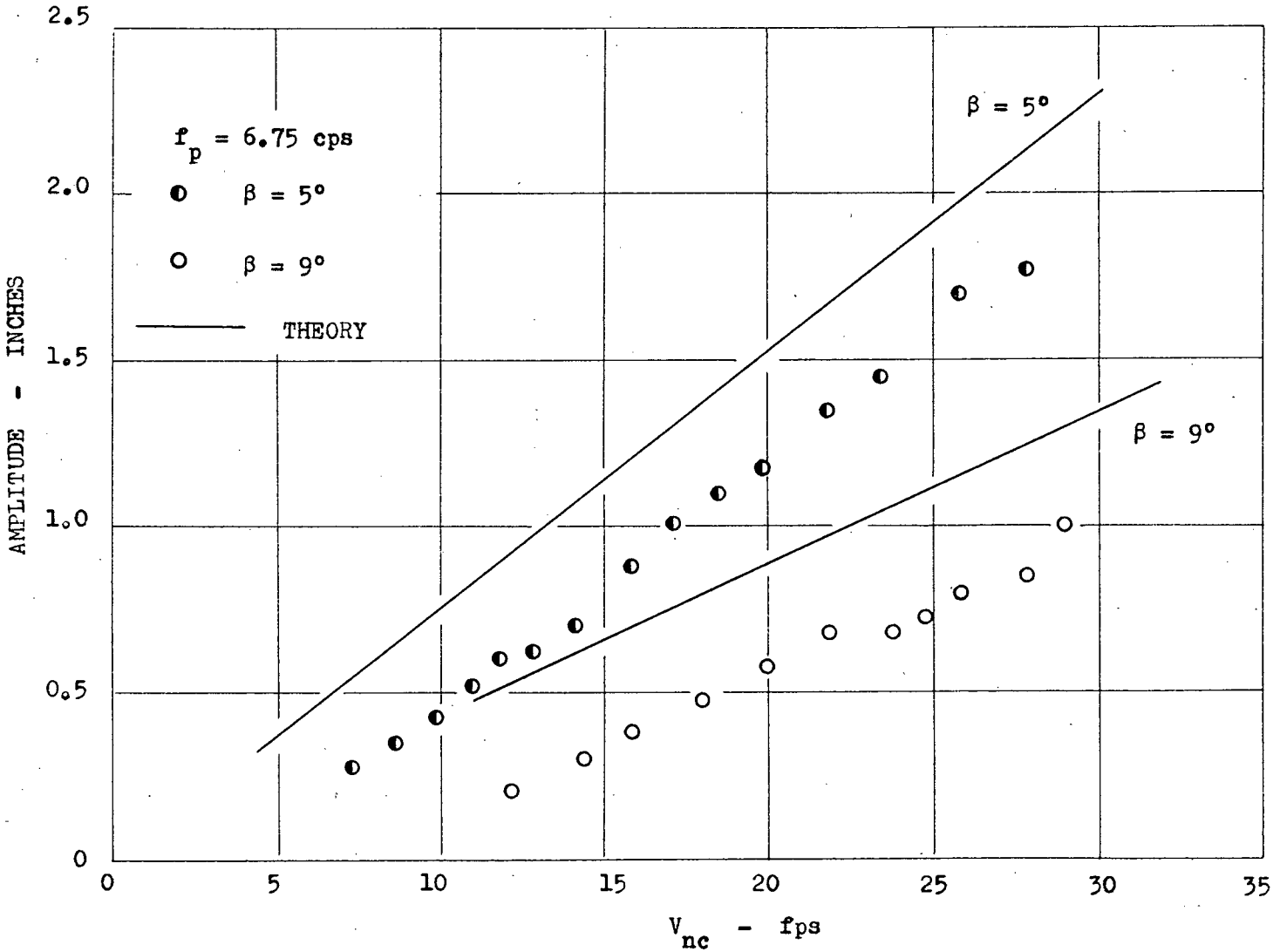

FIGURE 56 - AMPLITUDE RESPONSE FOR SQUARE SECTION CYLINDER FOR β = 5° & 9°

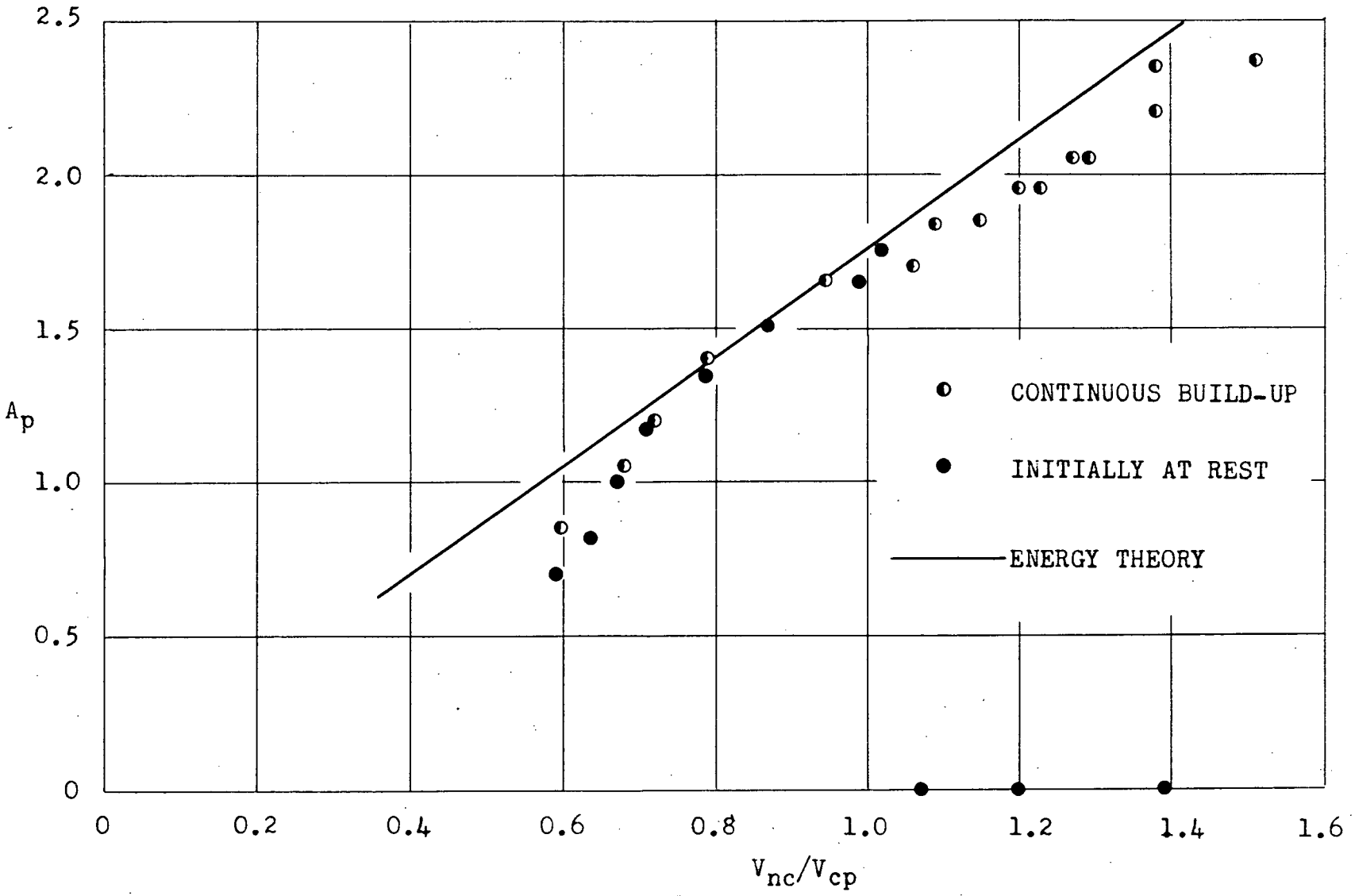

FIGURE 57 - AMPLITUDE RESPONSE OF D-SECTION SHOWING GALLOPING VIBRATION